Albert-Ludwigs-Universität Freiburg i. Br.
Institut für Hydrologie

Chris Fischer

Hydrological Modeling
of the Water Resources in the Nahal Harod, Israel.

Diplomarbeit unter der Leitung von Prof. Dr. Ch. Leibundgut
Freiburg i. Br., Main 2007

Albert-Ludwigs-Universität Freiburg i. Br.
Institut für Hydrologie

Chris Fischer

Hydrological Modeling of the Water Resources in the Nahal Harod, Israel.

Referent: Prof. Dr. Ch. Leibundgut
Koreferent: Dr. J. Lange

Diplomarbeit unter der Leitung von Prof. Dr. Ch. Leibundgut
Freiburg i. Br., Main 2007

Acknowledgment

Thanks to Prof. Dr. Christian Leibundgut and Dr. Jens Lange for the supervision of this work and for all the classes, seminars and field trips throughout my studies.

I owe a special thank to Anne Gunkel for helping me with all the occurring problems during modelling and for the many written source code lines.

This work and my studies would not have been possible without the financial and moral support of my parents. Thank you mum, Thank you dad.

Finally, I would like to thank my girlfriend Ximena, my son Mateo and Señiora Wilma for all their love, support and patience.

Contents

List of figure

List of tables

Contents of the appendix

Notation

A_{sub}	area subbasin [m²]
A_{CS}	cross-section area of flow [m²]
c_p	heat capacity of air [J/kg]
Coef	runoff coefficient
C_{at}	atmospheric conductance [m/s]
E	Evaporation [mm]
FC	field capacity
IEOF	infiltration excess overland flow
LJRC	Lower Jordan River Catchment
K_S	saturated conductivity [cm/h]
$K(\Theta)$	unsaturated conductivity [cm/h]
m	Slope of the saturation vapor pressure curve
n	Manning's coefficient of roughness
N	Number of time Steps
NS	Nash-Sutcliffe model efficiency
P	wetted perimeter [m]
ρ_a	Density of air [kg/m³]
PWP	permanent wilting point
Q	Runoff [m³/s]
Q_{OBS}	observed runoff [m³/s]
$Q_{\overline{OBS}}$	mean observed runoff [m³/s]
Q_{SIM}	simulated runoff [m³/s]
QC	parameter fur runoff concentration
R_H	hydraulic radius [m]
rH	relative humidity
R_n	net irradiance [W/m²]
S	Slope
SVAT	Soil vegetation atmosphere transfer
SEOF	saturation excess overland flow
SSD	sun shine duration
T	temperature [°C]
u	wind speed [m/s]
v	flow velocity [m/s]
VE	volume error
x	time Step
γ	psychrometric constant [Pa /K]
Θ	soil water content
Θ_r	residual soil water content
λ	Brooks-Corey pore-size distribution index
λ_v	latent heat of vaporization [J/ kg]
μ	arithmetic mean
σ	standard deviation
ϕ	porosity

Summary

The coupled hydrological model TRAIN-ZIN is applied to the meso scale basin Nahal Harod in Israel. The study area is semi-arid with a Mediterranean climate which is characterized through hot and dry summers and a mild and wet winter. Rainfall events usually are only of local extent and have high intensities. They are highly variable in space and in time. River flow is periodic or ephemeral. Flood events of short duration occur mainly during winter months. Hydrographs show steep rising limbs and steep recession curves. Main runoff generating processes are infiltration excess and saturation excess overland flow. Surface runoff and groundwater are in no direct contact and indirect runoff processes (e.g. interflow) do not occur. The absence of a dense vegetation cover and crust building lead to very low infiltration capacities. Shallow soils reach saturation easily. Soil characteristics controlling infiltration and runoff generation are highly variable. This variability and the uncertainty of rainfall make the simulation of Mediterranean catchments with hydrological model difficult. Different approaches than for the more humid region have to be used.

The Nahal Harod basin is situated between Lake Tiberias and the Dead Sea in the Lower Jordan River Catchment. With 170km² it is a meso scale basin. The vast and flat valley is part of the lowered Jordan Rift. A thick quaternary alluvium lies on basalt from the Miocene. The South the basin borders to the West Bank. The limestone of the southern valley shoulder shows some karst formations. The existing soils are typical for the Mediterranean region. Vertisols are the dominant soil type in the valley basin. Because of the high content of clay minerals these soils swell and crack during alternating wet and dry seasons. On the slopes shallow Terra Rossas are found. Many rock outcrops alternate with pockets of soils. These areas are covered with Mediterranean scrubland. Most of the basin is agriculturally used. During the wet winter months mainly wheat is planted. The fields stay bare during the dry summer. 3% of the catchment is sealed by settlements and industry. Fishponds cover 4% of the basin's surface. These water bodies play an important role in the water balance. Spring discharge is taken to maintain the ponds and their sewage produces a continuous base flow at the catchment's outlet. Large amounts of water are lost through evaporation. An estimation is done with the Penman equation for evaporation from open water surfaces.

Runoff is simulated with the coupled TRAIN-ZIN Model. The SVAT-Model TRAIN simulates the vertical processes evaporation, transpiration and deep percolation in daily time steps. The rainfall-runoff model ZIN simulates the flashy floods in tine steps of five minutes. The soil moisture module connects the two models. During dry periods TRAIN estimates the soil water content. It is taken by the ZIN Model for the calculation of runoff generation in case of rainfall. After an event TRAIN again picks up the soil moisture estimation from ZIN. After the first successful application of the coupled model to a micro scale basin, it was now applied to a meso scale basin. Rainfall radar data with a high spatial and temporal resolution was used for rainfall input. A new runoff concentration routine was successfully integrated into the model. It takes the slope and the size of the model unit subbasin into account. Parameters were determined through an intensive literature study, the analysis of maps, satellite images and photographs, and through calibration. Landuse and soil grids were generated. The study area was divided in 142,899 cells of 50x50m². For runoff concentration 110 subbasins were delineated and the stream network was cut into 110 stream segments for channel

routing. No direct Measurements in the basin were made. Parameters of the routing routine and of the submodel TRAIN were not calibrated. The parameter for the new runoff concentration routine was adjusted during the first simulations. The soil characteristics infiltration capacity, initial loss, soil depth, saturated conductivity and initial moisture were subject to a more intensive manual calibration process.

With a predefined modeling strategy, the analysis of daily rainfall maps and of saturation maps an effective calibration could be conducted. Three single events were used during this process, each with different rainfall and runoff characteristics. With the determined parameter set a fourth event was simulated for model verification. Model efficiencies of 0.2-0.8 were achieved. After the event simulations the whole season 2002/2003 was modeled. Results were highly satisfactory and proved the functionality of the coupled model. The validated model was used to run landuse and climate change scenarios to predict their effects on runoff characteristics. A detailed discussion on the model, the parameterization, the simulation and the possible reasons of observed inaccuracies is given at the end of the work.

Keywords:

Semi-arid, Mediterranean, IEOF, SEOF, meso scale, Nahal Harod, Jordan, TRAIN Model, ZIN Model, TRAIN-ZIN, model coupling, landuse change scenario, climate change scenario.

Zusammenfassung

Mit dem gekoppelten hydrologischen Model TRAIN-ZIN wird das meso-skalige Einzugsgebiet Nahal Harod in Israel simuliert. In dem semiariden Gebiet herrscht mediterranes Klima mit trockenen, heißen Sommern und feuchten, kühlen Wintern. Niederschläge haben eine hohe zeitliche und räumliche Variabilität. Die lokal begrenzten Regenereignisse weisen meist sehr hohe Intensitäten auf. Flüsse führen nur periodisch oder ephemer Wasser. Abflussereignisse sind meist sehr kurz treten vor allem in den Wintermonaten auf. Sie sind gekennzeichnet durch einen starken Anstieg des Abflusses und ein schnelles Abklingen. Horton'scher Oberflächenabfluss und Sättigungsabfluss sind die zwei Hauptprozesse der Abflussbildung. Oberflächenwasser und Grundwasser stehen in keinem direkten Kontakt zueinander und indirekte Abflusskomponenten wie etwa Zwischenabfluss sind zu vernachlässigen. Das Fehlen einer dichten Vegetationsdecke und die häufig auftretende Krustenbildung führen zu sehr niedrigen Infiltrationsraten und begünstigen die Bildung von Horton-Abfluss. Geringmächtige Böden können wenig Wasser aufnehmen, so dass es schnell zu einer Aufsättigung und zur Bildung von Sättigungsabfluss kommt. Bodeneigenschaften, welche die Infiltration und die Abflussbildung beeinflussen sind räumlich sehr unterschiedlich. Aufgrund dieser Variabilität und dem ungewissen Niederschlag ist die Simulation von mediterranen Einzuggebieten äußerst diffizil. Andere Herangehensweisen als bei der Modellierung von humideren Gebieten sind nötig.

Das Einzugsgebiet Nahal Harod mit einer Größe von 170km² liegt zwischen dem See Genezareth und dem Toten Meer im untern Jordan Einzugsgebiet. Der weitläufige und ebene Talboden ist Teil des abgesenkten Jordan Grabens. Ein mächtiges quartäres Alluvium liegt auf tertiären Basalten. Im Süden führen teilweise verkarstete Hänge, aus der Kreide und dem Jura zur höherliegenden West Bank. Die Pedologie ist typisch für den Mediterranen Raum. Die Talböden weisen Vertisole auf und die Hänge werden von geringmächtigen Terra Rossas bedeckt. Durch den hohen Gehalt an Tonen quellen und schrumpfen die Vertisole bei Befeuchtung und Austrocknung. An den hängen wird die Bodendecke oft durch anstehendes Gestein durchbrochen. Der größte Teil des Einzugsgebietes wird landwirtschaftlich genutzt. In den Wintermonaten wird vornehmlich Weizen angebaut und im Sommer liegen die Felder brach. Die Versiegelung beträgt 3% und Fischteiche nehmen 4% der Fläche ein. Diese künstlichen Gewässer haben einen großen Einfluss auf die Wasserbilanz des Nahal Harod.

Die Abflussereignisse werden mit dem gekoppelten TRAIN-ZIN Model simuliert. Das SVAT—Model TRAIN beschreibt die vertikal ausgerichteten Prozesse Evaporation, Transpiration und Tiefenfiltration in Zeitschritten von einem Tag und das Niederschlag-Abfluss Model ZIN modelliert die *Flash Floods* in Zeitschritten von 5 Minuten. Die Berechnung der Bodenfeuchte stellt die Verbindung zwischen den beiden Modellen dar. In trockenen Perioden wird sie von TRAIN ermittelt und im Falle von Niederschlag an ZIN weitergegeben. Nach der erfolgreichen Simulation eines mikro-skaligen Einzuggebietes wird es nun auf ein größeres Gebiet angewendet. Es wurden Niederschlagsradardaten mit einer hohen zeitlichen und räumlichen Auflösung verwendet. Eine neue Methode zur Berechnung der Abflusskonzentration, welche die Größe und die Neigung der Teileinzugsgebiete berücksichtigt, wurde in das Model integriert. Die Parameter wurden mittels einer intensiven Literaturrecherche, dem Auswerten von Karten, Satellitenbildern und Photographien sowie durch Kalibrierung bestimmt. Das

Gebiet wurde in 142 899 Gitterzellen à 50x50m² unterteilt. Jeder Zelle wurde eine Landnutzung und ein Bodentyp zugewiesen. Zur Berechnung der Abflusskonzentration wurden 110 Teileinzugsgebiete mit jeweils einem Gerinne ausgewiesen. Die Bodeneigenschaften Infiltrationsrate, Anfangsverlust, Bodentiefe, gesättigte Leitfähigkeit und Vorfeuchte wurden während der Kalibrierung bestimmt. Diese konnte durch eine vorher bestimmte Kalibrierungsstrategie sowie durch die Einbeziehung von Niederschlagskarten und Bodenfeuchtkarten anhand von drei Einzelereignissen zügig durchgeführt werden. Ein viertes Ereignis wurde zur Verifizierung simuliert und anschließend wurden die so bestimmten Parameter für die Simulation der gesamten Niederschlagssaison 2002/2003 verwendet. Die guten Ergebnisse belegen die Funktionalität des Models und ermöglichen das Durchführen von Landnutzungs- und Klimaänderungsszenarien.

I. Introduction

The Jordan River is the most important surface water source of the Middle East. This area is characterized by scarcity of its water resources. The lack of sufficient water coupled with high population density and/or high population growth rates results in serious water crisis. The five riparian countries Palestine, Israel, Syria, Jordan and Lebanon together have a total population of over 35 million. The situation has aggravated with increasing population and their extension towards dryer and more hostile regions. The distribution of the river's water and its allocation between the riparian countries always was a matter of concern and still leads to political tension in the region. Most of the surface water is located in the upper basin of the Jordan River, which extends from its main sources on Mount Hermon down to Lake Tiberias. The annual water flow into the lake is around 660 Mm^3/yr. Only around 70 Mm^3/yr is released from the lake into the Lower Jordan. The Israelis export large amount of the lake's water to the south and beyond the basin (Ju'ub & Schetelig 2004). It is pumped to the coastal plain and distributed there by the national water carrier to the Negev in the South. In dry years an over-exploration of the existing resources in the lake (4000Mm^3) can be observed. This leads to a lower sea level. The Lower Jordan River receives additional water quantities of about 245Mm^3/yr. On the way to the Dead Sea it is nearly emptied. The decrease of discharge into the Dead Sea caused serious negative effects. A decline in its water level and a reduction in its area are visible. This brings about a sharp increase in salinity. As a result the unique ecological system in and around the Dead Sea is in serious danger.

Irrigation consumes more than 60% of the region's surface and ground water resources. The personal private demand makes up another 30%. In Israel total water consumption per day and capita of 330 liters is calculated, while the respective values of the Palestinian West Banks amount around 60 liters (Hötzl 2004). A sustainable socio-economic development in the whole region is hindered through the scarcity of water. The natural water resources are exhausted. Strategies on how to run the future water demand and a sustainable water resources management have to be developed.

The GLOWA Jordan River provides the scientific support for an integrated water resources management. The project is financed by the German Federal Ministry of Education and Research as part of the 'Global Change in Hydrological Cycle' research initiative. The interdisciplinary GLOWA JR addresses the vulnerability of water resources under global change. A multilateral research consortium with institutions from Israel, the Palestinian Autonomy, Jordan, and Germany develop a modeling framework to integrate data and methods from various disciplines. (URL 1).

.

II. Objectives

The assessment of the effects of climate and landuse change on spatio-temporal surface water availability and groundwater recharge is a major part of the GLOWA Jordan River Project. At the Institute of Hydrology process-based models are used for this purpose. In the scope of her dissertation A. Gunkel coupled the SVAT-model TRAIN (Menzel 1999) with the hydrological model ZIN (Lange et al. 1999). In order to achieve a simulation of the entire Lower Jordan River Catchment, the coupled model was first tested in a data-rich environment. Schütz (2006) modeled the micro scale basin of Wadi Anabe in Israel. Main objective of this work is a first application of the coupled TRAIN-ZIN Model to a meso scale basin. The runoff of the 170km² large Nahal Harod will be simulated. To set up a complete water balance, further components of the water cycle have to be addressed.

Unlike for the micro scale basin with a comprehensive data base, the model cannot be run non-calibrated for the Nahal Harod. Parameters have to be determined through calibration. No direct measurements are available. Through an intensive literature study and the analysis of thematic maps, photographs and satellite images a sufficient data base has to be created. The model then will be calibrated manually. Through a prior specification of a modeling strategy an effective calibration and simulation will be assured. In publications and reports of simulations with deterministic hydrological models, the calibration process is often not discussed sufficiently. Therefore another objective of this work was to give an exact and comprehensive report of the model adjustment. For further model applications, the sensitivity of the different parameters will be discussed. The transfer of the model from micro to meso scale requires further modifications. Rainfall-radar with a high spatial and temporal resolution will be integrated. A new method of runoff concentration considering the spatial variability of the model elements has to be developed and tested.

With a determined parameter set the functionality of the coupled TRAIN-ZIN Model and its modules has to be proven. Therefore the simulated hydrographs of single events and of the whole season 2002/2003 will be compared with measured runoff. An estimation of the effects of landuse and climate change on flood generation for the Nahal Harod was another objective. First landuse and climate change scenarios will be run with a validated model. The results and experiences made will be another step towards the simulation of the whole LJRC.

III. General aspects

3.1 Mediterranean climate

The climate of Israel as a whole is defined as a Mediterranean climate (Jaffe 1988). The common climatic classifications describe the Mediterranean climate as one with distinct seasons, a hot and dry summer followed by a cool and rainy winter. In the Köppen classification for the Mediterranean climate, the winter rainfall has to be at least three times as much as the summer rainfall. Indeed, in most of the Mediterranean, summer rainfall is virtually zero (Palutikof et al. 1997). Goldreich (2004) shows the general distribution of climate regions for Israel, using the Köppen classification (fig. 3.1). This system, from the beginning of the 20th century, is based on empirical natural vegetation boundaries and is still one of the most popular among climatologists.

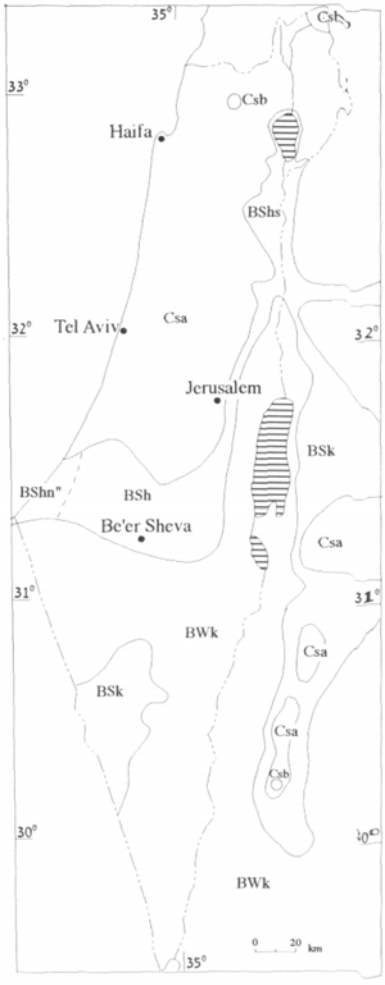

Figure 3.1: Köppen climatic classification of Israel (Goldreich 2003)

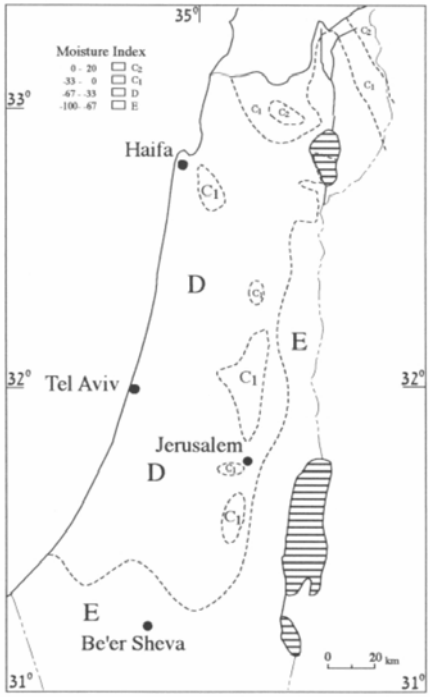

Figure 3.2: Moisture index of the Thorthwaite climatic classification (Goldreich 2003)

Climatic regionalization across Israel is difficult because of the abrupt differences in climate across relatively short distances (Kalma et al. 2004). Annual rainfall decreases from about 1000mm in the far north down to about 25mm in the extreme south of

Israel. The west-east differences depend on the distance from the Mediterranean Sea. The lower Jordan River Valley is just on the border between the Mediterranean (Cs) and the semi-arid (BS) climate. The distinction between the two is made by the total annual rainfall of 400mm. The famous Thornthwaite classification which takes the water balance of rainfall and potential evaporation into account defines most of Israel as semi-arid (moisture index D). The Bet She'an Valley, the study area of this work, belongs, according to Thornthwaite, to the arid semi-dessert class (moisture index E), even though the landscape is rather Mediterranean. The Köppen model seems to be more suitable in this case. For this reason, the Thornthwaite Map was excluded from the newer versions of the Atlas of Israel (Goldreich 2003). The following table gives an overview of common climate classification.

Table 3.1: Comparison of various climatic classifications (Goldreich 2003)

	Budyko (1974)	Thornthwaite (1955)	Köppen	Annual precipitation (mm)	Vegetation
30			BWhs	<200	desert
10		arid E		200-300	semi-desert
	desert		BShs	300-400	sub-humid
3		semi-arid	Csa	400-600	
	semi-arid	D			humid savannah
	savannah	sub-humid			
		C	Csb	600-1200	forest-sub-tropic
	sub-tropic forest	humid			
1					
	forest		Cfa		wet forest
			Cfb		

The summer months are characterized by warm and dry conditions associated with a strong high-pressure ridge which pushes over the Mediterranean from the Azores subtropical high (Wigley 1992). The high pressure prevents convection and the formation of occasional thunder storms which can be observed in the summer of the temperate, humid region. Temperatures of over 40°C under strong midday sun are not uncommon. The winter, which usually lasts from November to March, is the cold and rainy season. The relatively warm Mediterranean Sea attracts low pressure systems which migrate from west to the east, pass over Israel and may eventually trigger precipitation events. In Israel, approximately 92% of the mean annual rainfall is recorded in the winter with January being the wettest month (Jaffe 1988).

The mean annual temperature lies between 18°C in the south-east of the Mediterranean basin and 12°C in the northern and north-western parts. In winter the lowest mean temperatures are found in the north coast of the Adriatic Sea (6°C) and in summer it can rise over 26°C in Egypt and southern Turkey (Palutikof 1996). In the lower Jordan River Valley mean annual temperature is 22°C with 13°C in the coldest month January and 33°C in the hottest month August (Goldreich, 2003).

Annual rainfall in the semi-arid Mediterranean region of about 300-700mm is uncertain and patchy. Interannual rainfall variation is high and makes agricultural management and other rainfall-dependent economic considerations difficult. Although rainstorms are restricted to the winter period, their seasonal distribution, amount of rainfall, intensity

and span vary considerably. Precipitation is mainly associated with cyclonic disturbances, but it is also strongly influenced by local orographic effects and therefore the spatial variability is very high (Wigley 1992). Storm cells tend to be limited in their aerial extent and often do not reach a 10km diameter. Rainfall intensities of 50mm/h (or higher) are common (Nir 1973). Goldreich (2003) states that the Jordan Valley between Lake Tibereas and the Dead Sea is rich in storms with high intensity.

3.2 Hydrology of semi-arid environments

3.2.1 General aspects

Stream discharge cannot be observed continuously in most semi-arid environments. Periodic and ephemeral streams drain these regions. Dominating runoff processes are saturation excess and infiltration excess. Indirect runoff components (e.g. interflow) are not relevant. Surface and subsurface hydrology are separated (Lange 1999) and no groundwater storage contributes to stream runoff during the dry season. Spring discharge, diminished through transmission losses or usage of the population, does often not contribute to the main channel. In semi-arid environments a threshold of storm rainfall has to be reached. Below this amount no runoff is measured (Nir 1973). In a dry catchment or during rainfall events of small extent, runoff may be generated locally but never reaches a stream channel. Floods of regional dimension only occur a few times a year, mainly under wet conditions when large parts of the basin contribute to runoff.

A major difference to humid environments is the widely observed and reported large variability of hydrological variables and processes (e.g. Berndtsson & Larson 1987, Beven 2002, Merz & Plate 1997 and Yair & Lavee 1985). Temporal and spatial variation in runoff caused by the already mentioned high variability of precipitation may be enhanced by spatial variation of soil properties as soil water content and infiltration rates. Berndtsson & Larson (1987) performed 52 double-ring infiltrometer tests in a small, semi-arid catchment in Northern Tunesia with a very wide range of both initial and final infiltration capacities.

Table 3.2: Statistical properties of initial and final infiltration capacities (Berndtsson & Larson 1987)

	Infiltration capacity	
	Initial	final
Mean (mm/h)	545	85
Median (mm/h)	425	50
Standard deviation (mm/h)	505	95
Variation coefficient	0.93	1.12

3.2.2 Infiltration

Infiltration directly affects surface water runoff, water storage in the soil and groundwater recharge through deep percolation. Zones of low infiltration are the major runoff source area. Factors that control infiltration can be divided into two groups: biotic and soil factors. Vegetation cover tends to increase infiltration as compared to bare soils. Presence and activity of living and dead roots can increase the infiltration rate through the formation of macro pores. Vegetation prevents crust building and a

plant canopy diminishes the kinetic energy of falling raindrops. It reduces raindrop compaction and averts *Splash*-erosion followed by surface sealing. In semi-arid Mediterranean environments, bare or sparsely vegetated areas intervene with patches of vegetation (Bergkamp 1998).
The important soil characteristics that influence the infiltration rate are pore size distribution, bulk density, structure, chemical concentrations, topography, stone cover and water content (e.g. Cerda 1997, Hanks 1985). Initial soil water content just before a rainfall event is perhaps the most important factor involved in the rainfall-runoff relationship. It affects the infiltration capacity and the rainfall excess. Antecedent conditions play a significant role in both hill slope runoff and main channel hydrograph propagation (Shannon et al. 2002). Gomez-Plaza et al. (2001) recognizes the soil water content as an important factor controlling runoff in semi-arid environments and explains its spatial variability through the influence of many factors. Topography, soil properties, vegetation and soil depth are important. Among these factors which govern infiltration, the antecedent soil moisture is the most uncertain. It is highly variable in space and time (Karnielli & Ben-Asher 1993).

3.2.3 Infiltration excess overland flow

In arid environments the predominant runoff mechanism is IEOF (Castillo et al. 2003). High rain intensities and less permeable soils are the reason for the infiltration excess. The runoff response is more uniform and does not depend on initial soil moisture. If the rainfall exceeds an initial loss due to wettening and micro basin storage, intensities over the infiltration rate will generate runoff. This process, also known as Hortanian flow, is much more important than in more humid areas.

3.2.4 Saturation excess overland flow

In zones with more permeable soils even the high rainfall intensities of storm in the Mediterranean region might not reach the infiltration rate. In this case, no infiltration excess overland flow is generated. Soil storage is limited and after a certain amount of rain or run-on the soil is saturated. With a steady state infiltration rate, known as the saturated hydraulic conductivity, water percolates through the saturated soil (Cerdá 1997). This rate usually is lower than the rainfall intensity and so runoff is generated. The SEOF is more dependent on initial soil water content.

3.2.5 Runon-Runoff

As a result of high variability in vegetation and soil characteristics, infiltration rates might differ along a hill slope. Runoff generated on rock outcrops or impermeable soils does not reach the stream but infiltrates further down when it reaches highly permeable surfaces. These zones eventually reach saturation and contribute to storm runoff. This process known as run-on - runoff takes place in areas with a complex pattern of surface characteristics (Beven 2002).

3.2.6 Transmission losses

Water losses along channels eventually play an important role in ephemeral streams. Infiltration into the riverbed, which stands in no direct contact to groundwater, can be significant. Smaller floods often do not reach the outlet of a catchment. In arid environments these transmission losses are the only source of groundwater recharge. Runoff coefficients of semi-arid regions decrease with slope length or with the size of a basin. Moisture content, width, depth and the hydraulic conductivity of the alluvium together with the flow duration are the most important factors influencing the transmission losses. Large runoff events that leave the main channel, flooding additional areas along the riverbed, loose a large amount of water to the underground (Lange 2005).

3.2.7 Storm events

Generally, the hydrographs of ephemeral streams show a steep rising limp, with an almost instantaneous rise to peak flow and a steep recession curve (Shannon et al. 2002). Semi-arid catchments usually have a very short response time and no large reservoir, which could lead to runoff for longer time after the rain has fallen, exists. Discharge rises and falls quite rapidly (Scoging & Thornes 1979). The difficulties in estimating the magnitude of runoff events can be explained with the spatial and temporal variability of hydrological processes.

3.3 Rainfall-Runoff modeling in semi-arid environments

Hydrological models are an important tool in research and water management. There are a large number of common used and accepted definitions for rainfall-runoff models. Beven (2001) generally defines models through at least one functional component that accounts for the relationship between rainfall and runoff. A basic classification of modeling strategies differentiates between lumped and distributed, deterministic and stochastic models. Due to the lack of data, the paucity of time series, the variability in catchment response and the unpredictable nature of storm cells, hydrological simulation in arid and semi-arid regions can not be realized the same way as for perennial rivers in the humid zone (Pilgram et al. 1988, Shannon et al. 2002). The lack of data causes the validity of stochastic models to be highly questionable (Yair & Lavee 1985). The great spatial variability of processes makes it very difficult to combine geographical units for a lumped approach and the temporal variance and the rarity of rainfall and runoff impedes the use of statistical methods. Physically based models are necessary to describe runoff processes in semi-arid environments. They require the specification of descriptive, deterministic equations of hydrological processes and have to be distributed because the defined equations generally involve one or more space coordinates (Beven 1985). To solve the generally nonlinear partial differential equations, approximate numerical methods have to be used and a large number of parameters are needed. With the limited range of measurements in space and time these parameters often have to be estimated during calibration process. Starting values can be taken from literature and should have some physical justification. Empirical generalizations (e.g. Manning's law of channel flow) have to be made for complex hydrological processes with a large number of parameters that have not been well understood so far.

For hydrological modeling, continuous precipitation data is essential. In semi-arid environments where rainfall events are mostly only of local extent and short in time, this data has to be available in a high spatial and temporal resolution. Rain gauge networks are usually inadequate due to their limited sampling distribution and other methods have to be applied. Rainfall radar is a technique to determine rainfall patterns as well as integrated total rainfall amount. It operates under the principal of back-scatter and absorption of short electromagnetic waves by particles of ice, snow, or water. For a further explanation on the method and on the physical background, Huebner (1985) gives a clear introduction.

IV. Study area, Nahal Harod

4.1 General aspects

The Nahal Harod is a tributary of the Jordan River. It is situated between Lake Tiberias and the Dead Sea in the Lower Jordan River Catchment (fig. 4.1). The characteristics of the basin are typical for the semi-arid Mediterranean region. Flood events during the rainy season, produced by infiltration and saturation excess overland flow, usually last only from a few hours to one or two days. The 170 km^2 large Nahal Harod can be divided in three major units: The vast and flat valley bottom, the steep southern karstic shoulder which borders the West Bank and the smoother slopes which delimit the basin in the North-West. The mean slope of the stream network is 0.046 and altitude ranges from -212m at the catchment's outlet to 510m over sea level at the highest point in the western end of the basin.

Figure 4.1: Nahal Harod (Source: Google Earth)

4.2 Geology

The strong tectonic activities in the end of the preglacial Pleistocene lowered the Jordan Rift and were accompanied by an uplift of the Rift valley shoulders (Horowitz, 1988). This is the dominant factor of the current shape of the Israeli landscape. The new created endoreic system flows to the Dead Sea. The regions of the Rift in which there was tectonic down movement became sediment traps. Klein (1988) correlates the Harod valley with these basins, which were areas of swamplands before they were artificially drained by man. The lowered massif of the rift valley is covered by quaternary alluvium. Limestone and chalk from late Cretaceous and early Miocene dominate the geology of the West Bank. The southern shoulder of the Harod valley is part of this formation and shows some karst formation.

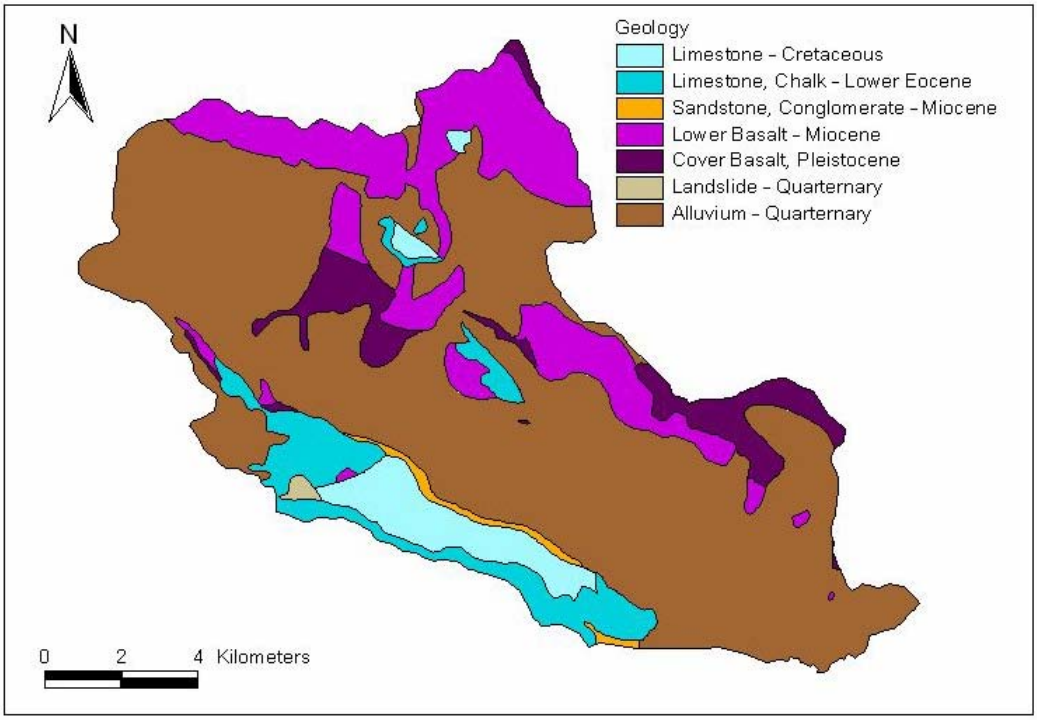

Figure 4.2: Geology, Nahal Harod (Geological Survey of Israel 1997, changed)

4.3 Soils

The dominant soils in the Nahal Harod are Vertisols. Dan et al. (1981) describes them as AC soils of heavy texture. The high content of expanding montmorillonitic clay minerals causes the soil to crack and swell during alternating wet and dry seasons. The origin of these clay is mainly aoelion and alluvial but also stems partly from basalt weathering. The swelling and cracking affects their physical properties, especially the infiltration (Battikhi & Suleiman 1999). After longer dry periods, cracks will spread widely over the surface and the infiltration rate will increase. During a precipitation event, the infiltration will decrease due to the swelling and due to the surface sealing process. While the swelling mostly depends on the soil structure and the soil resistance to swelling, the clogging by sediments is a function of rain intensity and vegetation cover. Without a protective plant cover, the falling raindrops cause *Splash*-erosion and the disengaged minerals seal the pores and cracks of the soil. Schröder (2000) found these factors to be the most important in the sealing-up of agricultural soils. In a wet condition bare Vertisols will so become highly impermeable (Duiker et al. 2001). Vegetation leads to a strong increase of infiltration due to the formation of macro pores. A dense cover absorbs the kinetic energy of the raindrops and so impedes *Splash*-erosion. It also prevents crust formation. Infiltration into Vertisols is highly dependant on soil water content and in case of agricultural fields on the current crop situation.

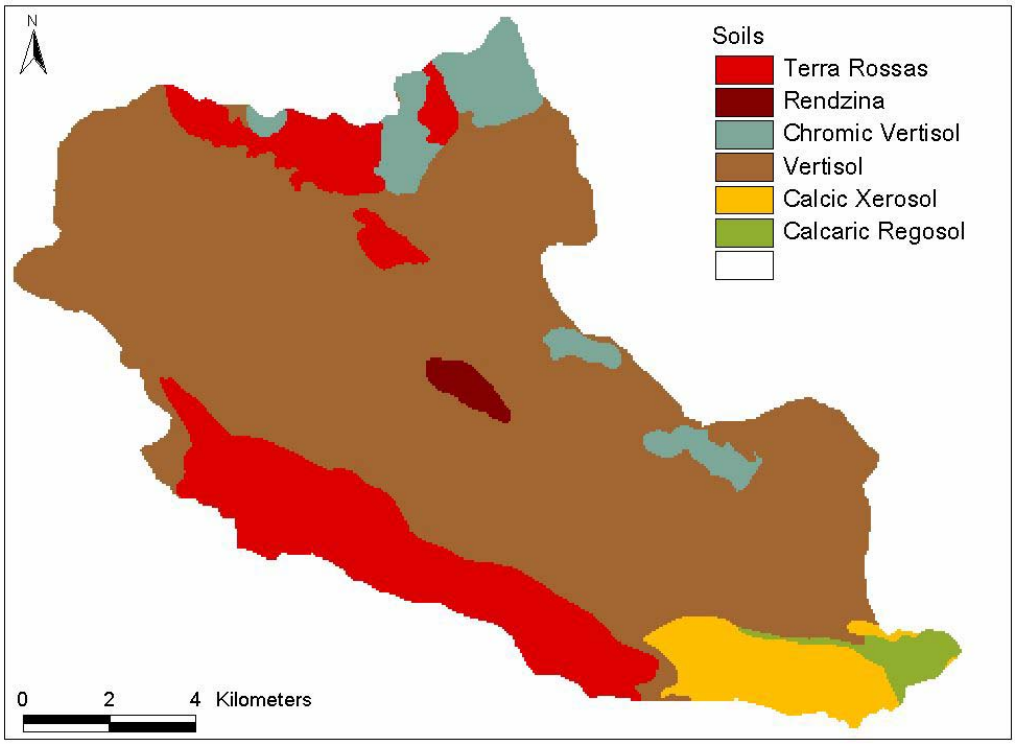

Figure 4.3: Soilmap, Nahal Harod

Besides the Vertisols in lowlands, shallow soils on nearly bare slopes are typical for the Mediterranean region (Yaalon1997). While the Vertisols have a thickness of several meters in the Nahal Harod, the Terra Rossas on the surrounding slopes of the basin are quite shallow and many rock outcrops appear. This wide spread soil type over the entire Mediterranean is a reddish brown, fine-textured, mostly non-calcareous soil on hard limestone. The Rendzinas, Regolsols and Xerosols play only a minor role in the Nahal Harod.

4.4 Landuse

The lower Jordan River Valley has been subject to severe changes during history. The fertile swampland was drained and used mainly for agriculture throughout centuries. Today agricultural fields occupy over 53% of Nahal Harod. During the rainy winter months wheat is mostly planted. After the harvest in early spring, these fields are bare until next winter. Besides a few small sites, no irrigation is applied. Citrus fruit orchards make up another 15% of the basin. Where there is hardly any human influence the slopes are covered by scattered shrubs of *Zizphus lotus* and other typical herbaceous Mediterranean grasses. Some spiny trees of Sudanian origin like the *Ziziphus spina-christi* can also be found (Dan 1988). For the landuse map (fig. 4.4) and also for modeling, these types were merged into the same class of Mediterranean scrubland. The many fishponds, which cover a little over 4% of the basin, are mainly situated in the lower parts. About 3% of the catchment's surface is sealed, mainly by loose settlement, transportation and small industrial facilities.

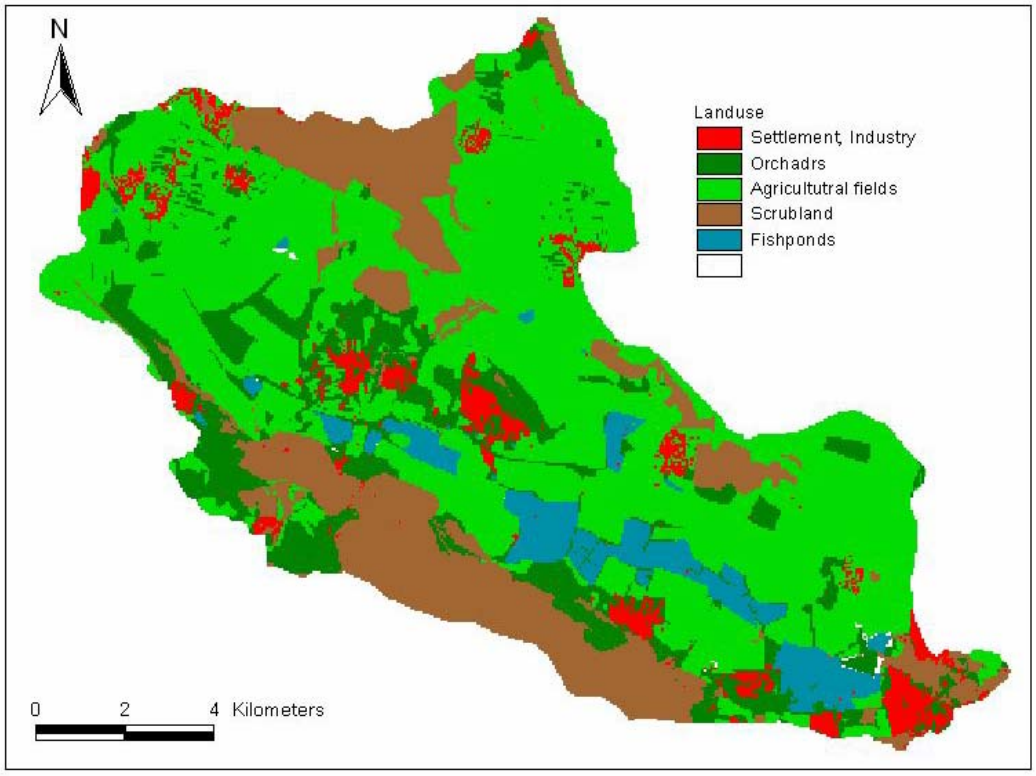

Figure 4.4: Landuse, Nahal Harod.

4.5 Fishponds

Fishponds cover 6.94 km^2 or 4% of the catchment. The satellite image was used for the determination of the open water surface. This was more exact than the landuse map. The water for the fishponds is taken from karst-sources at the south of the basin, bordering to the West Bank. The continuous base flow of the Nahal Harod of about 100 l/s is the outflow of these ponds. Furthermore, these ponds do not play any role in runoff generation and their surface does not contribute to floods. Natural channel flow

is not in contact to these ponds. During a precipitation event, the rainfall which falls directly on the open water surfaces is stored in the water bodies and only leaves the system through evaporation. It can be assumed that even during extreme rainfall events the ponds will not overflow and so will not contribute to storm water runoff.

4.6 Climate

The model was applied for the hydrological year 2002/2003. For this purpose the meteorological data from the station Gilboa was analyzed.

Table 4.1: Gilboa meteorological station, 01.10.2002 – 30.09.2003

	Annual	Winter (10.-03.)	Summer (04.-09.)
mean temperature [°C]	21.6	16.4	26.7
average wind speed [m/s]	3.9	3.1	4.6
relative humidity [%]	57.3	63.2	51.4
rainfall [mm]	527.5	527.5	0.0

Annual rainfall for the same period calculated from the rainfall radar is 580.4mm. This slightly higher value can be explained with the number of rainfall events in the higher parts of the catchment. Several storms took place locally at the western and the southern border of the Nahal Harod without any precipitation at the Gilboa station at the valley bottom. Rainfall calculated from the rainfall radar for the higher Shizafim subbasin is 682.8mm, and 624.7 for the Merhavia subbasin.

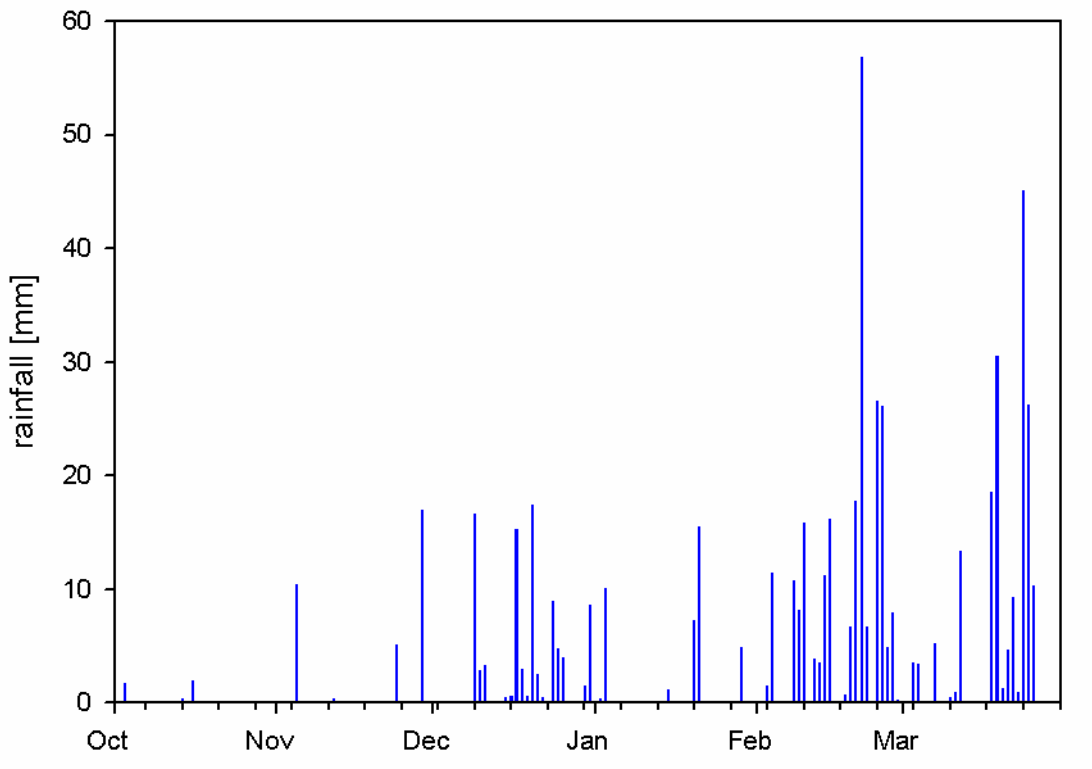

Figure 4.5: Daily rainfall, calculated from the rainfall-radar.

4.7 Hydrology

4.7.1 General aspects

The Nahal Harod is a perennial river with runoff all year through. It also shows some typical features of ephemeral streams which are common for the semi-arid Mediterranean realm. The low base flow is interrupted by huge runoff events. These flash floods occur mainly in winter months. The source of the base flow is a number of karst springs which drain the West Bank. The stream network of the Nahal Harod is mainly man-made. The main channel is an artificial trapezoid canal. Trenches draining the agricultural fields merge to larger ditches along roads and then flow into the main channel. Natural riverbeds can only be found in the steep slopes of the southern valley shoulder.

4.7.2 Flood events

In the season 2002/2003 thirteen floods were gauged. The first event of the hydrological year with a peak runoff of 4.3m³/s was observed in November. In December and January floods of up to 15m³/s were measured. With 36m³/s the biggest flow occurred in February. This equals a water yield of 0.211 m³/s*km². The hydrographs of all these events show the typical characteristics for floods in semi-arid environments. The fast rise of the water table is followed by a steep recession curve. After a few hours, runoff has nearly fallen to base flow. A number of multiple peak events with runoff peaks following each other in short time over 2-4 days up to a week were also observed.

Table 4.2: The five biggest floods in peak discharge.

	Start	Stop	Peak [m³/s]	Vol. [m³]	Vol [mm]	Rain [mm]	Coef.
1	24-Feb-03	27-Feb-03	36	1,735,700	10.21	65.65	0.16
2	19-Feb-03	22-Feb-03	18.6	834,500	4.91	87.97	0.06
3	4-Feb-03	5-Feb-03	13.93	223,560	1.32	13.09	0.10
4	17-Dec-02	21-Dec-02	13.6	339,840	2.00	39.98	0.05
5	24-Mar-03	27-Mar-03	10.72	500,760	2.95	82.45	0.04

The wide range of runoff coefficients can be explained with different soil moisture contents. The floods with low coefficients all occurred after a period of consecutive dry days with no initial soil moisture. The two floods with high runoff coefficients of 0.10 and 0.16 took place during rainy days, with higher antecedent soil moisture.

4.7.3 The Merhavia and Shizafim subbasin

This 6.4km² large section of the Nahal Harod is not representative for the whole basin. Unlike the Nahal Harod in the Merhavia sub-basin no flat valley bottom is found. It is a part of the western edge and consists out of steeper hill slopes. The landuse also differs significantly. 15% of the surface is sealed. The rest is mainly agricultural fields and orchards. In the hydrological year 2002/2003 two large floods were observed. On November the 5th peak flow reached 28,79m³/s and on February the 24th it reached 30,9m³/s. Runoff coefficients for this two events range from 0.19 to 0.15.

The 31.9km² large Shizafim subbasin has less than 3% sealed surface. 22% of the subbasin is Mediterranean scrubland and 75% are agricultural fields and orchards. It differs from the whole Nahal Harod also through the higher mean slope. On November the 5th the largest flood of the hydrological year 2002/2003 was measured. Peak flow with 5.52m³/s is smaller than for the Merhavia subbasin.

4.7.4 Transmission losses

Due to the artificial and compacted, in places even concreted riverbed, large transmission losses should not take place. Floods do not leave the main channel, so no overland flow with resulting additional water loss occurs. However, the hydrographs of the flood event on November the 5th give evidence to losses along the stream channel (fig. 4.6). After strong rainfall over the settlement of Affula, 28,79m³/s peak flow was measured at the Merhavia runoff gauge. 0nly 4.34m³/s were observed at the Nahal Harod catchment's outlet.

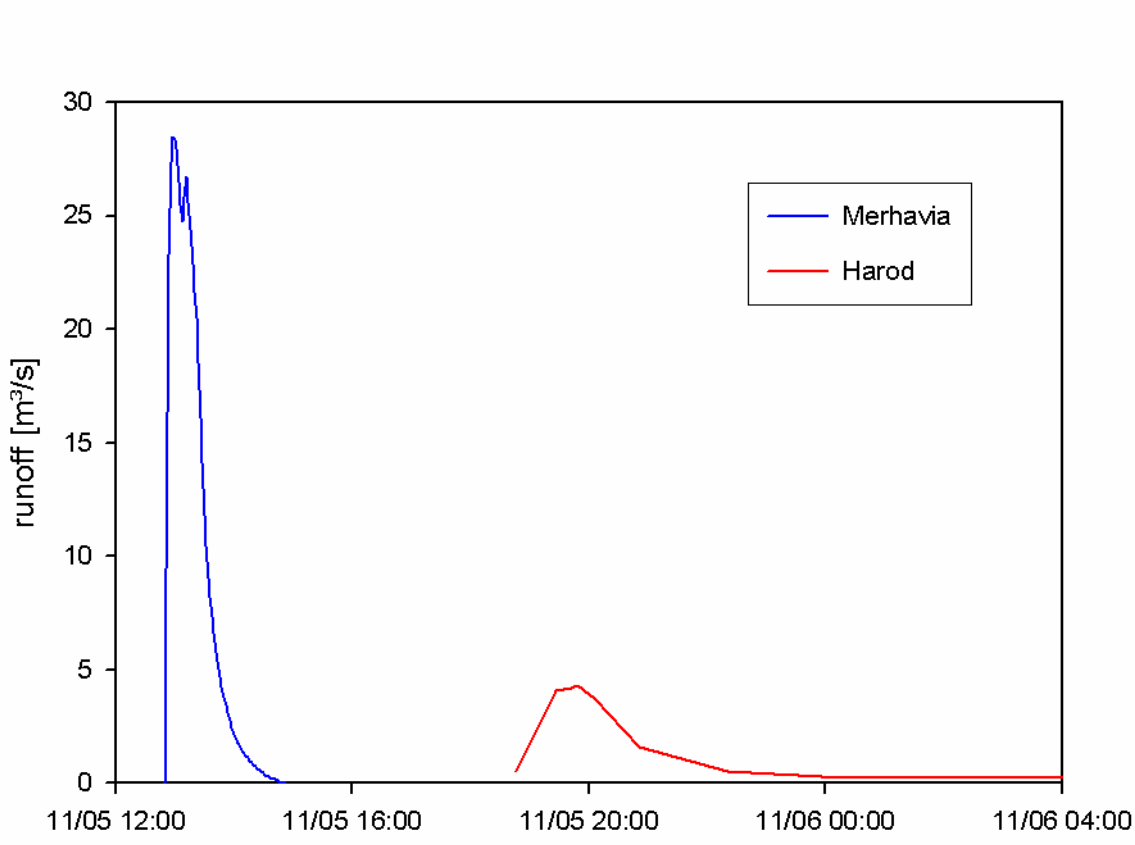

Figure 4.6: The Nov. 5th flood event at the Merhavia and Nahal Harod gauge.

The decrease of runoff volume was not so significant. The channel between these two gauges has a length of 24km. Travel time of the wave is a little over six hours, so the average speed of the wave is 1.1 m/s. The upper parts of the stream channel were completely dry before the event. Base flow originates from the fishponds in the lower parts of the basin. Therefore an amount of water is lost through wetting, a small part is lost through evaporation and another infiltrates into the riverbed. Exact information on the properties of the river bed for an estimation of transmission losses was not available. No further event to affirm the observed transmission losses was found. In hydrological year 2002/2003 no other observed flood only took place in the Merhavia or Shizafim subbasin. A calculation of transmission losses by simply subtracting the measured

runoff at the Nahal Harod station from the observed runoff at Merhavia or Shizafim therefore was not possible. The observed flood events all had contributing areas outside of one of the two subbasins, so flood waves grew in size and volume on their way from the gauged subbasins to the Nahal Harod catchment's outlet.

In chapter 8.1.2 inconsistencies in the runoff data from the Merhavia and Shizafim gauge are shown. The data is invalid and will not be used for this work. Nevertheless, the figure 4.6 and noted runoff measurements above was not erased. The approach used to estimate transmission losses prior to a model application should always be done, when runoff data from subbasins is available.

4.7.5 Water Balance

Throughout the Mediterranean region the water balance is negative most of the year. Potential evaporation normally exceeds rainfall. In case of the Nahal Harod additional water fluxes besides rainfall and runoff have to be considered. Spring discharge provides water the whole year. The karstic springs are located on the southern shoulder of the valley. The difficulty of delineating the basin of springs in a karstic environment is a known fact (Dreybrodt, 1988). However, it is definite that the Nahal Harod is not the main contributor of these springs, due to the location of the springs near the catchment's border. Runoff probably is fed by a large aquifer under the higher West Bank. The spring discharge supplies the fishponds. From the open water surfaces large amounts of water are lost through evaporation. To draw the complete water balance these losses have to be quantified. Other terms of the balance are evaporation from bare surfaces and transpiration, rainfall, storm runoff and base flow. As already mentioned, the continuous base flow is the sewage of the fishponds.

4.8 Conclusion

The Nahal Harod is a meso scale semi-arid basin. It is situated in the Lower Jordan River catchment. The climate is Mediterranean with a hot and dry summer followed by a cool and rainy winter. The present soil types are typical for the Mediterranean environment. Clay rich Vertisols in the valley basin and Terra Rossas on the karstic valley shoulders cover most part of the basin. Besides these common characteristics, some particularities of the Nahal Harod have to be taken into account during modeling. 3% of the surface is sealed and 4% is occupied by fishponds. A large amount of water is lost from the open water surface through evaporation. Spring discharge maintains the fishponds. The vast and very flat valley bottom is the biggest geomorphologic unit. Floods occur only during winter months after high intensity rainfall events.

V. Methodology

5.1 Penman equation for evaporation

The evaporation from the fishponds is a major part of the water balance and has to be quantified. Therefore Penman's formula for evaporation from open water surfaces is used. This physically based method takes atmospheric and thermodynamic parameters into account. Radiation, temperature, wind speed and relative humidity set the base for Penman's calculation (Schrödter 1985). All values used in the equation can be calculated from these meteorological data. The further development of this formula, the Penman-Montheith-equation for the calculation of evapotranspiration is standard in most rainfall-runoff models today.

$$E = \frac{mR_n + \rho_a c_p C_{at} \delta e}{\lambda_v (m + \gamma)} \qquad \textbf{(eq. 5.1)}$$

m = Slope of the saturation vapor pressure curve (Pa K^{-1})
R_n = Net irradiance (W m^{-2})
ρ_a = density of air (kg m^{-3})
c_p = heat capacity of air (J kg^{-1})
C_{at} = atmospheric conductance (m s^{-1})
δe = vapor pressure deficit (Pa)
λ_v = latent heat of vaporization (J kg^{-1})
γ = psychrometric constant (Pa K^{-1})

Equation 5.1: Penman equation for evaporation (E) from an open water surface.

The obtained daily evaporation is compared with published values of the region. For the total amount of water, which is lost to the atmosphere, results have to be multiplied with the total surface of the fishponds.

5.2 The TRAIN Model

The physically-based model TRAIN (Menzel 1999) has been designed to simulate the spatial pattern of actual evapotranspiration. The distributed model includes information from comprehensive field studies of the water and energy balance. Components of the water balance can be modeled with different spatial and temporal resolution. Due to its modular structure, individual simulations of processes of the soil-vegetation-atmosphere interface, e.g. evaporation, interception and radiation balance, can be performed. The direction of theses processes modeled by TRAIN is mainly vertical (fig. 5.1).

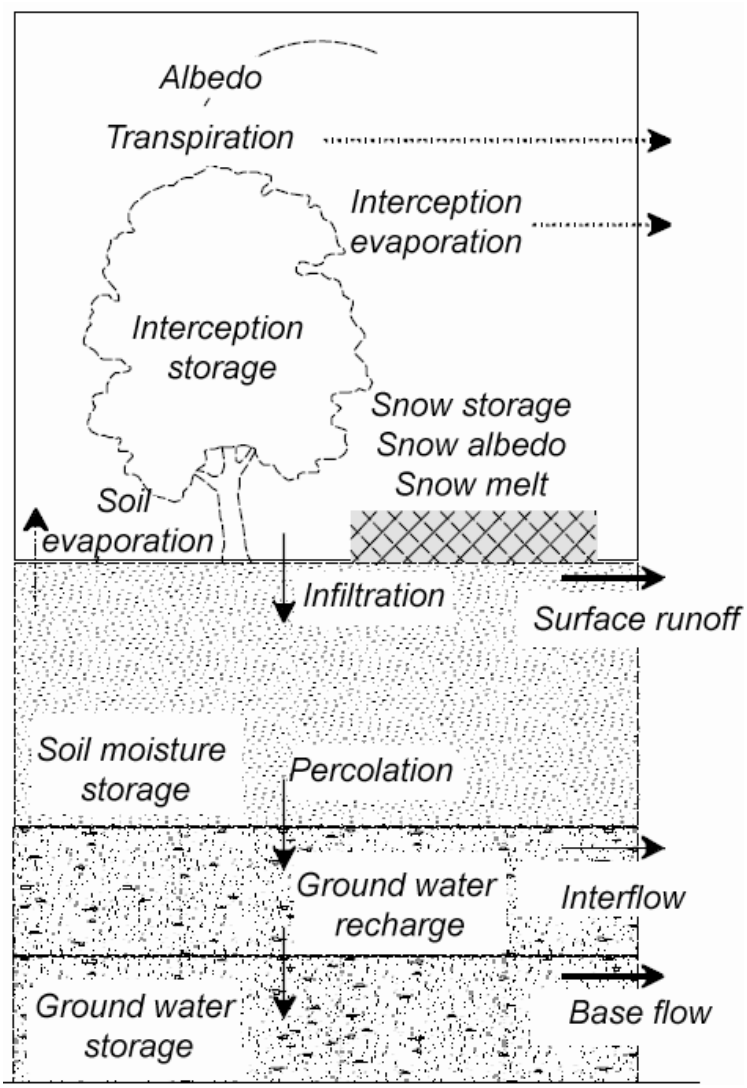

Figure 5.1: Processes simulated with the TRAIN Model

Soil moisture storage, deep percolation and evapotranspiration are components with longer term temporal fluctuations and do not vary within short time steps. The temporal resolution of one day is sufficient for good results. Spatially, the area is divided into raster cells. Evapotranspiration is calculated with the Penman-Montheith equation. Meteorological input is temperature, rainfall, relative humidity, wind speed, sunshine duration and radiation. Large study areas and area with an extent over different altitude zones are cut into different climate zones for the regionalization of this data. A soil grid and a landuse grid assign every cell a corresponding value. There are 15 land cover categories and 8 soil types in the TRAIN database to choose from. A digital elevation model is needed to calculate exposition and shade correction. TRAIN was developed for the estimation of evapotranspiration of the Swiss Alps, but has already been applied in the Jordan region. It has been validated successfully at selected sites, where continuous climate data series and information on soils and land-cover were available.

5.3 The ZIN Model

The distributed rainfall-runoff model ZIN has been developed for high magnitude floods in arid desert environment. The physically-based model originally was applied without calibration with measured runoff data, but required a number of parameters with a high spatial resolution. This data is usually not available in the catchment scale, so spatially homogenous sub-units have to be determined. Each of the three modules of the model is lumped in a different way (fig 5.2): For runoff generation, sub-units with different terrain types have to be outlined. Subbasins are the spatial unit for runoff concentration. The channel is subdivided into segments for channel routing and for the modeling of transmission losses. A short description of each module is given in the following chapters. For detailed description see Lange (1999). The model was first applied in the Nahal-Zin but has also proved its functionality in other regions and for other purposes (e.g. application in a small hyper arid catchment (Thormählen 2003), in the Kuiseb catchment in Namibia (Lange 2005 and Leistert 2005) and for urban hydrology in dry karst areas (Leibundgut et al. 2003)

.

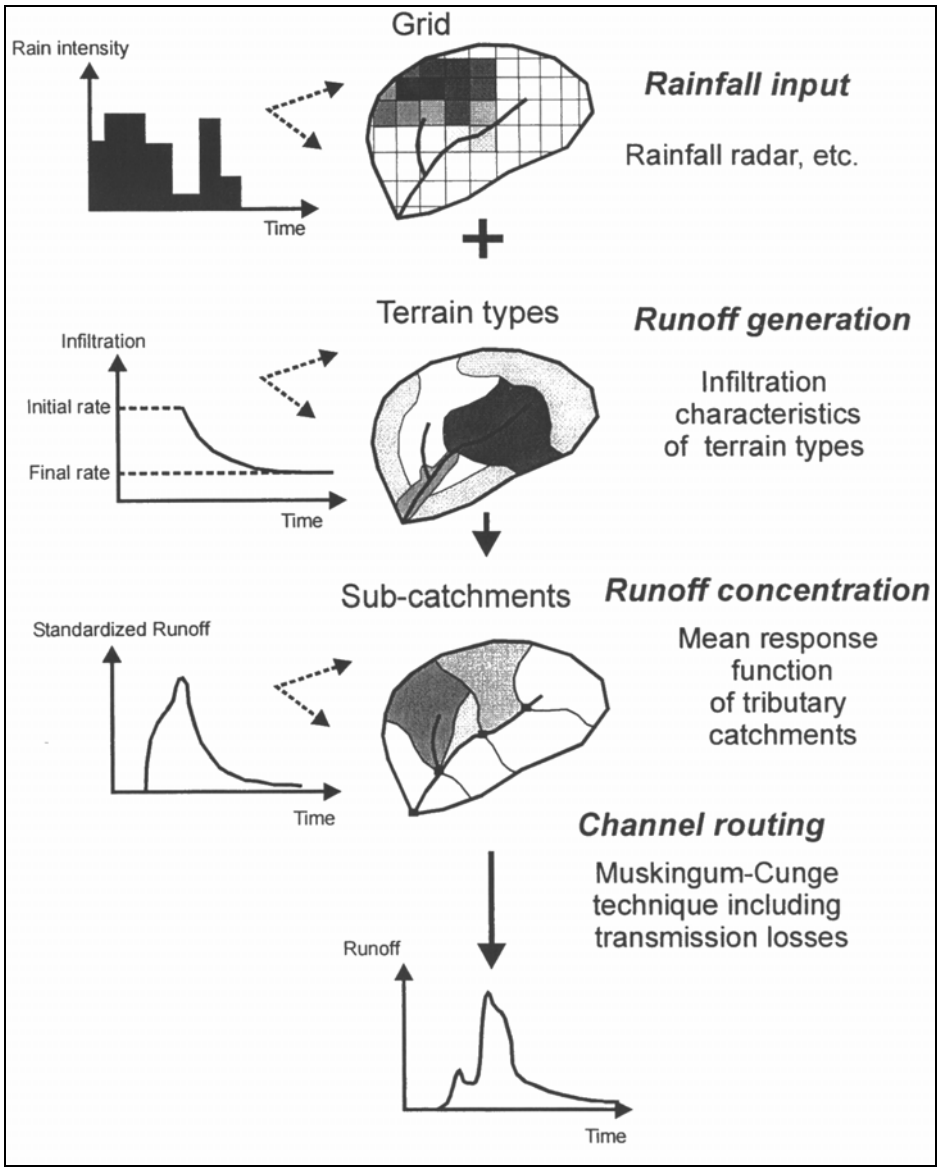

Figure 5.2: Flowchart of the ZIN Model (Lange 1999)

5.2.1 Runoff generation

Precipitation input are spatial and temporal distributed rainfall intensities derived from rainfall radar. The high initial infiltration rate declines to a constant rate which equals the saturated hydraulic conductivity. To represent this behavior, an initial loss is subtracted for each terrain type. After this amount is reached, rainfall intensities higher than the constant final infiltration rate of the terrain type generate Hortonian overland flow. Lower intensities are added to the soil storage, and may eventually generate overland flow when saturation will be reached. Soil storage is emptied by a constant evaporation and a constant deep infiltration.

5.2.2 Runoff concentration

Model elements for the runoff concentration routine are subbasins. These units are delineated by topography. The transformation of generated infiltration excess and saturation excess overland flow to channel flow is done by a mean response function. This function times the lateral runoff delivery to the channel segments and consists of a hydrological time lag and a standardized shape. For the estimation of these parameters, hydrographs of storm events from smaller catchments have to be analyzed. The size of theses catchments should be similar to the delineated subbasins, which make up the model elements for the runoff concentration routine.

5.2.3 Channel routing and transmission losses

The channel network is cut into segments according to the delineated subbasins. These channel segments are classified considering their morphological features (percentage covered by inner channels, bank-full stage, Manning n, depth of the alluvium and infiltration). The flow through the stream segments from node to node, is calculated with a distributed routing scheme. This mathematical method predicts the changing magnitude, speed and shape of flood waves as they propagate through waterways (Fread 1985). The ZIN-Model uses the MVPMC3 method (Ponce & Changanti 1994) of the Muskingum-Cunge technique. The channel segment properties slope and length together with the morphological features form the input for the channel routing. Velocity of flow in channels is estimated with the empirical formula of Manning. It relates the velocity to parameters of cross-section and slope.

$$v = \frac{1}{n} \times R_H^{2/3} \times S^{1/2} \qquad \textbf{(eq. 5.2)}$$

$$R_H = \frac{A_{CS}}{P} \qquad \textbf{(eq. 5.3)}$$

v	flow velocity [m/s]
R_H	hydraulic radius [m]
Acs	cross sectional area of flow [m²]
P	wetted perimeter [m]
S	Slope
n	Manning's coefficient of roughness

Constant infiltration rates are assigned to the channel segments to estimate the transmission losses. Leistert (2005) modified the ZIN-model by integrating the Green-Ampt infiltration model to simulate transmission losses.

5.4 Model coupling

ZIN simulates short term runoff processes and TRAIN models longer term fluxes. The combination leads to an improved simultaneous modeling of processes with a different temporal and spatial scale. The resolution of the calculation can be adjusted flexibly to data availability. During times of rain, ZIN describes the filling of the soil storage and runoff generation in time steps of minutes. Runoff concentration and routing can be conducted in even smaller time steps. During dry and rainy days, TRAIN calculates the emptying of the soil storage by evapotranspiration and deep percolation. With time steps of one day it provides the missing long term simulation of soil moisture to ZIN. Hence antecedent soil water content plays a vital role in runoff generation in semi-arid environments ZIN requires this information for the simulation of longer periods.

The structure of a model coupling is characterized by the interface between the models and by their spatial and temporal resolution. Gunkel (2006) realized the coupling by using the soil module as the main interface between TRAIN and ZIN (fig. 5.3). Although the models are not directly linked through an iterative solution, a tight coupling was achieved. The models are not run parallel, but successively. TRAIN passes the values of one day of simulation to ZIN, which, in the case of rainfall, then starts its calculation for the same day in shorter time steps. Daily values of evaporation are converted into values for the ZIN time steps considering the hourly radiation and rainfall. ZIN uses the passed-on soil moisture content as initial moisture for its calculations. In this way, feedback and exchange between the models is done in real-time.

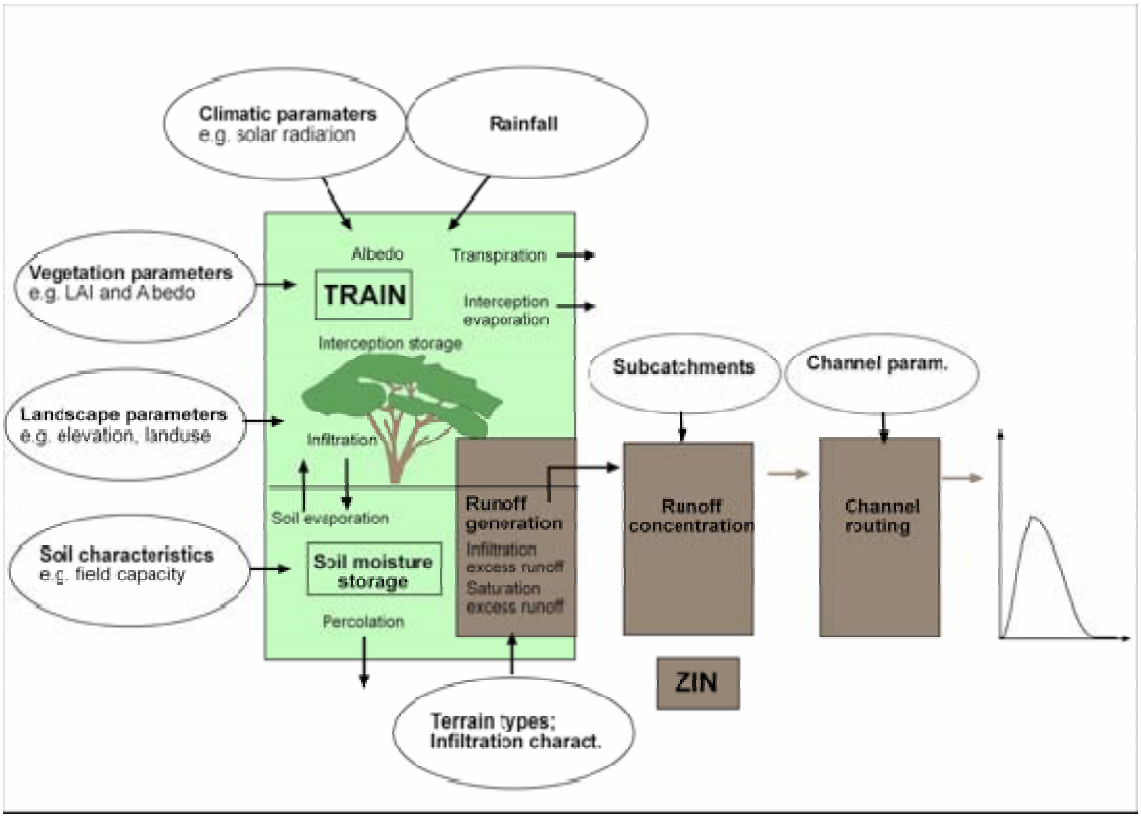

Figure 5.3: The TRAIN-ZIN Coupling (Gunkel 2006)

Both models were written in different programming languages. Therefore, a solution which allows the different codes to run parallel had to be found. The TRAIN code is written in FORTRAN77 and ZIN is available in C++. With the help of special software the TRAIN code can be run in a C++ environment. The connection was made without major modifications in the cores of each model.

5.5 First application

A first application of the coupled model was accomplished by Schütz (2006). TRAIN-ZIN was successfully applied to a micro scale catchment in the foothills of the Judean Mountains. Steinmann et al. (2003) investigated runoff generation processes of semi-arid environments with tracerhydrological and hydrometric techniques in this catchment, so a comprehensive data base existed. For the 1.1km² large basin, detailed meteorological data and runoff data were available. With TDR sensors, the soil moisture content was measured continuously at two sights. Soil samples, infiltration tests and an accurate mapping of the different soil and surface types enabled Schütz (2006) to apply the TRAIN-ZIN without calibration. Two new model routines were integrated, a function describing deep infiltration and the conceptual catchment storage model CaStor. The model produced acceptable simulations and functionality was proven. The deviation between the simulated and observed hydrographs showed the difficulty to reproduce runoff events with hydrological models without calibration. The necessary high spatial resolution of input parameters can hardly be achieved.

5.5.1 Percolation module

In the original ZIN version deep percolation was quantified with a constant value. The new routine simulates water losses through deep percolation with a dynamical function based on van-Genuchten (1980). The unsaturated hydraulic conductivity is determined as a function of the actual soil moisture.

$$\frac{K(\Theta)}{K_S} = \left(\frac{\Theta - \Theta_r}{\phi - \Theta_r}\right)^{1/2} \left\{1 - \left[1 - \left(\frac{\Theta - \Theta_r}{\phi - \Theta_r}\right)^{1/m}\right]^m\right\}^2 \quad \textbf{(eq. 5.4)}$$

$$m = \frac{\lambda}{\lambda + 1} \quad \textbf{(eq. 5.5)}$$

$K(\Theta)$	unsaturated hydraulic conductivity [cm/h]
K_S	saturated hydraulic conductivity [cm/h]
Θ	soil water content (volume fraction)
Θ_r	residual water content (volume fraction)
ϕ	porosity (volume fraction)
λ	Brook-Corey pore-size distribution index

The Brook-Corey pore-size distribution index and the residual water content are determined with empirical functions of the pore size distribution. In Rawls et al. (1992) these parameters are listed for the most common texture classes.

5.5.2 Conceptional catchment storage model

In the model, the soil storage controls saturation and the generation of saturation excess overland flow of each model unit. To integrate the already mentioned runon-runoff process a second soil storage was defined. This second catchment storage (CaStor 2) receives water through rainfall and additionally through generated runoff from the cells above. The soil storage of the upper parts of the slopes is represented through CaStor 1, which only receive water from rainfall. The CaStor 2 reservoir was applied for cells in the valley, close to the stream channel and at the foot of slopes. Runoff generated upslope entered the storage and first after its saturation, runoff was passed to the next cell and eventually to the stream channel. With this routine the small scale runon-runoff processes in pockets of soil on a bare slope cannot be simulated but retention of deeper soils in the valley can be considered. The observed higher threshold of rain and the delay of runoff and channel flow can now be simulated more adequately.

5.6 Modifications

5.6.1 Radar

The first application of the coupled model (Schütz 2006) was run with a uniform rainfall input. For the small basin with an extant of the 1.1km² this generalization already showed a significant inaccuracy. For the simulation of a meso scale catchment rainfall radar with a high spatial and temporal resolution has to be used. In the original ZIN Model this was already integrated. For the TRAIN Model the rainfall amount in time steps of five minutes, derived from the radar data had to be summarized to daily values. This time-consuming calculation was only made for the first model run. For further simulations the daily rainfall amounts from the first run were read in by the TRAIN Model and did not have to be determined again.

5.6.2 Runoff concentration routine

In the ZIN-model generated runoff is transformed to stream flow by a mean response function. To set up the equation, hydrographs from basins similar to the delineated subbasins have to be analyzed. A time lag and standardized shape is to be determined. The Nahal Harod was separated into 110 subbasins. The area of these units range from 0.04 to 6.5 km² and the slope varies between 0.003 and 0.19. Runoff concentration acquired from a single mean response function does not seem to be adequate for model elements with such a wide range of size, shape and slope. To overcome this problem, a Gaussian distribution to transform the runoff into stream flow was set up for every subbasin. With the help of this equation, generated runoff was distributed over a number of time steps. In bigger subbasins, generated runoff needs more time to reach the channel. The number of time steps and the two parameters, arithmetic mean and standard deviation for the adjustment of the distribution had to be determined for every element.

$$N = \frac{A_{SUB}}{QC \times S} \quad \textbf{(eq. 5.6)}$$

N	Number of time Steps
A_{SUB}	Area of the subbasin
QC	Parameter for Runoff Concentration
S	Slopegroup

The parameter QC was subject to calibration. From first model runs with a constant delay good results were obtained with 25 time steps of 5 minutes or two 2.05h of concentration time. Five minute time steps for the ZIN model were used for this work. As a starting value for calibration, QC was chosen so that the average number of time steps for the 110 model elements was 25.
The influence of the slope on runoff generation was included through a slope factor. Fig. 5.4 shows the distribution of the slope of the 110 subbasins. Three groups were outlined. Over 50% of the subbasins belong to the first group with less than 0.026 of decline. They are all situated in the vast and flat valley bottom. Members of the second group with intermediate slopes are mainly in the western part of the catchment. The subbasins of the third group with slopes of up to 0.17 lie in the steep shoulder up to the West Bank. The assumption that runoff in these units reaches the channel three times faster than in the flat subbasins does not underlie any measured data, but seemed to be plausible and was verified during calibration.

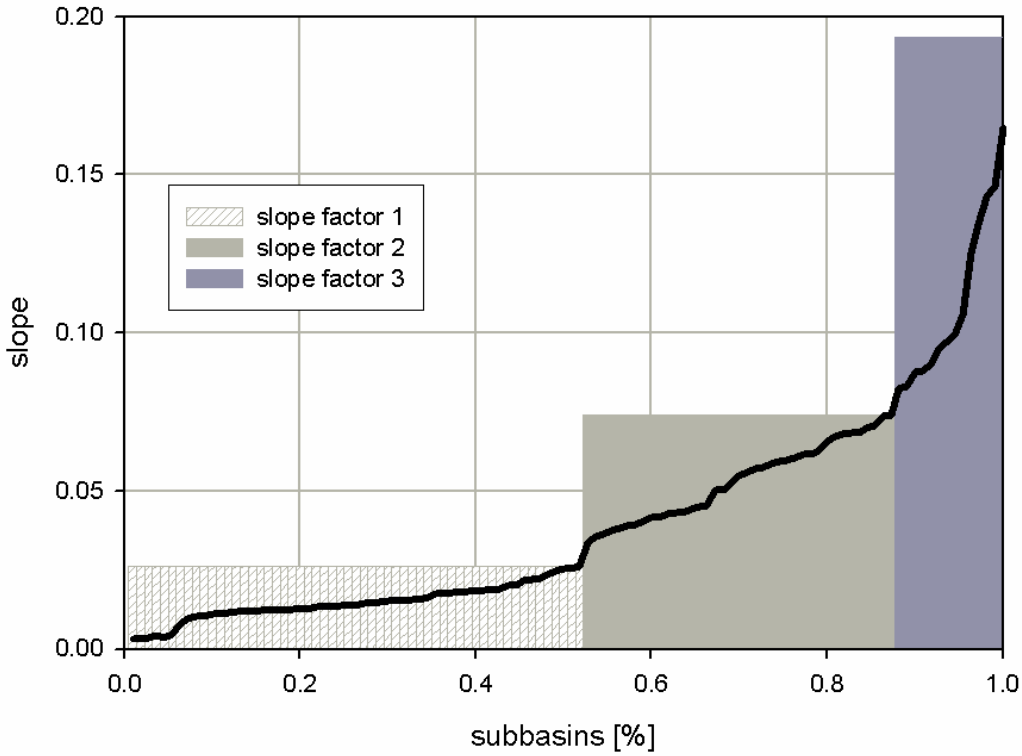

Figure 5.4: Slope of the 110 subbasins

The arithmetic mean marks the peak of the Gaussian distribution. Since a symmetric distribution with no skewness was assumed the arithmetic mean equals the mode and the median. At this time the relative biggest part of generated runoff reaches the stream. The arithmetic mean for each subbasin was predefined as μ=N/2, so the peak of the Gaussian distribution passed in half of the total concentration time.

$$F(x) = \frac{1}{\sigma\sqrt{2\pi}} \cdot \int_{-\infty}^{x} \exp\left[\frac{(x-\mu)}{2\sigma^2}\right] dx \quad \textbf{(eq. 5.7)}$$

x	time steps
μ	arithmetic mean
σ	standard deviation

The standard deviation determines the shape of the normal distribution. About 68% of values drawn from a standard normal distribution are within one standard deviation from the mean and about 95% of the values are within two standard deviations. It was set to σ= N/4. For a subbasin with a calculated total runoff concentration time of 50 time steps, an arithmetic mean of 25 and a standard deviation of 12.5, 68% of the generated runoff would reach the stream in between the 12^{th} and 38^{th} time step.

5.7 Conclusion

Through the coupling of the physical-based rainfall-runoff model ZIN with the evapotranspiration model TRAIN, a flexible hydrological tool was built. Processes with a different spatial and temporal resolution can be modeled simultaneously. ZIN is able to simulate the flashy floods of semi-arid environments in small time steps and TRAIN determines the daily water loss through evaporation, transpiration and deep percolation. With the integrated van-Genuchten equation for the simulation of water loss through deep percolation, and the estimation of evaporation and transpiration, the soil content can be simulated continuously. In this way, runoff in semi-arid environments can also be modeled for longer time periods with the event model ZIN. For applications of the coupled model to meso scale catchments two further modifications were implemented. With rainfall-radar, precipitation-input enters the model in a high spatial and temporal resolution. A newly integrated method estimates runoff concentration considering the size and the slope of each subbasin.

VI. Parameterization

6.1 Radar

The C-band radar system is located at Ben-Gurion International Airport, Tel Aviv. The distance to the center of the Nahal Harod catchment is 80km. Radar data resolution is 5 min in time and 1.4° x 1km in space with radar scans at several elevation angles. With an ARC-Workstation, polygons with rain intensities for every time step were derived. In the study area the polygons have an extension of about 1800x1000m². Rain intensities are a function of radar reflectivity. For quantitative precipitation estimation, the calculated rainfall-intensities have to be corrected. Huebner (1985) summarizes possible disturbances of the reflection signal. Absorption and reflection depend on the condition of aggregation of the water drops. In mountainous regions, two effects have to be considered: Signal contamination by ground clutter and beam blockage. To overcome this annoyance, radar with higher elevation angles is used. The radar beam then has a clear sight but might not detect surface-near clouds and precipitation events. Morin & Gabella (2006) conducted quantitative precipitation estimations with the radar data from Ben-Gurion Airport. Radar data was adjusted by correlating it to rainfall gauge measurements with two different methods: A 1-coefficient bulk-adjustment and a 4-coefficient weighted multiple regression. The adjustment coefficients were derived for twenty-eight storms using 60 independent gauges. Results were validated with an independent data set of gauges located in eleven 20x20km² validation areas. For his diploma thesis, Wiesendanger (2007) corrected this data for the entire Lower Jordan River Catchment with 90 rainfall gauges for every precipitation event of the rainfall season 1991/1992. Unfortunately the corrected data for the rainfall season 2002/2003 was not available for this work and is still to be generated. For model input the data set from Morin was used. This data was adjusted with rainfall events among others with storms of the 2002/2003 season. A high accuracy can be expected, hence the Nahal Harod lies in one of the eleven validation areas.

The polygons were converted into grids, and to minimize computation time, were cut to the extent of the Nahal Harod basin. Time steps with no rain were extracted and rain intensities were converted into rainfall amounts. For the TRAIN Model daily sum grids were generated (fig. 6.1). The ZIN model reads in all data sets during precipitation events. For the calculation of total rainfall and runoff coefficients, cell values were summarized to an amount for the whole catchment and for the subbasins Merhavia and Shizafim.

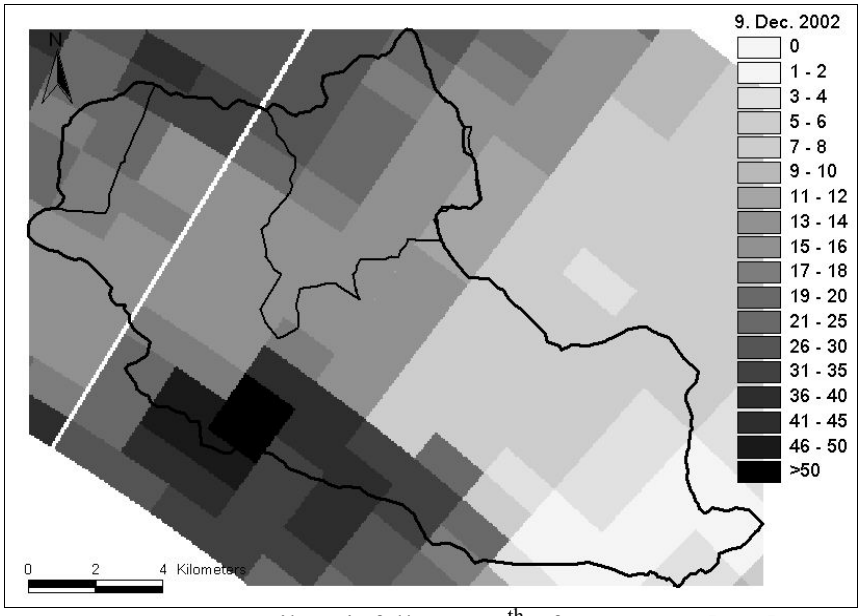

Figure 6.1: Daily rainfall map, 9th of Dec. 2002 [mm]

Daily rainfall maps for of all simulated events can be found the appendix.

6.2 Parameters for the TRAIN Model

The TRAIN Model requires climate data and geographical information on landuse, soils and altitude. The daily value of temperature, relative humidity, wind speed, and sunshine duration mark the meteorological input (table 6.1). The relative sunshine duration is additionally connected to hourly radiation data to insert a quantitative energy value into the model.

Table 6.1: climate data from the station Gilboa

Year	Month	Day	T [°C]	rH [%]	u [m/s]	SSD
2002	10	1	30.87	0.43	5.72	0.74
2002	10	2	27.48	0.55	6.01	0.58
...	...	...	...	...	...	...

Since the Nahal Harod is a mainly even and uniform basin data from only one meteorological station was used and no further regionalization procedures were applied. The Gilboa meteorological station is situated in the valley bottom (fig. 7.2)

The geographical information is stored in a grid. The catchment was divided into 142,899 cells of 50x50m² in 427 columns and 327 rows. The landuse grid was created out of the landuse map and an analysis of a satellite image. Each cell was assigned to one of the 15 land-cover classes of the TRAIN database. The soil grid with the nine possible soil classes out of the database was generated with the soil map.

6.3 Parameters for the ZIN Model

6.3.1 Input for the runoff generation module

Grid files read in by the ZIN Model had the same spatial resolution as the TRAIN grids. A soil grid with a corresponding soil properties table constitutes the input for the runoff generation module. The grid differs from the soil data needed for the TRAIN Model. Hence the ZIN Model does not need information on plant parameters, no landuse grid is required. The land-cover class settlement and the class fishpond were a different class in the ZIN soil map with altogether 8 soil types.

Infiltration capacity, initial loss, soil depth and effective porosity are very sensitive parameters and were subject to the calibration process. With the very high values for the soil type *fishponds,* it was achieved that these ponds did not play any role in runoff generation and their surface did not contribute to floods as explained in chapter 4.5.

Table 6.2: Soil properties (starting point of the calibration process.)

	Soilnr	infCap [mm/h]	initLoss [mm/h]	soilDepth [m]	Poreff [/]
Pelosol	1	12	45	4	0.5
Vertisol	2	12	45	4	0.5
Terra Rossa	3	43	10	1	0.46
Regosol	4	61	10	1.5	0.4
Rendzina	5	30	10	2	0.4
Xerosol	6	65	10	1	0.35
Fishponds	7	1000	1000	10	1
Settlement	8	5	5	0.25	0.3

Starting point of the calibration process and input of the first model run were infiltration rates taken from literature (e.g. Agassi et al. 1985, Cerda 1997, Duiker et al. 2001, Scoging & Thornes 1979). Due to the complexity of factors influencing infiltration and their high variability, a wide range of infiltration rates for the same soil types has been published. Therefore, no exact values from a single source were considered, but an average from various publications.

The capacity of the soil storage was determined with the porosity and the soil depth. For the calculation of the unsaturated hydraulic conductivity with the van-Genuchten equation further soil characteristics had to be determined. Schütz (2006) was able to estimate the parameters wilting point, field capacity and saturated hydraulic conductivity with grain size distributions of the soil samples. The SPAW hydraulic properties calculator (Saxton 1986) estimates saturated conductivity and water holding capability based on the soil texture, organic matter and gravel content. The equations of this tool are derived from statistical analysis of over 2000 soil samples from the USDA/NRCS National Soil Characterization data base. For this study, no soil samples were taken and the soil water characteristics had to be taken from literature (e. g. Battikhi 1983, Berndtsson 1987, Duiker et al. 2001). Not all the soil water characteristics for the different types of soils were found. Therefore published grain size distributions were used to calculate the missing soil water characteristics with the

SPAW calculator. The complete soil properties table with the values from calibration and the determined soil water characteristics can be found in appendix (tab. 12.1, tab. 12.2).

An estimation of the initial moisture of the soil had to be made for the simulation of single events. For events without rainfall in previous days it was set to zero and for runoff following a wet period it was subject to calibration. Soil water content is modeled by TRAIN-ZIN, so for the simulation of the whole season, the initial moisture was set to zero at the beginning of the wet season and did not need further calibration.

6.3.2 Input for the runoff concentration module

The Nahal Harod was divided into 110 sub-basins. Each sub-basin contains one channel segment. Due to the very low slope of the major part of the terrain the division could not only be done with the DEM as usual. Additionally, the satellite image had to be considered.

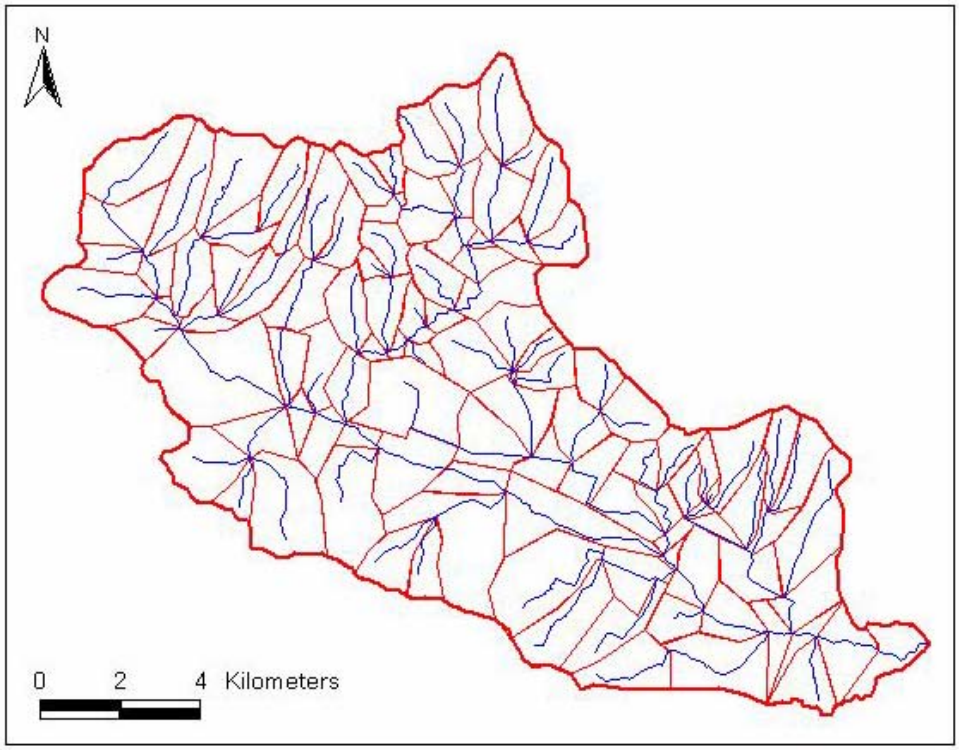

Figure 6.2: Sub-basins and stream network

In the flat bottom of the valley, model units often just are a field and its draining trench. These artificial subbasins mostly are delineated by a road or a track cart. The parameter QC for the calculation of the time steps needed for the runoff concentration was determined through calibration of the first model runs and then kept unchanged for further simulations.

6.3.3 Input for the routing module

The 110 channel segments were divided into five groups with similar characteristics. In the channel properties table, values of the slope, length, and width were summarized together with the channel type of each segment. The length of the channel segments could be determined quite accurately in a GIS. The width of the channel was measured in the satellite image with a resolution of 0.8x0.8m². For smaller channel segments with widths of less than two meters no exact measurement was possible. For a more precise slope the altitude difference between the beginning and the end of a segment was identified analyzing the digitalized contour lines. The DEM with a horizontal resolution of 50x50m² was not suitable for this task.

Table 6.3: channel properties.

Segment	LastSeg	NextSeg	Trib1	Trib2	Slope	Length	Width	Type
1	0	2	0	0	0.0389	2491	10	2
2	1	5	0	0	0.0124	1611	11	1
…	…	…	…	…	…	…	…	…
110	109	0	0	0	0.0153	1564	20	1

Table 6.3 is an extract of the whole channel properties table, which can be found in the appendix. The Muskingum-Cunge method of the channel routing needs the numeration of the channel segments to pass the calculated runoff from one segment to the next one. A channel segment receives water from the unit above and eventually from up to two tributaries. Further information on the channel segments was summarized in the description of the five groups. The parameters of these groups are Manning's roughness, depth of the full channel, percentage of the inner channel of the whole riverbed and depth of the alluvium. A single value counted for every segment of each group.
In Chow (1959) the Manning coefficient of roughness is listed for different channel types. Photographs of channel cross-sections help to select matching values. According to Azmon (1992), who studied the Manning coefficients along the Soreq stream in Israel, the determination of the coefficient with tables in the hydrological literature is problematic. For long reaches, the application of published coefficients is sufficient, while for specified cross-sections, it is not advisable.

Table 6.4: Channel types with similar characteristics

	1	2	3	4	5
Manning's n	0.029	0.042	0.055	0.045	0.09
% of the inner channel	0.70	0.60	0.75	0.30	0.20
Depth [m]	3.5	2	1.5	0.4	2.5

channel type 1: main channel, channel type 2: tributary channel, channel type 3: trenches along agricultural fields, channel type 4: furrow on agricultural fields, channel type 5: steep canyons of the valley shoulders

The depth of channel segments was estimated on the basis of photographs. The percentage of the inner channel of the whole riverbed also was derived from these images. This parameter is important for the modeling of ephemeral streams, where over bank flow takes place during floods. For the Nahal Harod it was not significant. Since transmission losses were not modeled, the parameter depth of the alluvium played no

role for the simulation. The determined channel characteristics were not changed during simulation and were not subject to calibration.

6.4 Sensitivity runs with artificial rainfall

After the determination of the input data, model runs with an artificial uniform rainfall impulse were conducted. Functionality of the sub routines was checked. Routing correctly passed the generated runoff from segment to segment. The new runoff concentration routine incorporated the size and the slope of the subbasins in the transformation from generated runoff to channel flow. Results showed that no water left or entered the system besides the modeled fluxes and mass conversation is obtained. The sensitivity of model parameters was tested. Changes on specific parameters lead to expected changes in the modeled output. After the model passed this examination, first runs with actual rainfall data could be carried out.

6.5 Conclusion

Parameters for the physically-based model cannot be measured in an adequate resolution for a meso-scale basin. Generalization of point-measurements, remote-sensing, and published data from similar environments were used to form the model input of the Nahal Harod. With the help of a GIS this data was processed and several grid files were prepared. Channel properties were determined through photographs. The data preparation of the rainfall radar included the conversion from intensities into rainfall amounts and the transformation in ASCII grids with the help of an Arc workstation. Meteorological time series were taken form the Gilboa station. No field trip to view the study area personally was taken and this work is totally depended on published data and remote sensing. General functionality of the model and of the input data was tested in model runs with artificial rainfall.

VII. Water balance

The annual rainfall and spring discharge are listed on the positive side of the annual water balance. For the hydrological year 2002/2003 rainfall cumulates to 580.4mm. This equals a total volume of 98.67×10^6 m³. The real number of springs in the Nahal Harod and the total volume of spring discharge are unknown. For six important springs monthly discharge data is available. Fig. 7.1 shows a nearly constant flow throughout the year. This is an indicator for a huge aquifer and another argument for the theory that the Nahal Harod basin cannot be the only source for these springs. Total discharge volume of these six springs was 51.72×10^6 m³.

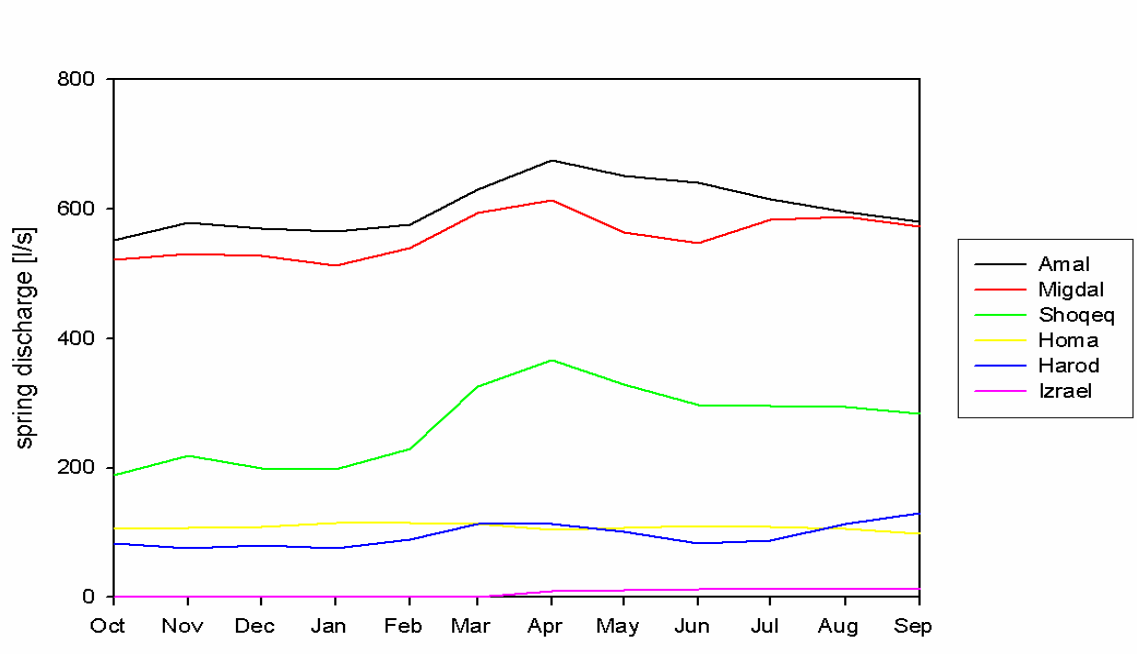

Figure 7.1: Monthly discharge of springs in the Nahal Harod basin.

The system looses water through superficial runoff, evaporation, transpiration and deep infiltration. No data on groundwater level, groundwater recharge, groundwater flow and an eventual use of groundwater is available. Superficial runoff can be divided into the storm runoff and the base flow. 13 floods between November and March were observed in the hydrological year 2002/2003. Total storm runoff volume was 3.94×10^6m³. The exact annual base flow could not be determined. The runoff time series of the Nahal Harod is incomplete. An estimation of an annual mean flow of 100l/s with 20l/s during summer and 180l/s during winter months seems appropriate. This would cumulate to a total annual volume of 5.62×10^6m³. The sewage from the fishponds forms the base flow.

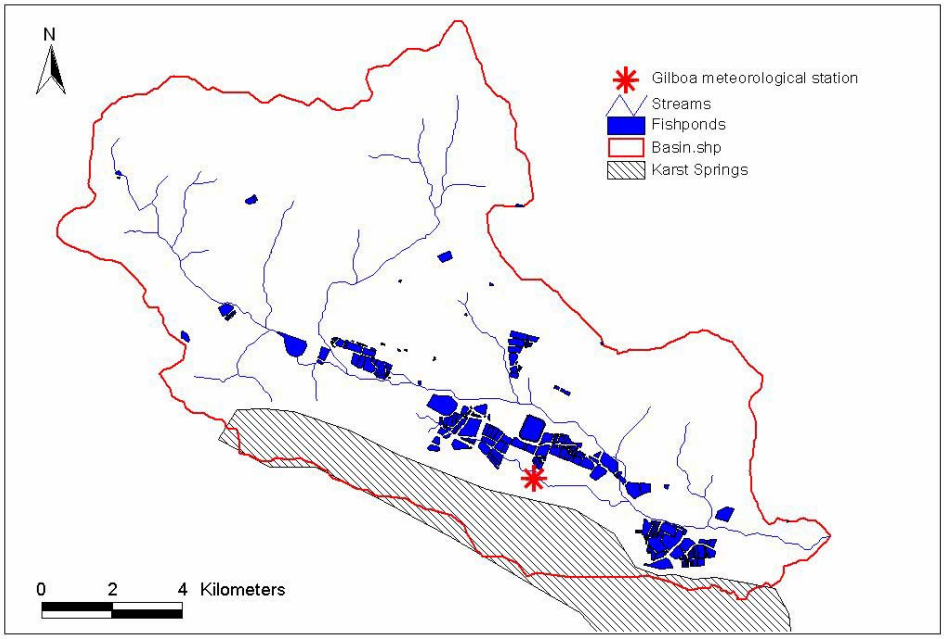

Figure 7.2: Fishponds and karst springs, Nahal Harod

The annual evaporation from these fishponds was calculated with data from the meteorological station Gilboa in the valley of Nahal Harod. With the Penman equation 1,417mm were determined for the hydrological year 2002/2003. For the total surface of all fishponds (6.94km²) a total amount of 9.82×10^6 m³ evaporated. This is equivalent to a flow of 300l/s.

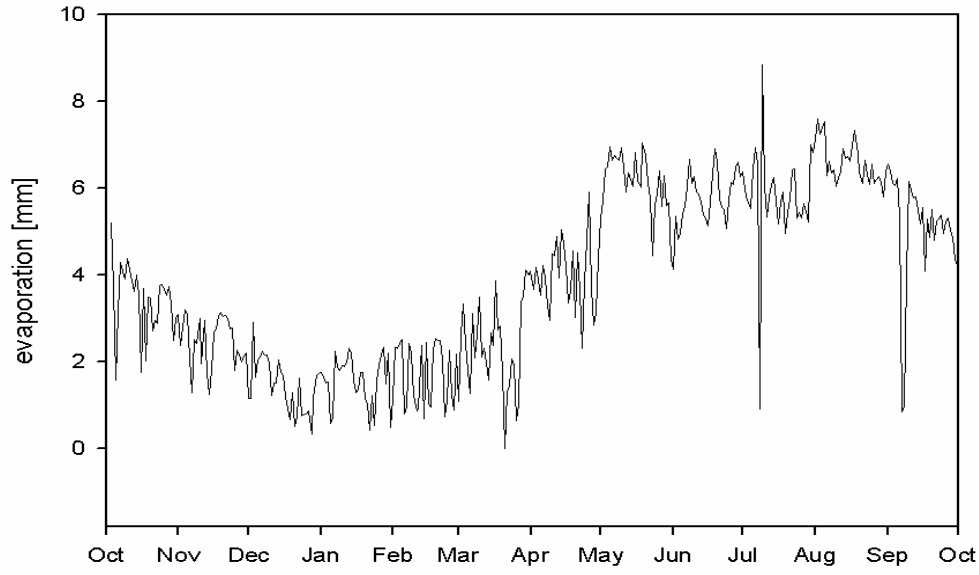

Figure 7.3: Daily potential evaporation, calculated with the Penman equation

Evaporation pan measurements in Tirat Zevi, Lower Jordan River Valley of 2,210mm annual verify the result. To adjust pan evaporation measurements to open water surfaces the values have to be multiplied by the pan coefficient of 0.7 (Goldreich 2003). 2,210mm annual evaporation equals 1,547mm open water surface evaporation. Rimmer & Gal (2003) estimated the water balance of Lake Tiberias for the period of 1968-2001.

Evaporation, calculated with the energy balance method, ranges from 1,386mm to 1,867mm. Transpiration and bare surface evaporation were not estimated. The TRAIN-ZIN Model only was applied to the months of October to March.

The water for all the fishponds is taken from the springs. Therefore it should be possible to relate the determined evaporation and the base flow with the spring discharge. The sum of the six gauged springs though is much higher than the calculated evaporation added to the measured base flow. It can only be assumed how the additional water loss arises. Transmission losses, irrigation in small private garden plots and other recreational usage might be responsible. Because the bigger springs lie near the catchment's outlet, in the base of the Jordan valley, water probable flows through tubes and artificial canals to fishponds outside the Nahal Harod basin. In the upper valley of the LJRC fishponds are quit common. Further investigation on the spring flow, its origin and its use would be necessary to determine an exact water balance, but was not part of this work. The simulated flood events had a magnitude of several m^3/s, so base flow only had a negligible small percentage. For this reason it was not taken into account during modeling.

VIII. Simulation

8.1 General aspects

8.1.1 Modeling strategy and calibration

The accuracy of model results is a function of the accuracy of the input data and the degree to which the model structure correctly represents the hydrological processes (DeVries & Hromadka 1996). For physically-based distributed models, a large amount of data is required. This data often is not available and so becomes subject to calibration. Sorooshian & Gupta (1995) define calibration as the process by which model parameters are selected so that the model closely simulates the behavior of the study site. A possible problem of deterministic models is that equal or similar simulation results can be obtained with different sets of parameter. Beven (2001) terms the ability to reproduce acceptable simulations with different parameter sets as equifinality. Therefore a parameter set should always be checked on its physical justification and compared with measured or reported values. Hence no direct measurements were conducted for this study; starting values for the calibration process were taken out of prior publications.

Because of the large number of raster cells and different parameters, model runs were computationally expensive. Automatic calibration techniques, as used for lumped models were not practicable and the model fitting had to be done with manual calibration. Through a trail-and-error process, parameters were adjusted one at a time and the simulated and observed hydrographs were visually compared after each model run. Besides the generated hydrograph for the whole Nahal Harod, it was possible to output hydrographs for the Shizafim and the Merhavia subbasin. This way the parameters for the land use class eight settlement, would have been adjusted more accurately. 15% of the Merhavia subbasin is sealed. By analyzing the estimated hydrograph of the Shizafim basin, the parameters for the Mediterranean scrubland, which makes up 22% of the subbasin would have been calibrated more detailed. Unfortunately the data from the gauges of the two subbasins did not seem to be consistent (chapter 8.1.2) and so were not used for model calibration. The possibility to adjust certain parameters by analyzing observed and simulated floods in subbasins with distinct properties might facilitate the fitting of the TRAIN-ZIN model in further applications.

From the first model runs with artificial rainfall, the sensitivity of the most important parameters was known. Before starting the calibration process some thoughts considering the order of the addressed parameters were made. After an event with mainly IEOF a second event with more SEOF was used for calibration. The simulation of a third event should have served as verification. Unfortunately two events were not sufficient for parameter determination and the third event also had to be used for calibration. The original planned model strategy had to be changed and all three events had to be simulated simultaneously for good results.

For the simulation of single events the parameter initial moisture had to be determined before running the model. To avoid the calibration of an additional open parameter, first model runs were executed for a rainfall-runoff event after a longer dry period. This way the parameter initial loss could be set to zero. The selected event implicated another advantage. Because of the short duration and the low amount of total rainfall, no SEOF is expected. Calibration therefore could focus on the parameters which influence the generation of IEOF, particularly infiltration capacity and initial loss. The value of parameter QC for runoff concentration was adjusted during these first runs.

After a good simulated hydrograph was achieved, the parameters were used to simulate a second event. The chosen event took place after several rainy days. Assuming that the soil was close to saturation, initial moisture was set to one for first simulations. With the values for infiltration capacity and initial loss from the first simulated event no satisfying results were reached. The process of SEOF was now much more important. A parameter set for good simulations of both events was found after alternating calibration of the first and the second flood.

For parameter verification a third event with again different characteristics was simulated. Since the data set did not produce a satisfactory result, a new calibration process had to be started for the third event. Even after several calibration runs a good simulation was not possible. Analyzing the results, it became clear that it would be necessary to change another parameter besides the already adjusted infiltration capacity, the initial loss and the soil depth. After the adjustment of the parameter saturated conductivity for different soil types, good results for this third event were achieved.

Now for each event good hydrographs were produced but with different parameter sets. The data set of one event lead to bad simulations for the other events. *'Good results because of wrong reasons'*. All the parameter sets withstood a check on their physical background. For further application of the model a parameter set which would fit all three events had to be found. The three events had to be calibrated simultaneously and intermediate results had to be brought into line with the other parameter sets.

For the verification of the model and the obtained soil properties a fourth event, which was not used during calibration was simulated. In the whole calibration process only the soil properties infiltration capacity, initial loss, soil depth and saturated conductivity were changed. Porosity, field capacity and wilting point were kept untouched. For runoff concentration, the parameter QC was adjusted during the first model runs. Channel characteristics for the routing and all parameters of the TRAIN model did not undergo any calibration. After a short description of event characteristics, calibration and simulation results are presented for each event in the following chapters. The presented simulated hydrographs were all obtained with the final parameter set which fitted on all events. Although better results were possible for single events, these simulations were not considered.

After the modeling of single events the calibrated TRAIN-ZIN was applied for the whole rainy season 2002/2003 lasting from October to March.

8.1.2 Inconsistencies of the Merhavia and Shizafim gauge

After the rainfall-radar was analyzed, the measured runoff from both gauges showed unexplainable inconsistencies. No runoff was measured even after major rainfall events in the subbasin. In the month of December the gauge for the Merhavia subbasin did not observe any flood event. On Dec. 9th, 20.81mm of rain fell over the area (Annex) and no runoff was observed. For the mentioned large event of Nov. 5th only 11.15mm rainfall were derived from the rainfall radar. The Shizafim gauge did not measure any runoff on Feb. 21st after a daily rainfall of 50mm and more over the whole subbasin (Annex). These are only two examples of gauge outfalls. Examples for gauge failures are given below. On November the 5th floods were observed at both stations. The Shizafim gauge measured 5.52m³/s. This was the highest peak flow of the whole season. The passage of the flood wave was described by only 3 measurements. Nevertheless the event was simulated. The calibrated model reproduced a peak flow of less than 1m³/s.

Table 8.1: measured runoff at the Shizafim gauge

time	runoff [m³/s]
05/11/2002 13:40:00	0
05/11/2002 14:13:30	5.52
05/11/2002 14:30:49	2.68
05/11/2002 14:53:20	0.66
05/11/2002 15:04:50	0

A simulation of the Merhavia subbasin with the validated model produced nearly no runoff. Measured was nearly 30m³/s. The functionality of the model for the whole Nahal Harod was proven during this work. The measured values cannot be explained. For the Merhavia subbasin an additional test was executed. All soils of the basin were assumed to be totally impermeable. Produced runoff by the model still did not exceed 3m³/s. The delineation of the Merhavia subbasin goes through the settlement of Affula. The area is flat, so uncertainties in the catchment size can be expected. However, the immense deviation of the measured and simulated hydrograph cannot be explained with the inaccuracies.

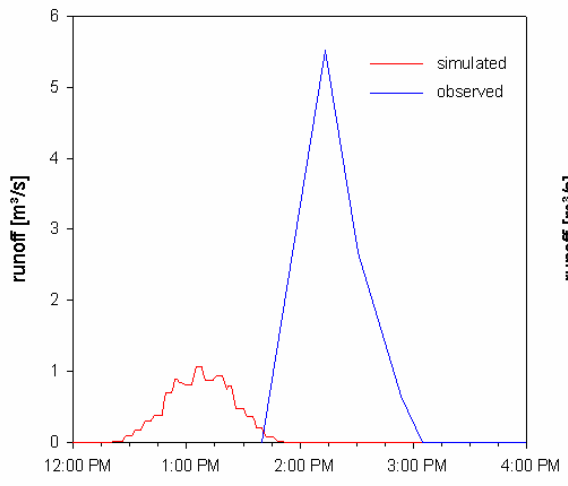

Fig. 8.1: observed and simulated runoff at the Shizafim station, Nov. 5th 2002.

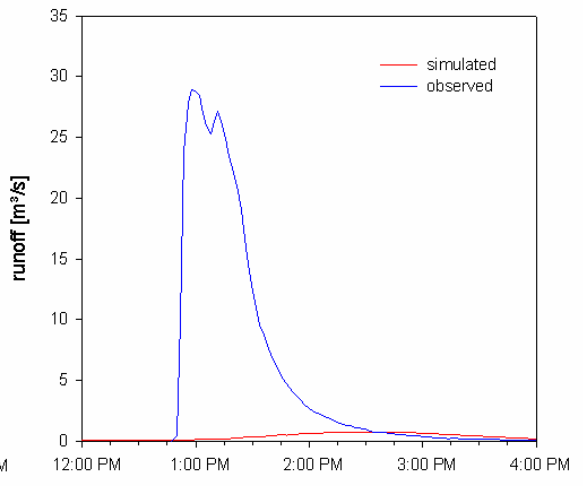

Fig. 8.2: observed and simulated runoff at the Merhavia station, Nov. 5th 2002.

Data from both gauges were unemployable for calibration and validation of the model and were not further considered in this work. The described floods and runoff characteristics of the two subbasins in the chapters 4.6.3 and 4.6.4 should not be taken into account.

8.1.3 Validation

Model performance during calibration was evaluated only by visual comparison of the observed and simulated hydrographs. Further validation of good runs was done with statistical methods. The *model efficiency* from Nash & Sutcliffe (1970) is a widely accepted method to assess the accuracy of hydrological models.

$$NS = 1 - \left(\frac{\Sigma (Q_{OBS} - Q_{SIM})^2}{\Sigma (Q_{OBS} - Q_{\overline{OBS}})^2} \right) \quad \textbf{(eq. 8.1)}$$

Q_{OBS} observed runoff [m³/s]
Q_{SIM} simulated runoff [m³/s]
$Q_{\overline{OBS}}$ mean observed runoff [m³/s]

Possible values of the dimension-less *model efficiency* range from -∞ to 1.0. A perfect model fit has a *model efficiency* of 1.0. The value of 0 indicates that with a constant value, the mean of the measured time series, a similar performance would have been obtained. Bad simulations exhibit negative *model efficiencies.*

The square deviation between simulated and measured values is used to determine the *model efficiency*. Therefore, for the simulation of runoff, peak flow with high absolute values is overrated in comparison with the simulation of low flow. Since runoff in semi-arid environments is characterized by large and flashy floods, the Nash & Sutcliffe *model efficiency* is ideal for model validation.

For model runs, which demonstrate the right magnitude and shape of flood waves, but with an error in their timing, the Nash & Sutcliffe *model efficiency* would declare a very poor performance. Therefore, additionally the volume *error* VE was determined. It specifies the deviation between measured and simulated runoff and assesses the model performance with an emphasis on total runoff volume.

$$VE = \frac{\Sigma (Q_{OBS} - Q_{SIM})}{\Sigma Q_{OBS}} \quad \text{(eq. 8.2)}$$

By dividing with the observed total runoff, the volume error is standardized and different simulations can be compared.

A good model performance can be achieved for a specific data set, e.g. one event. For the verification of the model functionality a second data set which was not used for calibration has to be tested. Therefore, a fourth event was simulated with the obtained parameter set from the calibration of the other events.

8.2 Event simulation

8.2.1 The Dec. 9th-12th Event

Event characteristics

The second runoff event of the season occurs on Dec. 9th. After 10 days without any precipitation, 16.67 mm of rain fell during the first day and another 3mm on each of the following two days. At about midnight of the first day peak runoff reached 7.2m³/s. At 4.00h in the morning a second peak of 5.3m³/s was observed. Runoff fell to the initial value in matters of hours. In the early hours of Dec. 12th another small flood wave of 0.7m³/s passed the river gauge. The total volume of the flood was 163,000m³ and the runoff coefficient of the whole event is 0.041. From the daily rainfall maps (Appendix) two major rainfall cells can be outlined. On Dec. 9th over 50mm of rain fell on the southern shoulder of the basin. The second rainfall cell was located over the north-western border of the Nahal Harod near Affula and with about 20mm of rain, less intensive than the southern cell. After the long dry period, it can be assumed that soil moisture content is very low and due to the relative low amount of total rainfall, saturation will not be reached. The generated runoff should be from the infiltration excess type.

Calibration

The first model run produced a hydrograph which fitted the observed hydrograph in form and also in timing surprisingly well. Only smaller changes of the assumed QC parameter had to be done. The initial parameter set was characterized through low infiltration capacities to trigger IEOF (table 12.1, appendix). Various authors (e.g. Agassi et al. 1985, Battikhi & Suleiman 1999) assume low infiltration rates of even under 10mm/h for Vertisols because of swelling processes and surface sealing on these soils with very high clay content. There was no information available, whether there were any crops on the fields. With a vegetation cover, no IEOF will be generated and infiltration capacities are a magnitude higher. For Mediterranean scrubland covered partially with Terra Rossas infiltration rates from 30mm/h (Duiker et al. 2001) up to 300mm/h (Cerdá 1997) can be found in literature. Depending on measurement techniques (e.g. infiltrometer, artificial rainfall on plots), vegetation cover, season, orientation and steepness of slopes values vary in a wide range. The low infiltration rates of first model runs however were not applicable for the second event. The generation of SEOF required different parameters, particularly high infiltration rates. The daily rainfall map indicated that most rain fell over the Mediterranean scrubland, so increased infiltration rates of the soil types in the valley basin had only little influence on the simulated hydrographs. During the event no runoff, whether of infiltration excess type or of saturation excess type was generated on the agricultural fields. The shallow soils on the Mediterranean scrubland reached saturation very fast, so these areas also contributed small amounts of SEOF. Rainfall with very high intensities may have triggered IEOF on Mediterranean scrubland. Most runoff was generated on the sealed areas. The model produced good hydrographs with the higher infiltration capacities from the calibration of the Dec.17th-20th event and with the final parameter set. It was possible to output the fraction of SEOF and IEOF of the generated runoff. This feature was useful for calibration and in this case confirmed the assumption that most runoff generated is from the infiltration excess type.

Results and Discussion

In figure 8.1 the observed and the simulated hydrograph is plotted. The simulated graph was produced with the determined final parameter set after the calibration of three events. It was not possible to reproduce the double peak, but the small impulse two days after the main flood wave was detected by the model. The first amplitude of the simulated hydrograph could not be compared with measured data. The gauge started recording a little later. Even though the form and also peak flow did not match the measured curve exactly, the duration of the flood was reflected correctly. The Nash-Sutcliffe model efficiency of the simulation is 0.55 and volume error is 3.3%.

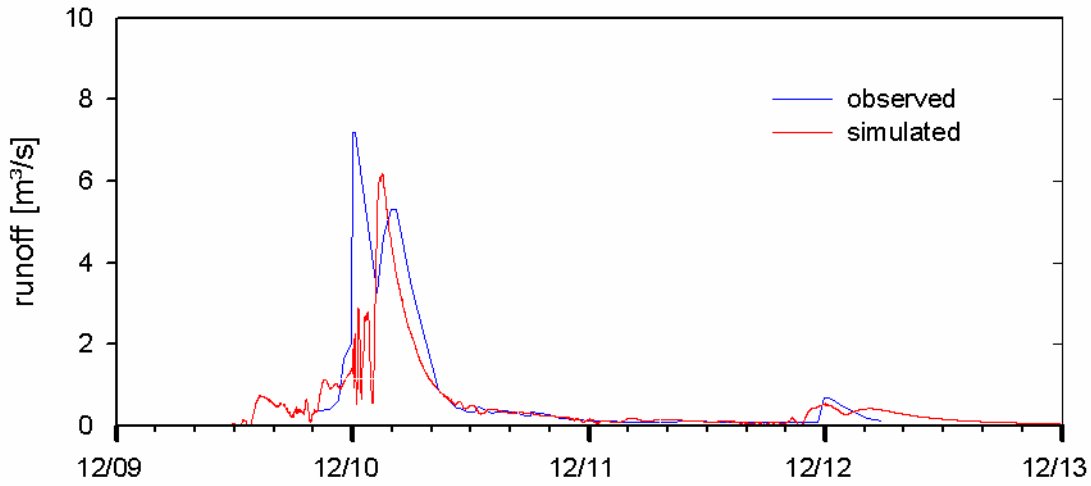

Figure 8.1: Simulation of the Dec. 9th-12th Event.

Only a few measured points form the curve of the main flood wave. About ten minutes lie between the particular measurements. Runoff in semi-arid environments can alternate in very short time. The shown runoff between these points therefore only can be seen as an approximation. For a better calibration and a more precise validation measured data with a higher temporal resolution would be necessary.

The calibration of this first event focused on the parameter infiltration capacity and initial loss. The sensitivity and the interaction of the parameters were studied. Model results prove the importance of IEOF for the runoff generation in Nahal Harod. Over 90% of generated runoff was IEOF. Hence rain mainly fell over the Mediterranean scrubland and settlements, model runs with very low (<10mm/h) and very high infiltration rates (>100m/h) for the agricultural fields produced good results. No statement on the infiltration capacity and on the vegetation cover (e.g. crops) of this landuse class could be made.

8.2.2 The Dec. 17th-21st Event

Event characteristics

The second simulated runoff event was about twice as large in total runoff volume and in peak flow as the first modeled event. 40mm of total rain, unequally distributed over 5 days produced 339,840m³ of discharge. Runoff coefficient for the 5-day event is 0.05. Two main precipitation events on 17th and on 20th cause two major runoff peaks, the first peak with 6.06m³/s and the second with 13.6m³/s of runoff. The daily rainfall maps (appendix) again indicate two major rainfall cells, one over the southern shoulder of the basin and the other one close to the town of Affula. This time precipitation of over 15mm on both days was detected in the Nahal Harod valley, between the cores of the two rainfall cells. Due to light prior precipitation on Dec. 15th and Dec. 16th saturation of soil storage could be expected for the following days.

Calibration

The main difference to the first application was the fact that initial moisture could not be set to zero. It was assumed that a fraction of the generated runoff would be SEOF. Therefore initial soil moisture and the soil depths were additional parameters to be considered. From the first model runs the parameter QC was adopted. The low starting values for infiltration capacities produced far too much runoff. Initial moisture was, as expected, a very sensitive parameter for the onset of SEOF. During calibration it was set to 0.68. Due to a possible vegetation cover, the infiltration rate for the agricultural fields was set to 100mm/h. This way the model did not generate any IEOF for these surfaces, which agrees with the general understanding of runoff generation on flat areas with a dense vegetation cover. Due to the too high initial values of all soil depths, no saturation was reached and thus no runoff was generated. There was no data on the soil depths available. The thickness of the layer was estimated with the help of the geological map, digital elevation model and several photographs of various spots in the basin. Soil storage is calculated by multiplying the depth with porosity. Saturation and the onset of SEOF therefore were in direct relation to soil depth which turned out to be another vital parameter. After the adjustment of the soil depth, good simulations were achieved. As mentioned the new parameter set was returned to the simulation of the first event. After a few simultaneous runs good hydrographs for both events were produced.

Results and discussion

The TRAIN-ZIN Model was able to reproduce the event after the calibration of the parameters initial moisture, infiltration capacity, initial loss and soil depth and proved its capability to simulate SEOF. With the final parameter set a model efficiency of 0.34 was reached. With the parameters adjusted only for this event a minimal better simulation was achieved. The passage of the second flood wave was predicted too early. The third peak could not be generated by the model with any parameter set.

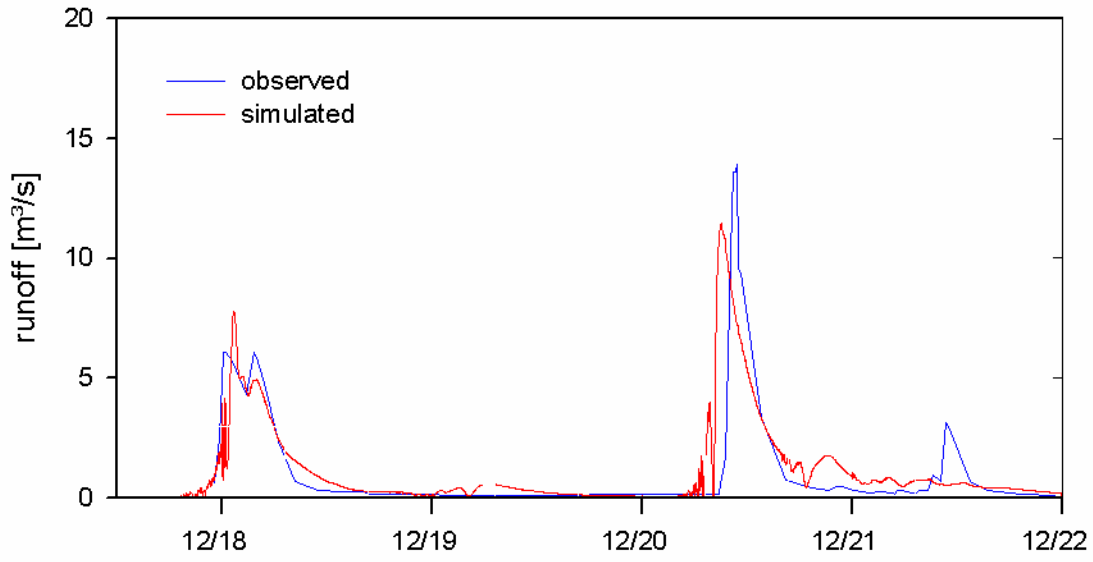

Figure 8.2: Simulation of the Dec 17th-21st Event

Responsible for the peak flow is mainly SEOF. It makes up over 60% of the first and 76% of the second peak. It is doubtful whether the timing of the second wave could be predicted more precisely after a calibration of the routing parameters. The first flood was timed exactly. To figure out why the model could not picture the third peak, knowledge about its generation would have been necessary. Without knowing where and how this runoff is formed, only speculations on possible errors of the model or of measurement can be made. Nevertheless with a volume error of 2% and the good fit of the hydrograph the result is satisfactory.

8.2.3 The Feb. 19th-22nd Event

Event characteristics

With a total rainfall of 88mm the third simulated event again was a magnitude higher. Peak flow was 18.6m³/s and runoff volume accumulated to 834,500 m³. Runoff coefficient of 0.06 also was a little higher than for prior events. After three dry days, rainfall rose from 6.8mm on the 19th to 17.7mm on the 20th and 56.8mm on the 21st. In contrary to the December events, the rainfall of the 21st was not limited to local cells but evenly distributed over most part of the basin (appendix).

Calibration

After the good simulation of two different events with the same parameter set, this third event initially should have served as the verification of the model and of the obtained parameters. The model run did not produce an acceptable hydrograph. Even after several simulations no improvement was achieved by readjusting the values of infiltration capacity, initial loss, soil depth and initial moisture. The modeled runoff was too low. To generate additional runoff with the model either SEOF or IEOF had to be increased. With lower infiltration capacities and higher IEOF better simulations for this event were accomplished, but the same parameters were not applicable to the prior events. Therefore too little SEOF was generated. A possible reason is that too much

water was lost through the filling of the soil storage. With smaller soil depths and higher initial soil moisture saturation was reached earlier, but no major increase in runoff was produced. Outputted soil moisture maps showed low soil water contents for the Mediterranean scrubland, even right after a rainfall input. The emptying of the storage through evaporation or deep percolation was too fast. Estimated evaporation seemed to be in the right order of magnitude. Deep percolation is controlled by the parameter saturated conductivity. For the Terra Rossa on the Mediterranean scrubland it was estimated with the SPAW hydraulic properties calculator from grain size distribution out of literature. The initial value of 0.65cm/h was too high and the soil lost too much water to the underground. After the adjustment of this parameter better runs were conducted. Through the simultaneous modeling of the three events, the different parameter sets were combined to the final set which produced good results for all events.

Results and discussion

With a model efficiency of 0.80 and a volume error of 1.37% the best fit of the three simulations was achieved with the final parameter set. First peak is made up by 73% of IEOF and the second peak consists out of 79% SEOF. Initial moisture was set 0.53. Even with lower values the too steep first rising limb could not be leveled.

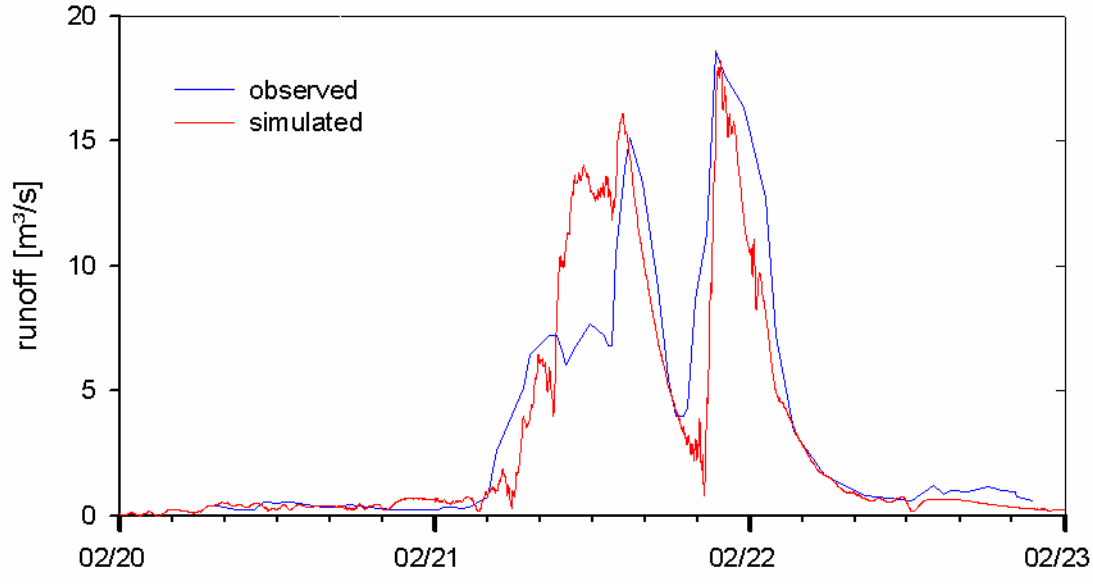

Figure 8.3: Simulation of the Feb.17th-22nd Event.

8.2.4 Verification with the Feb. 24th-Feb. 27th Event

Event characteristics

The largest runoff event in volume and peak flow occurred end of February. Total volume was $1{,}7 \times 10^6 m^3$ and the stream flow at the catchment's outlet rose to $36 m^3/s$. Only one dry day was between this and the previous events. Due to the high antecedent

moisture runoff coefficient of 0.16 was a lot higher than for earlier events. The hydrograph shows several smaller peaks following each other without a total decline of runoff in between.

Verification

The unchanged final parameter set of the calibration runs was used for verification. Only the initial moisture was adjusted. It was set to saturation. Model efficiency for this non-calibrated event is 0.20 and volume error 15%.

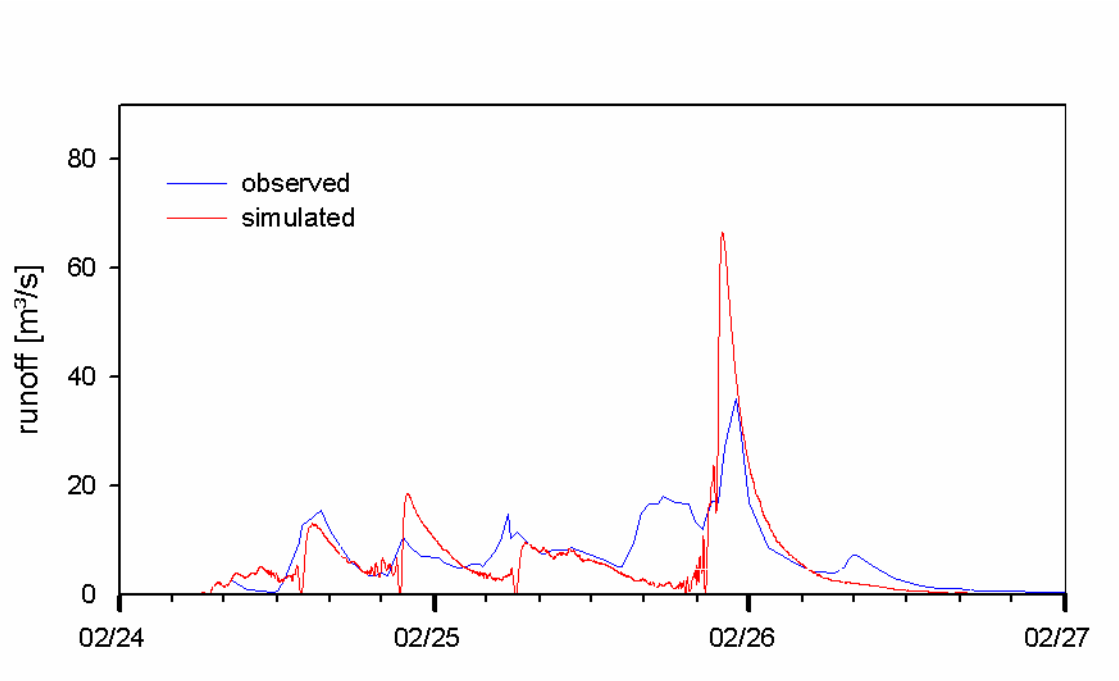

Figure 8.4: Simulation of the Feb.24th-27th Event.

Results and discussion

It is arguable whether the largest observed flood in the hydrological year is ideal for model verification. The ZIN model was developed for the simulation of large floods, so the coupled version also should be able handle extreme events. Eye catching is the high peak of the simulated hydrograph which more than doubles the observed peak flow. The runoff generated by the model for this flood is only SEOF. A possible explanation for this malfunction is that in reality the large flood leaves the channel and water is lost through infiltration of the over bank flow. In the model this process is not considered. The main channel in the lower part of the basin can carry easily the peak runoff of 36m³/s. The velocity for one segment was estimated with Manning's law. The cross sectional area which is required by 36m³/s flowing with a speed of 5.4m/s is about 7m². The main channel provides over 30m². This test could not be executed for all segments. Particular runoff in each channel was unknown. Smaller tributaries may overrun when a rainfall cell hits the distinct subbasin. The assumption of over bank flow cannot be disproved. The fact that the width and the depth of all channel segments were estimated and that such malfunction of the model was not observed during model runs of smaller events strengthens this possible explanation. Measurements on-site are necessary to verify these values. Only this way would it be able to state that simulated peak flow was so high because over bank flow occurred and the so caused transmission losses were not

considered by the model. When the two highest simulated values were not considered, model efficiency rose to 0.64.

Nevertheless the model verification was successful and the functionality of the TRAIN-ZIN model for the simulation of rainfall-runoff events in semi-arid environments was proven.

8.2.5 Conclusion

The TRAIN-ZIN model simulated rainfall-runoff events in an adequate way. SEOF and IEOF, the two important processes of runoff generation in semi-arid environments, were recognized and reproduced correctly. Even though no direct measurements in the basin were done, the number of parameters to be calibrated was not too big. Routing parameters did not undergo any adjustment, and the determination of the parameter QC for runoff concentration only needed a few runs. Three events with different rainfall and antecedent moisture characteristics were used for calibration. First the parameters controlling IEOF were adjusted with a short rainfall event on dry soils. Soil depth and saturated conductivity were addressed during the simulation of larger floods which were partly generated through SEOF on soils with high initial moisture contents. With a simultaneous calibration of the three events a parameter set for different antecedent conditions and rainfall characteristics was determined. Verification was done with a fourth event. All four events were run with the final parameter set and only initial moisture had to be alternated. Model efficiencies ranged from 0.2 to 0.8 and volume error stayed under 15% for all events.

8.3 Simulation of the season 2002/2003

8.3.1 Parameter

The parameter set was taken from the prior calibration with single rainfall-runoff events. For the simulation of events, the parameter initial loss had to be estimated before each model run. The TRAIN-ZIN calculates the actual soil moisture for days with precipitation and for periods in between rainfall events. The emptying of the soil storage is controlled by evapotranspiration and deep percolation. As already mentioned, parameters for the evaporation process where not adjusted during calibration. No regionalization of the meteorological data was done. Events of several days were simulated successfully and the correct continuous estimation of the soil water content and its effect on the onset and termination of SEOF was verified. For rainy days the water loss through evaporation is minimal, so water mainly leaves the soil through deep percolation. The adjustment of the saturated hydraulic conductivity during calibration assured good simulation results. For longer dry periods evaporation becomes more significant. Besides an evaluation of the continuous determination of the vertical fluxes, the modeling of the whole rainfall season 2002/2003 from October to March also can be seen as additional verification of the event simulation.

8.3.2 Simulation of runoff

For better inspection of the results, the simulated hydrograph of the whole season was cut into monthly segments. Due to the nearly constant base flow, which was not simulated, model efficiency and volume error were not applicable for model evaluation. The quality of the simulation was assessed though visual inspection. In October, runoff exceeding the base flow was neither observed nor simulated. The following months are shown below.

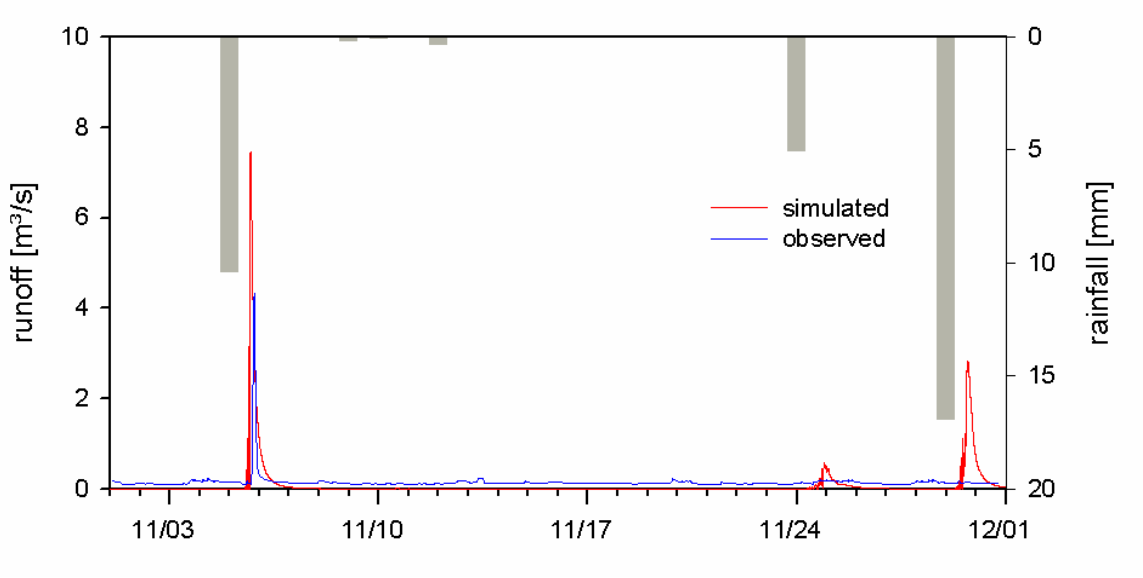

Figure 8.5: Simulation of November 2002

The first flood of the season was observed on November the 5th. Shape and timing was simulated correctly, but peak runoff was overestimated. In the end of November the model outputted two additional floods, which were not observed. All runoff generated by the model is from the infiltration excess type. An overestimation of IEOF was observed at various times and was subject to further discussion at the end of this chapter.

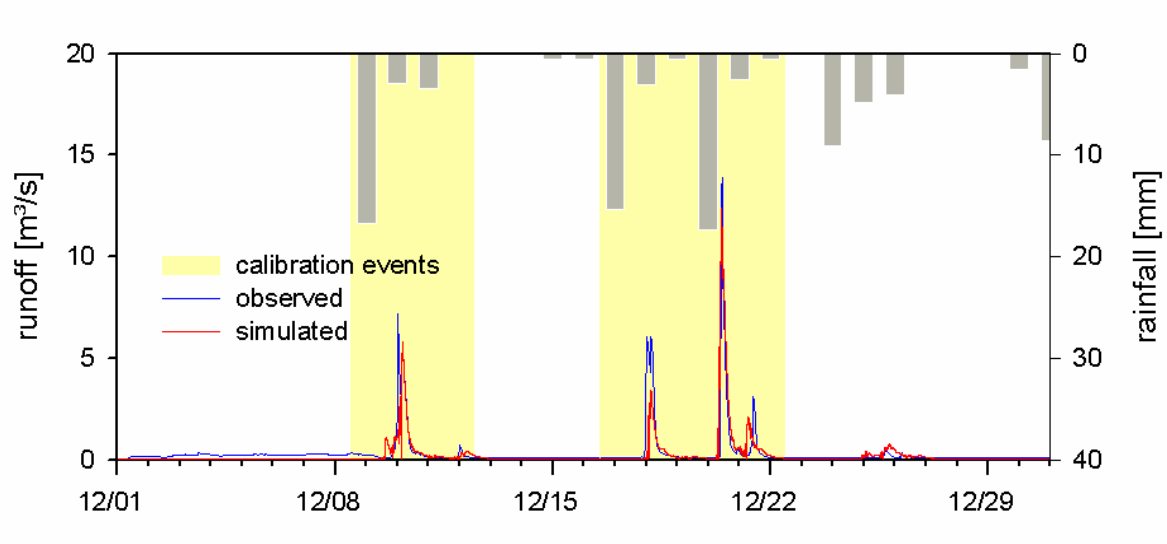

Figure 8.6: Simulation of December 2002

In December two major events were observed. Both were already modeled during the calibration process. The first event is mainly made up of IEOF. Initial soil moisture and its continuous calculation have no influence on model output. Therefore, the result of the season simulation equals the event simulation. The second event in December consists out of SEOF and IEOF and soil water content becomes more important for runoff generation. In fig.7.7 the hydrographs from the prior event simulation and from the simulation of the whole season are plotted together with the observed hydrograph.

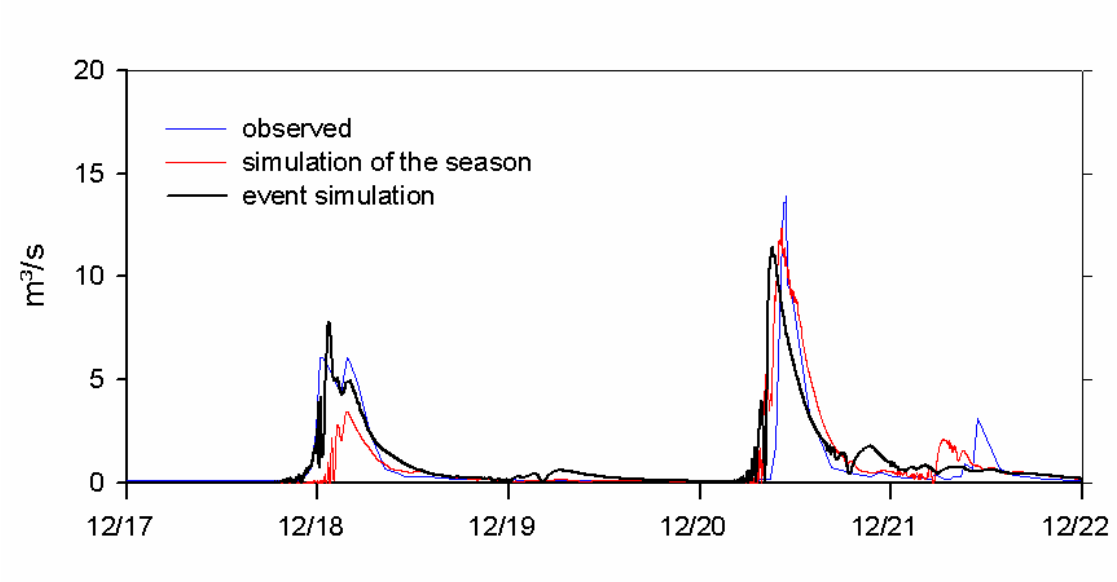

Figure 8.7: Comparison of event and season simulation of Dec. 17th- 21st

The first peak was underestimated during the season simulation. SEOF was not generated sufficiently. Reasons could be that the soil storage is emptied too fast through evaporation or deep percolation. Another possible reason is that the calibration of the event was done with too high initial moisture. The same parameter set applied to the whole season with the modeled initial moisture then produces too little runoff.

Both observed floods in January 2003 were reproduced by the model. The first event of the year was underestimated. The simulated hydrograph only reached 360l/s while 2.5m³/s were measured. If we add the base flow to the simulated hydrograph, the modeled peak discharge still lies far under the observed. An explanation of this malfunction, even after the analysis of rainfall map and saturation maps cannot be given.

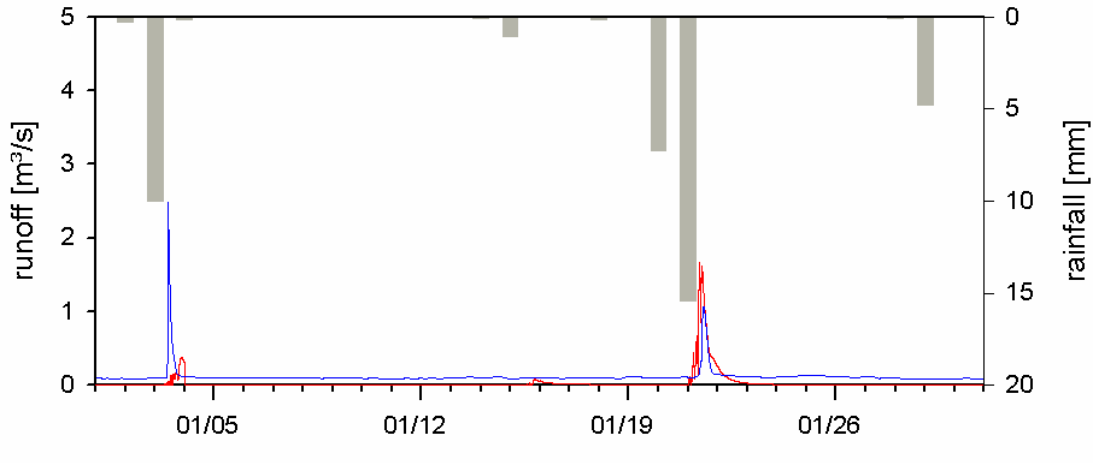

Figure 8.8: Simulation of January 2003

The second event in January was simulated more adequately. It is made up mainly of IEOF. The overestimation of the infiltration excess was already observed in the simulation results of November.

Two major floods occurred in February. The Feb. 19th – 22nd event was already modeled during calibration and the Feb. 24th – 27th event served as verification. Earlier runoff peaks were underestimated. It can be assumed, that a large fraction of the flood an Feb. 15th is derived from SEOF. Precipitation was observed on the four prior days so the soil should be close to saturation. In the model, again too much water is lost through the filling up of the soil storage and therefore cannot contribute to runoff. The simulated flood waves of Feb. 4th and Feb 15th not only show a too low peak discharge but also are smaller in total runoff volume. Deep percolation or evaporation is overestimated by the model and the soil storage is emptied with a too fast rate. The small simulated runoff peaks of February the 9th, 10th and 11th are made up of IEOF.

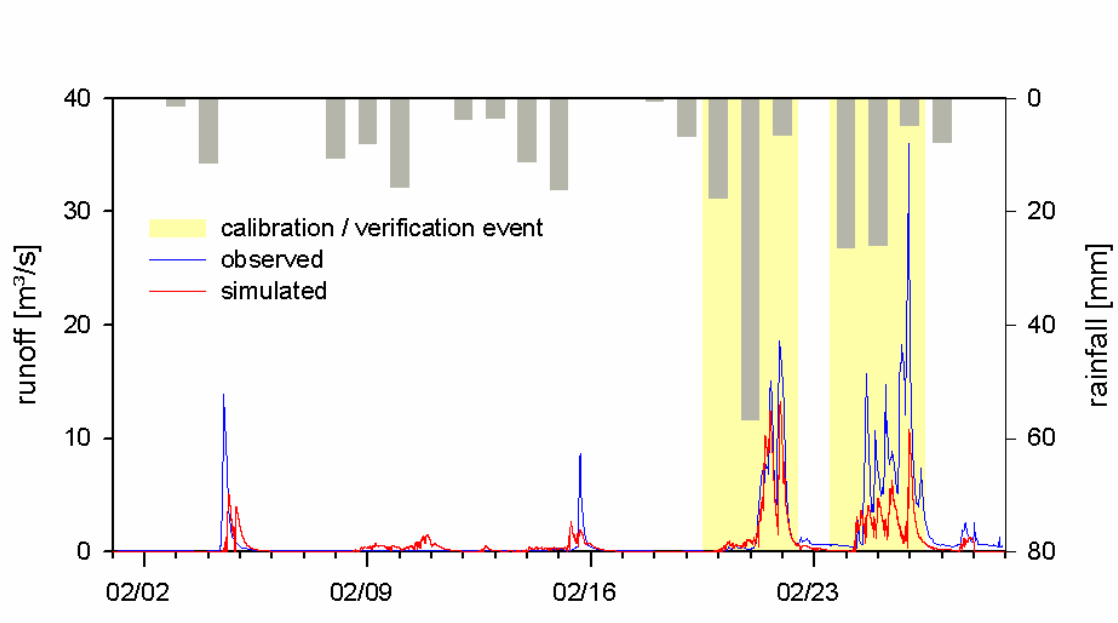

Figure 8.9: Simulation of February 2003

The comparison of the hydrographs of the event simulation and the season simulation with measured data of the December 17th – 21st event already showed, that initial moisture is too low or that the soil storage is emptied too fast during season simulation. This can be noticed again analyzing the two large events end of February. Therefore the hydrographs of the Feb. 19th – 22nd event are shown in Figure 7.10.

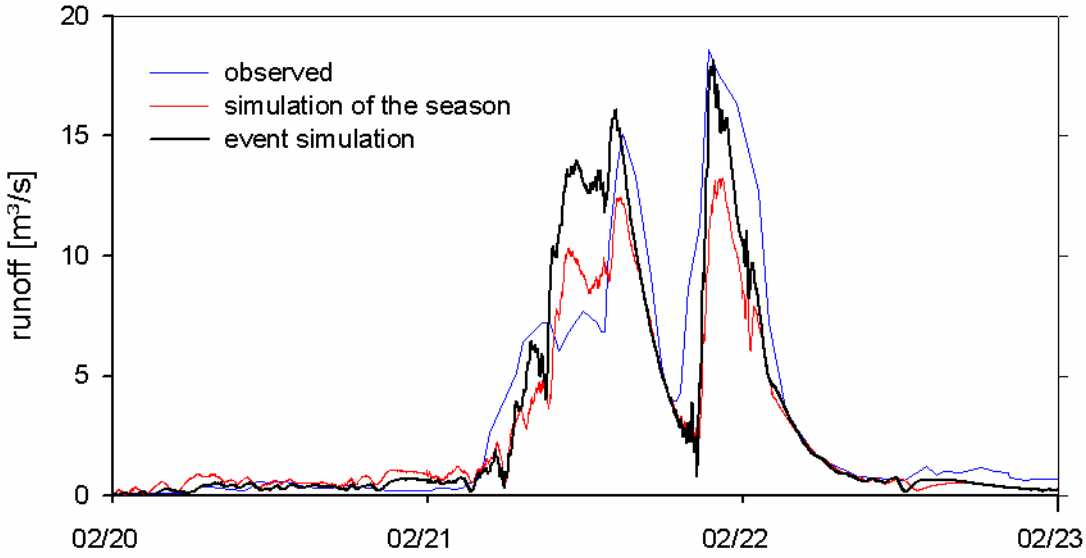

Figure 8.10: Comparison of event and season simulation of Feb.19th- 22nd

The largest flood of the whole season also was underestimated. The Feb. 24th-27th event was already used for verification. With the same parameter set plus the appointed initial moisture of one, the first small peaks of the flood were simulated much better (see chapter 8.2.4). The comparison of the hydrographs (fig. 8.11) makes the importance of the initial moisture and the continuous simulation of the soil water content visible.

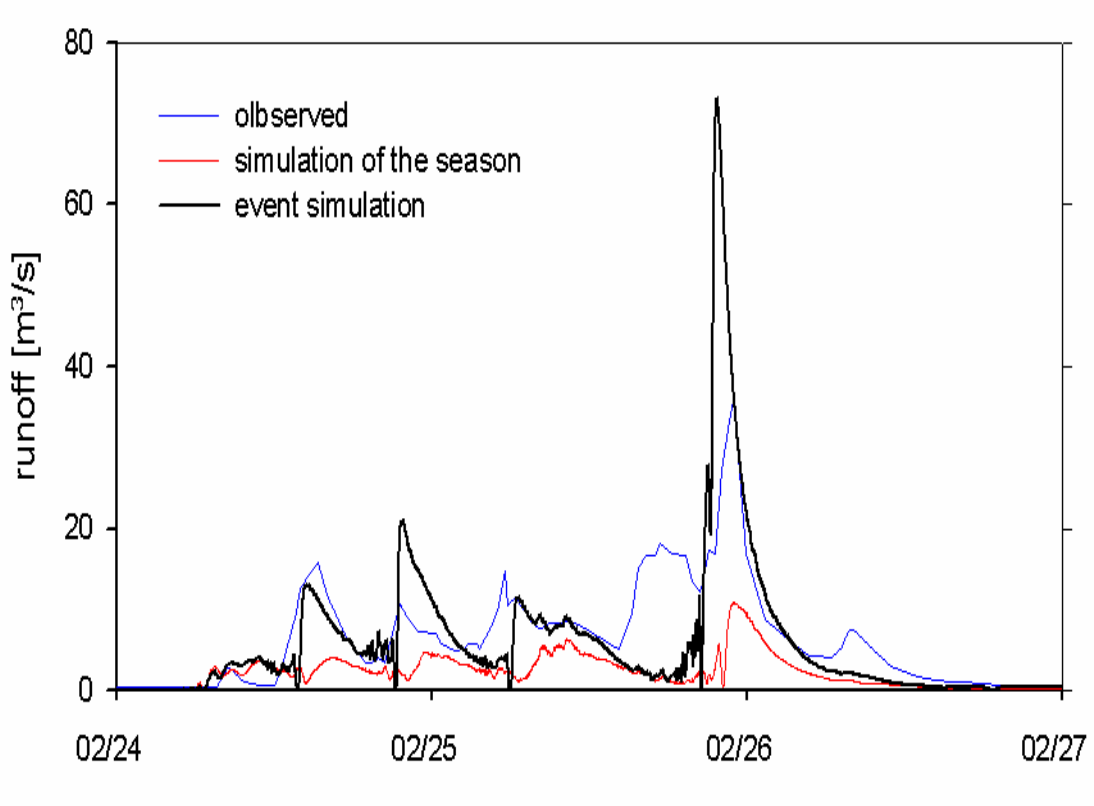

Figure 8.11: Comparison of event and season simulation of Feb. 24th-27th

For March 2003 the deviation between simulated and observed runoff probably has the same reason as the inaccuracies of the already regarded simulation results. All simulated peaks, excluding the last and largest flood wave, consist nearly totally of IEOF. During simulation IEOF again is overestimated. Because of the too low soil moisture, due to a too fast emptying of the soil storage the last simulated wave has a lower total volume than the observed. The overestimation of IEOF also leads to less infiltration and a later saturation of the soil.

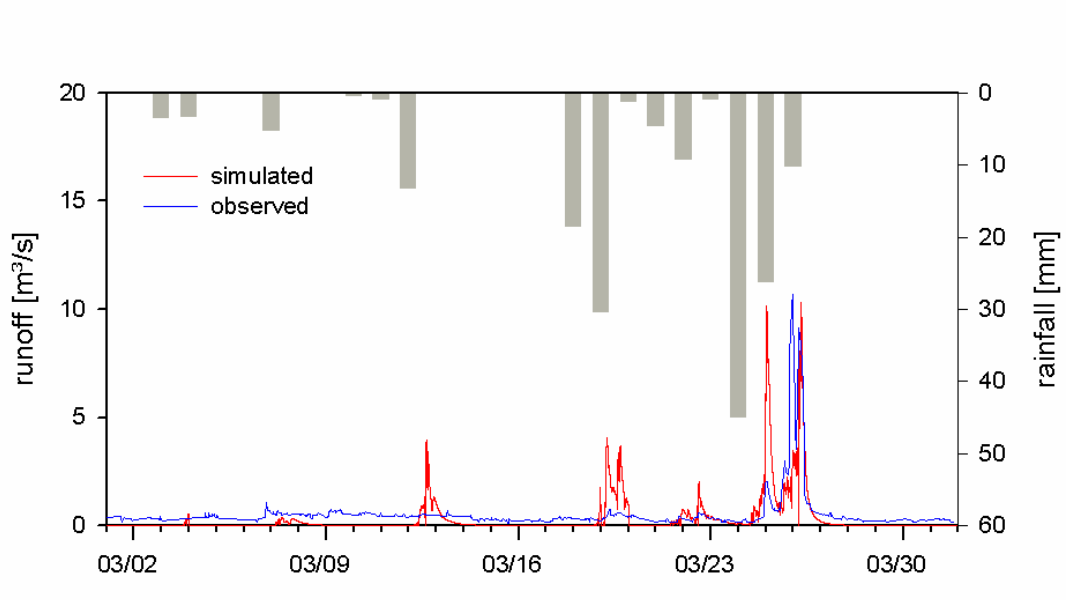

Figure 8.12: Simulation of March 2003

8.3.3 Simulation of evaporation

During the analysis of the simulation results, it became clear that the model did not generate enough SEOF due to the fast emptying of the soil storage. Percolation, evaporation and transpiration of the vegetation drain the soil. Percolation was subject to calibration through the adjustment of the saturated conductivity. There is no data available to check the determined parameters that control percolation. Parameters for the estimation of evaporation and transpiration were not calibrated. With the available data the estimated water loss through plant transpiration cannot be verified. However, simulated water loss from the fishponds can be compared with the values of the open water surface evaporation determined with the Penman equation (see chapter 7).
It is possible to output the daily evaporation of every raster cell. On October the 1st, the starting point of the simulation, initial moisture was zero. In fig. 8.13 the fishponds can be identified through the high daily evaporation ranging from 7.2 to 7.5mm. The surface and soils of all other land use classes are dry, so no actual evaporation occurs. With the Penman equation a daily evaporation of 5.2mm was determined for Oct. 1st. Open water surface evaporation estimated be the TRAIN Model is higher.

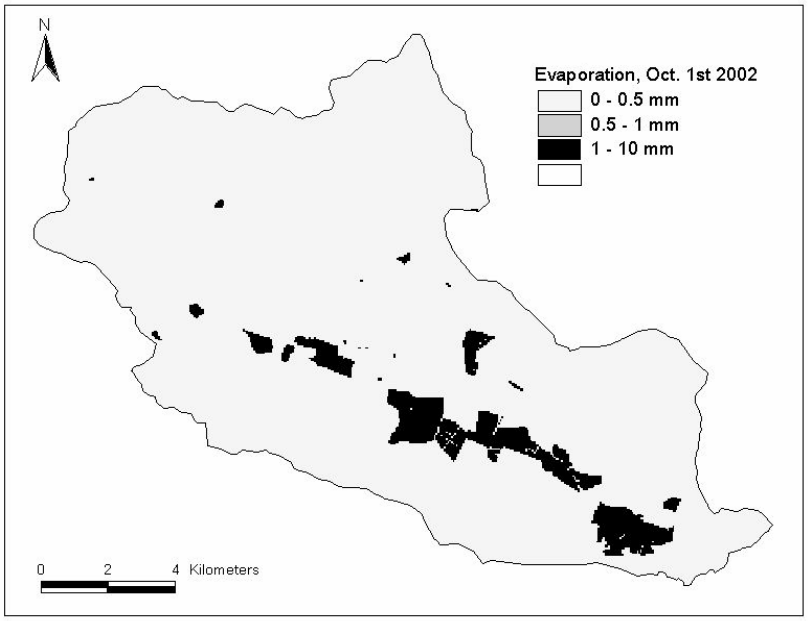

Figure 8.13: Evaporation, Oct 1st 2002

Dec. 27th is a day without any precipitation, following several wet days. Again the fishponds can be identified on the evaporation map (fig. 8.14). Unlike on Oct 1st, evaporation also takes place over other parts of the basin. After the rainfall of prior days, water is still stored in the soil storage and is lost to the atmosphere by evaporation or transpiration. Again the estimated evaporation from open water surfaces with the Penman equation of 1.18mm is lower than the estimated evaporation with the TRAIN Model of 1.65mm.

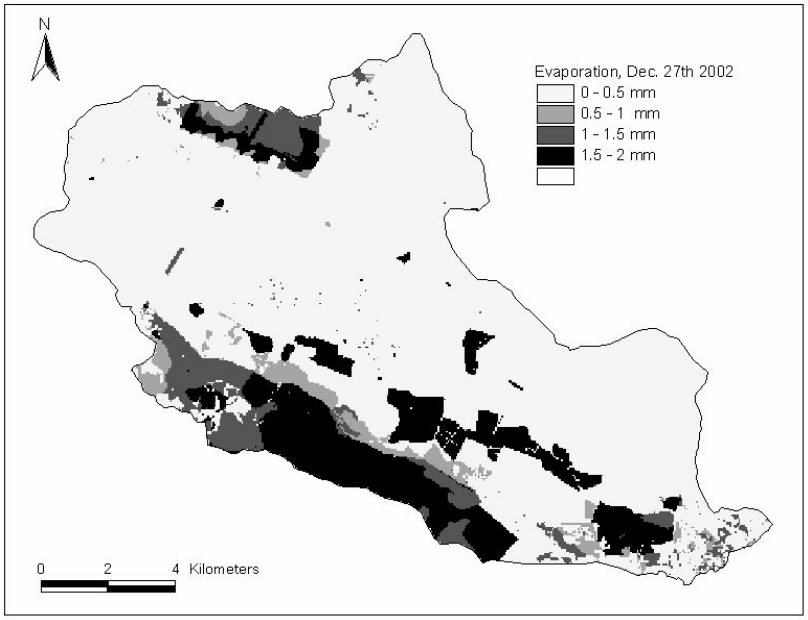

Figure 8.14: Evaporation, Dec 27th 2002

8.3.4 Conclusion

The TRAIN-ZIN was successfully applied to the rainy season 2002/2003. The model correctly timed all observed floods. The magnitude of peak runoff and volume was simulated adequately. The overestimation of runoff particularly in November and March can be explained with possible too low infiltration capacities and the additional generated IEOF. The rainfall of theses events is not concentrated only over the Mediterranean scrubland as often observed, but more evenly distributed over the total Nahal Harod, also over the vast valley basin. The infiltration rate of 100mm/h for agricultural fields is exceeded several times by rainfall storms with very high intensities. It can be assumed that Vertisols with a dense vegetation cover have higher infiltration capacities and do not generate IEOF as during model simulations. During calibration this overestimation of IEOF was not observed. Calibration events did not reach those high rainfall intensities over the agricultural fields. These inaccuracies therefore result from incorrect parameterization and not from possible errors in the conception of the model.

The underestimation of runoff mainly in February, but also end of December is the result of too little SEOF. The soil storage of the model looses water too fast to the atmosphere and/or to the underground. Therefore large amounts of rainfall are needed to keep the soil saturated for further SEOF. The estimation of deep percolation could not be validated. The saturated conductivity was determined through calibration. Measured data was not available. The water loss through evaporation and transpiration was estimated with given climatic and vegetation parameters. The water passage from the soil through the roots to the plant leaves and the transfer to the atmosphere is dependent on soil and vegetation parameters. This process neither was validated but a comparison of open water surface evaporation calculated by the model with evaporation estimated with the Penman equation gives evidence that the model overestimated the water loss through evaporation.

8.4. Scenarios

8.4.1 General aspects

One of the most important uses of rainfall-runoff models is to predict the effects of land use and climate change on a catchment's rainfall response, particularly for extreme events (Beven 2001). Physically based, spatially distributed models provide a potentially powerful tool for this purpose. The equations are valid for different parameters and changes can be implemented in their correct spatial context. Hydrologists and environmental consultants rely on models for an effective basin management. Decision-makers require these predictions on the impact of climate and land use changes.

Because of the natural variability of hydrological systems in space and time, and the generally short periods of available observations, it still is very difficult to study and to understand the effects of change, even with the most physically based distributed models available. Through improvement in measurement of physical parameters and a better understanding of hydrological processes in recent years, models are able to

picture reality more accurately. The advances in automatic data processing make it possible to handle complex models with a high resolution. However, model results always have to be handled with caution. Errors in measurement, in model concepts or in the prediction of parameters can cause significant uncertainties.

8.4.2 Landuse change

A high population growth with continuing urbanization is noticed throughout the Middle East (Hötzl 2004). The impact of gradually sealed surfaces is a problem in many urban areas. Huge storm water systems have to be built so that large rainfall events do not cause any damage. Settlements, roads and industrial areas do not store any precipitation and rainfall is followed by an immediate runoff response. The calibrated TRAIN-ZIN Model is used to predict the effects of urbanization. 3% of the Nahal Harod's surface is sealed. The distribution of the settlements and sealed surfaces can be taken out of the landuse map (fig. 4.4). No major agglomeration can be identified. For the scenario a landuse map with 6% and one with 15% instead of 3% sealed surface was generated. The additional areas were added along existing settlements with a concentration on the villages in the center of the basin. The spatial complexity of urban areas makes it difficult to simulate the rainfall response. House roofs, gardens with different soil depths, roads and recreational areas alternate nearly randomly. For the exact modeling these areas together with existing ditches and pipes have to be mapped. For the Nahal Harod all urban areas are generalized to a single landuse class and no distinction between different industrial and housing areas were made. 3mm/h infiltration capacity and 3mm initial loss were determined during calibration.

8.4.3 Climate change

The effects of global warming can already be observed and studied in many natural environments. Through an analysis of data sets that cover the period since 1970 the Intergovernmental Panel on Climate Change (IPCC 2007) leaves no doubt on the existence of a man-made climate change. Global circulation models (GCM) are used to predict regional climate changes. The Fourth Assessment Report of the IPCC (2007) summarizes the impacts, the adoption and the vulnerability of natural and human environments. Drought-affected areas will likely increase in extent. Heavy precipitation events, which are very likely to increase in frequency, will augment flood risk. Projected precipitation changes however vary significantly from model to model (Wigley 1992) Present GCMs are only available in a very large grid scale, in the order of 100x100km², which is equivalent to a basin of 10,000km². Exact regional predictions therefore are very uncertain. Nevertheless an increase in extreme daily rainfall and a decrease of annual rainfall is a widely accepted prediction for the Eastern Mediterranean region (Alpert 2004).

To assess the impact of increasing extreme daily rainfall producing large flood events, the model was run for two already simulated events, but this time with doubled rainfall input. The radar raster files with 5-minute rainfall amounts for every cell were multiplied with a factor 2, so intensities and total volume were doubled.

8.4.4 Results

The Feb. 19th-22nd event was already simulated during calibration. Of all model runs, the best model efficiency of 0.8 was achieved simulating this event. Rainfall on the 20th was mainly localized over the southern valley shoulder while on the 21st the rainfall was evenly distributed over the whole basin. The first peak of the flood was produced mainly by IEOF while the second consists of SEOF.

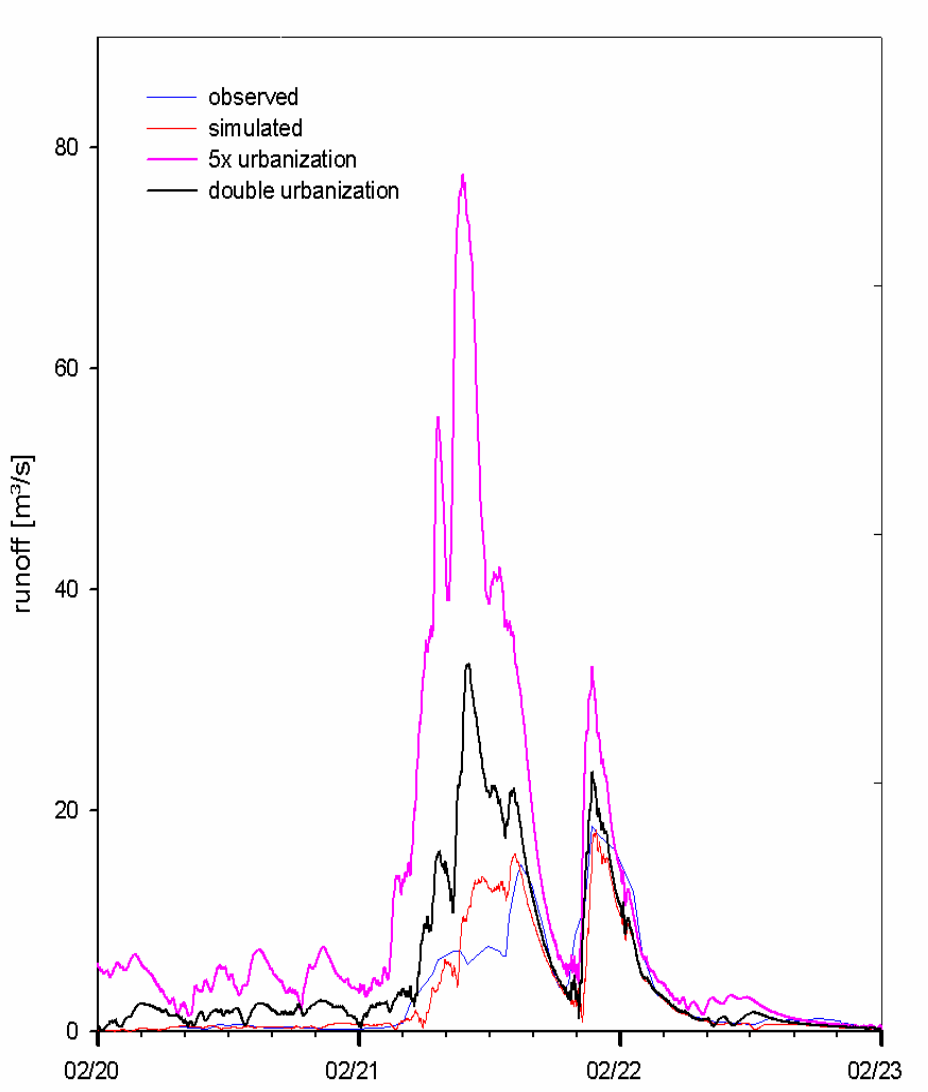

Figure 8.15: Urbanization scenarios of the Feb.19th-21st Event

The *double urbanization* scenario shows a significant increase in runoff in the beginning and at the first peak. This conforms with the general understanding, that urban areas produce a very fast response to rainfall. It can be assumed that the first peak of the observed hydrograph was produced mainly through IEOF generated on sealed surfaces. Through the doubling of this landuse class, the simulated peak runoff increases to nearly twice the size of the observed flood. The additional urban area has hardly any influence on the second peak which consists of SEOF. Total runoff volume increases by 43% with the same rainfall input and runoff coefficient rises from 0.055 to 0.092. The *fivefold urbanization* scenario shows the same tendencies: A strong increase in runoff for the first peak and little effect on the second peak. Total runoff volume is three times higher and runoff coefficient rises to 0.201.

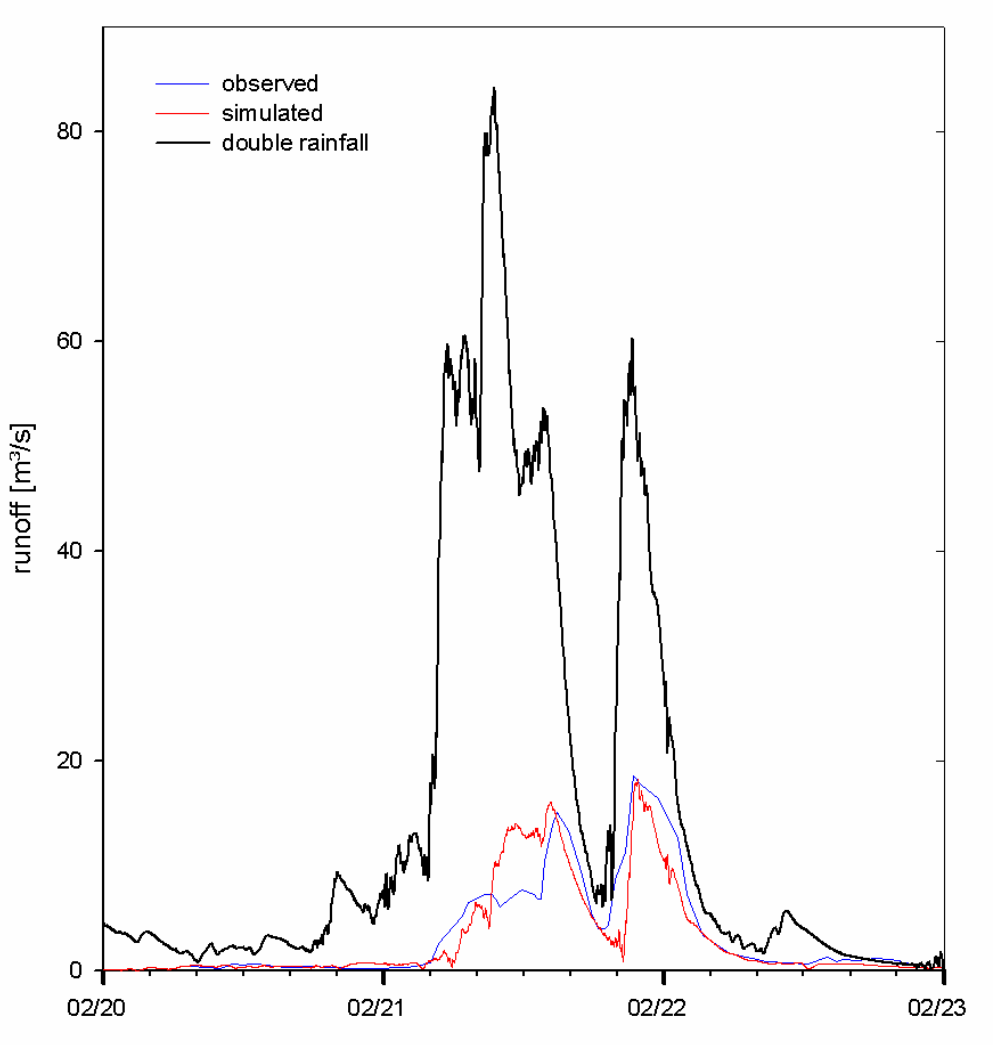

Figure 8.16: Rainfall scenarios of the Feb.19th-21st Event

With double rainfall input an enormous 84.3 m²/s is simulated. Rainfall input for the whole event now is 176 mm. Runoff volumes is four times larger and runoff coefficient reaches 0.132. The response to the assumed large rainfall event is disproportional high. For both, the scenario and the real event, the same initial loss is subtracted and the same amount of water is lost to the underground. These losses form 94.5% of total rainfall for the real event and only 86.8% for the scenario.

The Feb. 24th-27th event is the largest event of the 2002/2003 season. It already was used for the verification of the TRAIN-ZIN Model (Chapter 8.2.4). Accumulated rainfall for the whole event was 65.65 mm and was evenly distributed over the basin (appendix). The main runoff generation process was SEOF. The impact of change on extreme events is of special interest. Therefore scenarios of this event were run, even though only a model efficiency of 0.2 was reached and the peak discharge was strongly overestimated during verification.

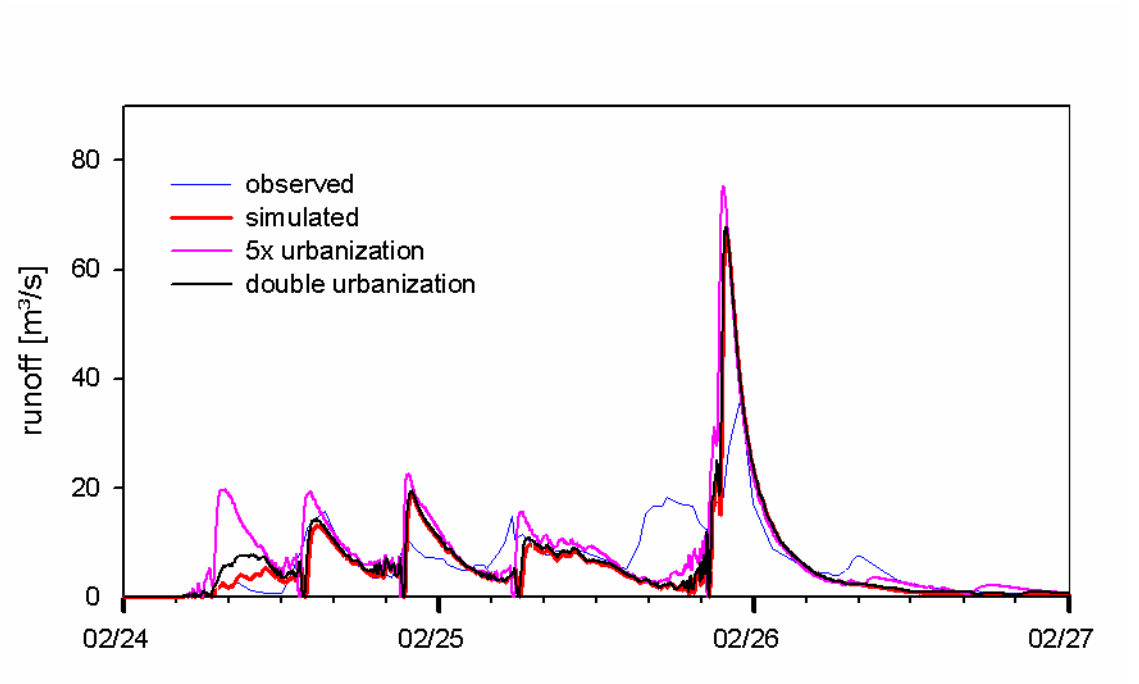

Figure 8.17: Urbanization scenarios of the Feb.24th-27th Event

Produced runoff of the *double urbanization* scenario is only a little higher than the simulated runoff volume of the real event. The two hydrographs are nearly identical. Only at the beginning of the event more IEOF is produced due to the additional sealed surface. The *fivefold urbanization* scenario neither shows a significant effect on the hydrograph. Again at the beginning of the event more IEFO is generated.. Rainfall with all intensities will produce runoff. Only the amount of water which is lost with a rate of the saturated conductivity does not contribute to runoff.

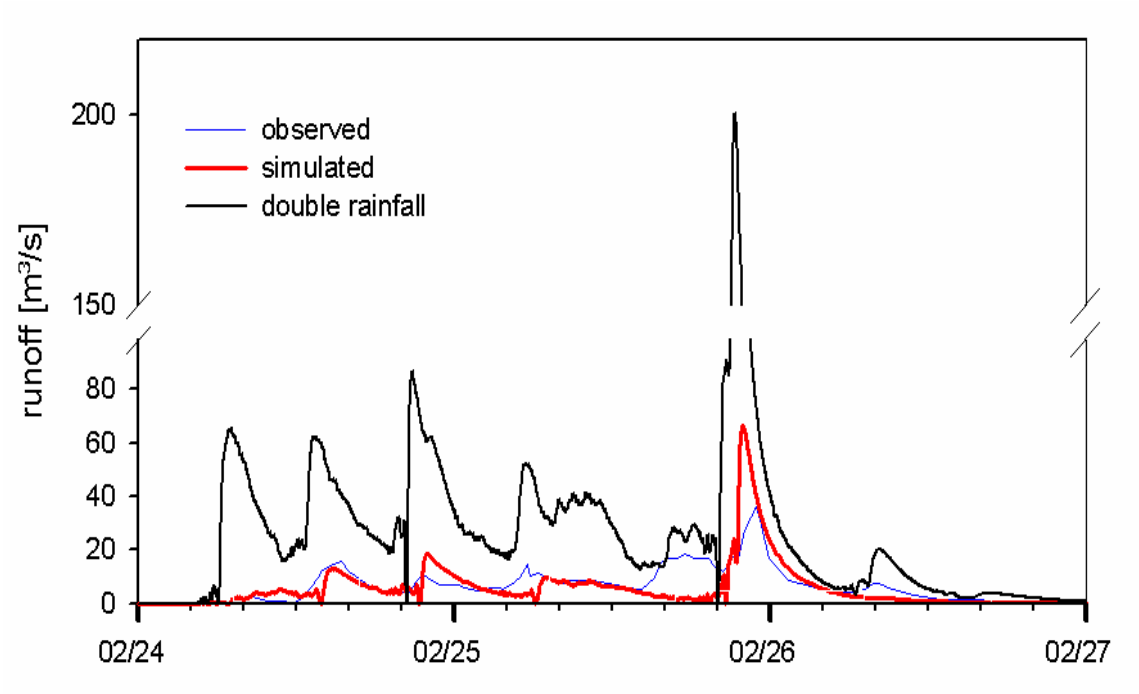

Figure 8.18: Rainfall scenarios of the Feb.24th-27th Event

Again a disproportional high response can be expected with higher rainfall. Runoff volume is nearly 5 times higher with double rainfall input. Large areas of the basin are saturated. For initial saturation and for maintaining this situation the same amount of total rainfall is needed during the two model runs. This loss is reached with a smaller fraction of the doubled rainfall. Runoff coefficient increases from 0.16 to 0.32. The simulated peak discharge of 201m³/s is afflicted with great uncertainty. The simulation of the real event already was inaccurate.

8.4.5 Conclusion

Two types of scenarios were run with the calibrated model: a landuse change and a climate change scenario. For the meso scale Nahal Harod a 100% and a 500% increase of urban area was assumed. The newly generated landuse maps then had 6% and 15% sealed surface. The effect on the largest observed flood in 2002/2003 was nearly negligible. For the other simulated event a significant increase of the first flood wave and an increase in total runoff volume were estimated by the model. This first flood wave consisted mainly of IEOF. Through the additional sealed area, more IEOF is generated. In the agricultural meso scale basin Nahal Harod a moderate additional sealing of surfaces through settlements and industry have only little influence on rainfall response of the whole basin. The effect in the settlement itself surely is much stronger. To study these changes models with higher resolution and a distinction of different settlement classes have to be applied. A strong urbanization would change the runoff characteristics of the Nahal Harod. Smaller floods, generated mainly by IEOF would increase significantly.

GCMs predict an increase of extreme daily rainfall. To estimate the effect of such storms, two events were simulated with double rainfall. The model predicts a disproportional high rainfall response. Outputted hydrographs show a significant increase in peak discharge and in runoff volume. For the first event a doubled rainfall would mean a total amount of 176mm in four days. A storm of this size would have a low probability also considering climate change. The second event which hits saturated soils would have a total rainfall of *only* 131mm. It produces a five times higher total runoff volume. In October 2006 the so far highest flood with a peak discharge of 128m³/s was observed. Floods with 150m³/s or even 200m³/s and runoff coefficients of .3 and higher are not unrealistic and have to be expected by basin managers.

IX. Conclusions and discussion

9.1 TRAIN-ZIN

After the successful application of the coupled TRAIN-ZIN Model to a micro-scale basin with sufficient data for a non-calibrated simulation, the model proved its functionality for meso scale catchments with parameters determined through calibration. The runoff generation processes IEOF and SEOF, runoff concentration and channel routing can be simulated with a high resolution. On dry days, changes in soil water content through evaporation, transpiration and deep percolation are modeled on a daily basis. This way an accurate simulation of the short flood events of semi-arid environments is possible for a whole season or longer periods. The determination of the parameters controlling runoff generation can be done with a feasible number of calibration runs and is not too time consuming. With the help of rainfall maps derived from rainfall radar and saturation maps showing the soil water content, the right direction of the parameter adjustment can be selected. Analyzing the model output, a determination of the main runoff contributing areas and the main runoff generation mechanism is possible. The newly integrated runoff concentration method considers size and slope of the subbasins for the transformation of generated runoff to channel flow. After the adjustment of the parameter QC, runoff concentration is simulated adequately for different subbasins. The Muscingum-Cunge method with its iterative approach for channel routing showed some instability and required a lot of attention. After an adjustment of the routing parameters and first correct flood wave propagations, no further calibration was necessary. The routing routine can be run separately with results from prior model runs and so parameters for channel flow and transmission losses can be calibrated without running the whole model. It is possible to output the hydrographs of every subbasin so calibration can be done focusing on distinct characteristics of subbasins.

Model results are promising for further applications. At the moment the TRAIN-ZIN Model only is available in a C++ shell. With a more user-friendly interface the coupled model is a powerful and useful tool for further research and for effective catchment management in times of significant climate and land use changes.

9.2 Parameterization

The author of this work never visited the study area and no direct measurements in the Nahal Harod were made. All input data was determined through an analysis of existing thematic maps (soil, landuse and geological maps), satellite images and photographs of the basin. Plant parameters were taken out of the TRAIN database. For the soil characteristics an intensive literature study was done. Published values were confirmed with the SPAW soil water characteristics tool. The preprocessing of the data was done with a GIS. Through model runs with artificial rainfall the sensitivity of the parameters was determined. An order of parameters to be calibrated was appointed. After the adjustment of parameters for runoff concentration and channel routing, the soil properties controlling the runoff generation were calibrated. With values taken from

literature and the analysis of maps and images as starting point, good results were achieved after manual calibration. A model strategy and additional model output as for example soil moisture maps help to shorten the calibration process.

With a few additional data the quality of simulation could be improved and parameter obtained through the calibration could be verified. The measurement of channel dimension and an analysis of samples of the major soil types could be accomplished without high expenses. A control of the catchment delineation especially in the settlement of Affula and near the outlet in the Jordan valley should clear some remaining doubts on the extent of the Nahal Harod. The TRAIN Model was developed for more humid environments. Typical Mediterranean landuse types as, for example, the Mediterranean scrublands are still not included in the TRAIN database. An approximation with the already existing landuse classes of the database had to be done. The assumptions considering the role of the fishponds in runoff generation have to be verified. Do they really absorb all rainfall and not contribute to any runoff? Vegetation has major influence on the infiltration on rainfall into the soil. Large areas of the basin are agricultural fields with a changing vegetation cover. Data on the type and on the schedule of cultivation would help to assign infiltration capacities more accurately and in a variable way depending on the season.

In spite of all these uncertainties good model results were achieved. The physically based TRAIN-ZIN Model can be run without any direct measured data. The number of parameters to be calibrated is manageable.

9.3 Simulations

After the calibration and verification of the model with single events, the whole season 2002/2003 was simulated. The most important processes of flood generation and the distribution of contributing areas were outlined. Both IEOF and SEOF play an important role for runoff generation in the Nahal Harod. Settlements and sealed surfaces produce runoff but are not responsible for the large floods. More runoff comes from the Mediterranean scrubland and the largest floods are generated in the entire basin, also on the agricultural fields. Local rainfall cells over one of the settlements may produce enough IEOF for floods at the catchments outlet. Locally large floods can occur. But during calibration and with the *urbanization* scenarios it became clear that sealed surfaces are not responsible for the largest flood events at the catchments outlet. The influence of the urban areas in the Nahal Harod is limited. It only occupies 3% of the total surface. Through additional urbanization the runoff characteristics of the catchment would not change significantly. Only a severe growth of settlements would affect the rainfall response. The largest runoff events were mainly made of SEOF. The main contributing area is the Mediterranean scrubland of the southern and north western valley shoulder. The shallow soil reaches saturation various times throughout the season. For the Terra Rossa a soil depth of 0.25m was obtained during calibration. With the porosity of 0.46 the soil storage is filled after 115mm of rain. The spatial distribution of rainfall often showed main rainfall cells over these areas and mean annual rainfall surely is higher. Initial loss and water loss through infiltration was exceeded several times, generating SEOF. Occasionally rainfall intensities topped the infiltration capacity of 72mm and IEOF was formed. The Mediterranean scrubland however was not solely responsible for flood generation. The largest floods of the season were generated after saturation of the whole basin, also of the agricultural fields. Runoff coefficient increases with storm intensity and duration. A coefficient of under

0.05 is observed for smaller events. For the largest event 0.16 and for the *double rainfall* scenarios 0.32 is reached. This also explains the disproportional high response to additional rainfall. The fraction of rainfall which is lost to wetting and saturation of the soil storage decreases with the amount of total rainfall.

Model functionality was proven. Possible explanations of the observed inaccuracies of model results are uncertainties in runoff and rainfall measurements. The temporal resolution of the runoff gauge might not be sufficient to determine precise flood volumes. The exact point of time of the flood wave passage may not be hit and so measured peak flow is too low. Due to many possible disturbances and interferences rainfall data derived from radar is always afflicted with uncertainties. Through the spatial resolution of 50x50m² small soil and landuse patterns are not taken into account. The influence of inaccuracies of the DEM of the mainly flat study area can be neglected. Beside these uncertainties in the input data, a further cause for the deviation of the modeled hydrographs is the inaccurate calibration. Results of the season show an overestimation of IEOF. The infiltration capacity of the Vertisols was set too low during calibration An underestimation of SEOF during very wet periods due to fast emptying of the soil storage was discussed. For the simulation of single events the parameter initial soil moisture had to be estimated prior every run. Even with a parameter set which was applied to different events and passed verification, the parameter initial moisture always stays open and has to be determined through calibration or measurement. For rainfall-runoff events during the wet period, initial moisture cannot be set to zero. With two or three prior days without precipitation a saturated soil may only have kept 40% of the soil moisture. These 40% now enter the simulation of the next event. The parameter initial moisture was equal for all soil types. This is the shortcoming of the model, because the emptying of the soil storage is dependent on porosity, pore size distribution and vegetation cover. Soil moisture is simulated by the model separately for each raster cell taken the rainfall, soil type and the vegetation cover into account. For longer periods the generalization of the entered initial moisture has no effect. Soil moisture in the beginning of the season usually is zero and can be set for all raster cells equally. Seasonal changes of infiltration rates were not considered. Beside the mentioned inaccuracies and their reasons no further model failures or uncertainties were observed.

The chosen model strategy of a successive approximation to the final parameter set through the calibration with single distinct events was effective. Event and season simulation results were satisfactory and made the execution of reliable landuse and climate scenarios possible.

X. Outlook

Within the GLOWA Jordan River Project the whole Lower Jordan River catchment is to be simulated for a better and sustainable water management. A. Gunkel therefore carried out a coupling of the rainfall-runoff model ZIN with the SVAT-model TRAIN. After the application to a micro scale basin, the newly TRAIN-ZIN was now modified for the meso scale. Simulation results are promising for successful application of the model to different basins throughout the semi-arid world, e.g. the macro scale LJRC. Through further development and modifications of the model an improvement of model performance can be achieved. Alternating infiltration capacities for certain soil types, in particular the soils of agricultural fields, should be used for a better simulation of surfaces with seasonal changes in vegetation cover. The integrated method for runoff concentration which already incorporates size and slope should also consider the shape of each subbasin. The transfer of generated runoff to channel flow could be estimated more accurately even for study areas with a wide range of different subbasins. For larger study areas thoughts about the spatial resolution are necessary. The temporal resolution of the TRAIN Model is far lower than for the ZIN Model. An also lower spatial resolution with larger grid cells would be sufficient for good TRAIN results. Saving computation times can be achieved this way. Despite these savings the spatial resolution will remain to be a limiting factor. Through the use of remote sensing techniques exact spatial information can be obtained for large areas. The processing of this high amount of data is very time consuming. A calibration with this data is not advisable. Faster calibration can be done with the simulation of subbasins. Through the use of subbasins with distinct characteristics the sensitivity of certain parameters and the quality of their calibration can be enhanced.

The rainfall scenarios showed a disproportional high runoff response to extreme rainfall events. A verification of these results is necessary. Therefore the observed event of October 2006 is to be simulated. With this additional proof of model functionality for such extreme events, further rainfall scenarios have to be conducted for the Mediterranean region. A more user-friendly model interface would make the model accessible to basin managers. The TRAIN-ZIN Model then can be used to study the effect of climate change and extreme rainfall events on flood generation in different basins. Simulation results in particular expected peak flows can then be considered within an integrated basin management.

XI. References

Agassi, M., Shainberg, I. & Morin, J. (1985): Infiltration and runoff in wheat fields in the semi-arid region of Israel. Geoderma, 36, 263-276.

Agnew, C. & Anderson, E. (1992): Water resources in the arid realm. Routledge. London.

Alpert, P. (2004): The water crisis in the E. Mediterranean – and relation to global warming. In: Water in the Middle East and in North Africa. Ed. by F. Zereini & W. Jaeschke, 55-62. Springer-Verlag, Berlin.

Azmon, B. (1992): Manning coefficient of roughness – a case study along Soreq stream, 1971-1981. Journal of Hydrology, 132, 361-377.

Battikhi, A. M. & Suleiman, A. A. (1999): Temporal variation of infiltration rate in a vertisol under lentil-wheat rotation. Journal of Agronomy & Crop Science, 183, 67-70.

Bergkamp, G. (1998): A hierarchical view of the interactions of runoff and infiltration with vegetation and microtopography in semiarid scrublands. Catena, 33, 201-220.

Berndtsson, R. & Larson, M. (1987): Spatial variability of infiltration in a semi-arid environment. Journal of Hydrology, 90, 117-133.

Beven, K. (1985): Distributed models. In: Hydrological Forecasting. Ed. by M. G. Anderson & T. P. Burt, 405-435. John Wiley & Sons. Chichester. England.

Beven, K. (2001): Rainfall-runoff Modeling. The primer. John Wiley & Sons. Chichester. England.

Beven, K. (2002): Runoff generation in semi-arid areas. In: Dryland Rivers. Hydrology and geomorphology of semi-arid channels. Ed. by L.J. Bull & M.J. Kirkby, 57-105. John Wiley & Sons. Chichester, England.

Castillo, V. M., Gómez-Plaza, A. & Martínez-Mena, M. (2003): The role of antecedent soil water content in the runoff response of semi-arid catchments: a simulation approach. Journal of Hydrology, 284, 114-130.

Cerdà, A. (1997): Seasonal changes of the infiltration rates in a Mediterranean scrubland on limestone. Journal of Hydrology, 198, 209-225.

Chow, Ven Te (1959): Open-channel hydraulics. McGraw-Hill Book Company. Singapore.

Dan, J. (1988): The soil of the land Israel. In: The Zoography of Israel. Ed. by Y. Yom-Tov & E. Tchernov, 95-128. Dr. W. Junk Publishers. Dordrecht. Netherlands

Dan, J., Gerson, R., Koyumdjisky, H. & Yaalon, D.H. (1981): Aridic Soils of Israel. Properties, genesis and management. Agricultural Research Organization. Israel.

DeVries, J. & Hromadka, T.V. (1996): Computer models for surface water. In: Handbook of hydrology. Ed. by D.R. Maidment, chapter 21. McGraw-Hill, Inc., New York.

Duiker, S. W., Flanagan, D. C. & Lal, R. (2001): Erodibility and infiltration characteristics of five major soils of southwest Spain. Catena, 45, 103-121.

Fread, D.L. (1985): Channel routing. In: Hydrological Forecasting. Ed. by M.G. Anderson & T.P. Burt, 15-36. John Wiley & Sons. Chichester. England.

Goldreich, Y. (2003): The climate of Israel. Kluwer Academic/Plenum Publishers. New York

Gómez-Plaza, A., Martínez-Mena, M., Albaladejo, J. & Castillo, V. M. (2001): Factors regulating spatial distribution of soil water content in small semiarid catchments. Journal of Hydrology, 253, 211-226.

Gunkel, A. (2006, unpublished): Kopplung der Modelle ZIN und TRAIN (Arbeitstitel). Dissertation zur Erlangung des Doktorgrades der Geowissenschaftlichen Fakultät der Albert-Ludwigs-Universität Freiburg i. Br.

Hanks, J. R. (1985): Soil water modeling. In: Hydrological Forecasting. Ed. by M.G. Anderson & T.P. Burt, 15-36. John Wiley & Sons. Chichester. England.

Hari Krishna, J. (1982): A parametric model to estimate runoff from small agricultural watersheds in the semi-arid tropics. Journal of Hydrology, 55, 43-51.

Hötzl, H. (2004): Natural scarcity of water resources in the semi-arid and arid Middle East and its economical implications. In: Water in the Middle East and in North Africa. Ed. by F. Zereini & W. Jaeschke, 3-13. Springer-Verlag, Berlin.

Horowitz, A. (1988) The quaternary environments and paleogeography in Israel. In: The Zoography of Israel. Ed. by Y. Yom-Tov & E. Tchernov, 45-58. Dr. W. Junk Publishers. Dordrecht. Netherlands.

Huebner, G. (1985): Use of radar for precipitation measurements. In: Hydrological Forecasting. Ed. by M.G. Anderson & T.P. Burt, 77-100. John Wiley & Sons. Chichester. England.

Intergovernmental Panel on Climate Change (2007): Forth Assessment Report. Climate Change 2007: Climate Change Impacts, Adaptation and Vulnerability. Summery for Policymakers. www.ipcc.ch (April, 2007).

Jaffe, S. (1988): Climate of Israel. In: The Zoography of Israel. Ed. by Y. Yom-Tov & E. Tchernov, 79-95. Dr. W. Junk Publishers. Dordrecht. Netherlands.

Ju'ub, G & Schetelig, K. (2004): The Jordan River: Natural flow and current consumption by the riparian countries. In: Water in the Middle East and in North Africa. Ed. by F. Zereini & W. Jaeschke, 31-39. Springer-Verlag, Berlin.

Kalma, J. D. & Stewart, W. F. (2004): Rainfall in arid and semi-arid regions. In: Understanding water in a dry environment. Ed. by I. Simmers, 15-63. A.A. Balkema Publishers. Lisse. Netherlands.

Karnieli, A. & Ben-Asher, J. (1993): A daily runoff simulation in semi-arid watersheds based on soil water deficit calculations. Journal of Hydrology, 149, 9-25.

Klein, M. (1988): The geomorphology of Israel. In: The Zoography of Israel. Ed. by Y. Yom-Tov & E. Tchernov, 59-78. Dr. W. Junk Publishers, Dordrecht. Netherlands.

Lange, J. (1999): A non-calibrated rainfall-runoff model for large arid catchments, Nahal Zin, Israel. Freiburg Schriften zur Hydrologie, Band 9. Institut für Hydrologie, Albert-Ludwigs-Universität Freiburg i. Br..

Lange, J. (2005): Dynamics of transmission losses in a large arid stream channel. Journal of Hydrology, 306, 112-126.

Lange, J., Leibundgut, C., Greenbaum, N. & Schick, A. P. (1999): A noncalibrated rainfall-runoff model for large, arid catchments. Water Resources Research, Vol. 35, No. 7, 2161-2172.

Lange, J., Greenbaum, N., Husary, S., Ghanem, M, Leibundgut, C. & Schick, A. P. (2003): Runoff generation from successive simulated rainfalls on a rocky, semi-arid, Mediterranean hillslope. Hydrological Processes, 17, 279-296.

Leibundgut, C., Lange, J. Tamimi, A.R., Ghanem, M., Husary, S., Enzel, Y., Grodek, T. & Lekach, J. (2003): The impact of urbanization on integrated drainage basin hydrology and water resources, West Bank and Israel. Abschlussbericht DFG-Forschungsprojekt LE 698/10-1-3.

Leistert, H (2005): Modeling transmission losses; Application in the Wadi Kuiseb and the Nahal Zin. Diplomarbeit am Institut für Hydrologie, Albert-Ludwigs-Universität Freiburg i. Br.

Menzel, L. (1999): Flächenhafte Modellierung der Evaporation mit TRAIN. Potsdam-Instiut für Klimafolgenforschung (PIK), Potsdam, PIK Report No 54.

Merz, B. & Plate, E. J. (1997): An analysis of the effects of spatial variability of soil and soil moisture on runoff. Water Resources Research, Vol 33, No 12, 2909-2922

Michaud, J. & Sorooshian, S. (1994): Comparison of simple versus complex distributed runoff models on a midsized semiarid watershed. Water Resources Research, Vol. 30, No. 3, 593-605.

Milliman J. D., Leftic L. & Sestini G. (1992): The Mediterranean Sea and Climate Change. An Overview. In: Climatic Change and the Mediterranean. Ed. by L. Leftic, J.D. Milliman & G. Sestini, 1-15. Arnold. London.

Morin, E. & Gabella, M (2006): Radar-based quantitative precipitation estimation over Mediterranean and dry climate regimes. Submitted to: Journal of Geophysical Research. Submission date: 31st October 2006.

Nash, J.E., Sutcliffe, J.V. (1970): River flow forecasting through conceptional models. Part I, a discussion of principles. Journal of Hydrology 10, 282-290.

Nir, D. (1973): The Semi-arid World: man on the fringe of desert. First published in Hebrew. Translated into English by Gottlieb, R.. Longman. New York

Palutikof, J.P., Conte, M., Casimiro Mendes, J. Goodess, C.M. & Espirito Santo, F. (1997): Climate and climatic change. In: Mediterranean desertification and land use. Ed. by C. Brandt & J. Thornes, 43-86. John Wiley & Sons, Chichester. England.

Pilgrim, D. H., Chapman, T. G. & Doran, D. G. (1988): Problems of rainfall-runoff modeling in arid and semiarid regions. Hydrological Sciences Journal, 33, 379-400.

Ponce, V.M. & Chaganti, P.V. (1994): Variable-parameter Muskingum-Cunge method revisited. Journal of Hydrology, 162, 433-439.

Rawls, W. J., Ahuja, L. R., Brakensiek, D.L. & Shirmohammadi, A. (1992): Infiltration and soil water movement. In: Handbook of Hydrology. Ed. by D. R. Maidman, Chapter 5. McGraw-Hill, Inc., New York.

Rimmer, A. & Gal, G. (2003): Estimating the saline springs component in the solute and water balance of Lake Kinneret, Israel. Journal of Hydrology 284, 228-243.

Saxton, K.E. (2006): SPAW Soil-Plant-Atmosphere-Water Field and Pond Hydrology. (http://hydrolab.arsuda.gov/SPAW/Index.htm, Mar. 2007), latest model version.

Saxton, K.E., Rawls, W.L. (1986): Estimating generalized soil-water characteristics from texture. Soil Science Society of America Journal, 50, 1031-1036.

Scheffer, F. & Schachtschabel, P (2002): Lehrbuch der Bodenkunde. 15. Auflage. Spektrum Akademischer Verlag, Heidelberg.

Schröder, R. (2000): Modellierung von Verschlämmung und Infiltration in landwirtschaftlich genutzten Einzugsgebieten. Bonner Geographische Abhandlungen. Sankt Augustin.

Schrödter, H.(1985): Verdunstung, Anwendungsorientierte Meßverfahren und Bestimmungsmethoden. Springer-Verlag, Berlin.

Schütz, T. (2006): Prozessbasierte Niederschlags-Abflussmodellierung in einem mediterranen Kleineinzugsgebiet. Diplomarbeit am Institut für Hydrologie, Albert-Ludwigs-Universität Freiburg i. Br.

Scoging, H.M., Thornes, J.B. (1979): Infiltration characteristics in a semiarid environment. In: IAHS-AISH Publ. no. 128. The hydrology of areas of low precipitation. Proceedings of the Canberra Symposium

Shannon, J., Richardson, R. & Thornes, J. (2002): Modeling event-based fluxes in ephemeral streams. In: Dryland Rivers. Hydrology and geomorphology of semi-arid channels. Ed. by L.J. Bull & M.J. Kirkby, 129-172. John Wiley & Sons. Chichester. England.

Sorooshian, S. & Gupta, V.K. (1995): Model calibration. In: Computer models of watershed hydrology. Ed. by V.P. Singh, 23-64. Water Resources Publications. Highlands Ranch. USA.

Steinmann, A., Lange, J., Leibundgut, C., Grodek T., Lekach, J. (2003): Experimental studies on runoff generation in a semi-arid area – a combination of hydrometric and tracerhydrological techniques. Geophysical Research Abstracts, Volume 5, European Geophysical Society, 2003. (Abstract EAE03-A-02512)

Thormählen, A. (2003): Hydrological modeling in a small hyperarid catchment – Nahal Yael, Israel – runoff generation and transmission losses. Diplomarbeit am Institut für Hydrologie, Albert-Ludwigs-Universität Freiburg i. Br.

Van Genuchten, M. Th. (1980): A closed-form equation for predicting the hydraulic conductivity of unsaturated soils. Soil Science Society of America. Journal, 44, 892-898.

Wiesendanger, C. (2007): Ereignis-basierte Datenkorrektur der Radarniederschlags-messung. Anwendung im Einzugsgebiet des Unteren Jordan. Diplomarbeit am Institut für Hydrologie, Albert-Ludwigs-Universität, Freiburg im Breisgau.

Wigley, T.M.L. (1992): Future Climate of the Mediterranean Basin with particular Emphasis on Changes in Precipitation. In: Climatic Change and the Mediterranean. Ed. by L. Leftic, J. D. Millimann and G. Sestini, 15-45. Arnold. London.

Yaalon, D. H. (1997): Soils in the Mediterranean region: what makes them different? Catena, 28, 157-169.

Yair, A. & Lavee, H, (1985): Runoff generation in arid and semi-arid zones. In: Hydrological Forecasting. Ed. by M.G. Anderson & T.P. Burt, 183-220. John Wiley & Sons. Chichester. England.

URL 1: http://www.glowa-jordan-river.de (May 2007)

XII. Appendix

Tab.1: Initial soil parameters

	SoilNr	infCap [mm/h]	initLoss [mm/h]	soilDepth [m]	Poreff [/]	PWP [/]	FC [/]	λ [/]	K_S [cm/h]
Pelosol	1	12	45	4	0.5	0.31	0.43	0.16	0.29
Vertisol	2	12	45	4	0.5	0.31	0.43	0.16	0.29
Terra Rossa	3	43	10	1	0.46	0.2	0.32	0.36	0.65
Regosol	4	61	10	1.5	0.4	0.17	0.28	0.32	0.92
Rendzina	5	30	10	2	0.4	0.2	0.35	0.24	0.74
Xerosol	6	65	10	1	0.35	0.08	0.18	0.38	4.8
Fishponds	7	1000	1000	10	1	0.01	1	0.1	10.0
Settlement	8	5	5	0.25	0.3	0.01	0.01	0.1	0.01

infCap: Infiltration capacity, initLoss: initial Loss, Poreff: effective porosity, PWP: permanent wilting point, FC: field capacity, λ : Brook-Corey pore-size distribution index, K_S: saturated hydraulic conductivity.

Tab.2: Final soil parameter set after calibration

	SoilNr	infCap [mm/h]	initLoss [mm/h]	soilDepth [m]	Poreff [/]	PWP [/]	FC [/]	λ [/]	K_S [cm/h]
Pelosol	1	100	12	2	0.5	0.31	0.43	0.16	0.4
Vertisol	2	100	12	2	0.5	0.31	0.43	0.16	0.4
Terra Rossa	3	72	9	0.25	0.46	0.2	0.32	0.36	0.17
Regosol	4	65	8	1	0.4	0.17	0.28	0.32	0.92
Rendzina	5	45	8	1.5	0.4	0.2	0.35	0.24	0.74
Xerosol	6	70	8	1	0.35	0.08	0.18	0.38	4.8
Fishponds	7	1000	1000	10	1	0.01	1	0.1	10.0
Settlement	8	3	3	0.25	0.3	0.01	0.01	0.1	0.01

infCap: Infiltration capacity, initLoss: initial Loss, Poreff: effective porosity, PWP: permanent wilting point, FC: field capacity, λ : Brook-Corey pore-size distribution index, K_S: saturated hydraulic conductivity.

Tab. 12.3: Channel properties

Segment	LastSeg	NextSeg	Trib1	Trib2	Slope	Length	Width	Type
1	0	2	0	0	0.03894491	2491	10	2
2	1	5	0	0	0.01241277	1611	10	1
3	0	5	0	0	0.02022672	989	5	4
4	0	5	0	0	0.04035351	2850	5	3
5	2	11	3	4	0.01200466	1250	15	1
6	0	11	0	0	0.01744385	2006	4	3
7	0	10	0	0	0.09936621	2415	6	3
8	0	9	0	0	0.134337	1935	3	3
9	8	10	0	0	0.03740558	1470	5	2
10	7	11	9	0	0.02555112	2192	8	3
11	5	17	6	10	0.01034907	966	19	1
12	0	17	0	0	0.0355716	618	2	4
13	0	14	0	0	0.08972776	1449	5	4
14	13	16	0	0	0.04281665	2569	3	3
15	0	16	0	0	0.041437	1279	5	4
16	14	17	15	0	0.01454645	1100	10	2
17	11	26	16	12	0.00907415	3527	22	1
18	0	21	0	0	0.02525325	1505	2	3
19	0	21	0	0	0.06980498	1304	5	5
20	0	21	0	0	0.0684872	2599	7	5
21	19	26	18	20	0.03636069	1705	3	3
22	0	24	0	0	0.08805767	1817	7	4
23	0	24	0	0	0.05475079	1425	5	4
24	23	25	22	0	0.03828193	1959	10	2
25	24	26	0	0	0.02629581	2016	10	2
26	17	28	25	21	0.00465282	645	20	1
27	0	28	0	0	0.02483657	1127	5	3
28	26	57	27	0	0.00325849	921	20	1
29	0	31	0	0	0.05034277	2284	4	4
30	0	31	0	0	0.08779195	866	2	4
31	29	35	30	0	0.02037191	2013	3	3
32	0	34	0	0	0.04173763	2204	4	4
33	0	34	0	0	0.01832991	1637	4	4
34	33	35	32	0	0.01233375	973	3	3
35	34	44	31	0	0.0032018	625	5	2
36	0	38	0	0	0.04318333	1667	4	4
37	0	38	0	0	0.10551371	2189	4	3
38	36	43	37	0	0.02183367	1557	5	3
39	0	41	0	0	0.09689931	1176	3	4
40	0	41	0	0	0.14298705	1322	3	4
41	40	42	39	0	0.06713866	462	5	4
42	41	43	0	0	0.04553969	1515	5	3
43	42	44	38	0	0.02201	818	3	2
44	43	45	35	0	0.01359824	1030	5	3
45	44	47	0	0	0.00628681	1273	5	2
46	0	47	0	0	0.07070438	1570	5	4
47	45	48	46	0	0.00416574	960	4	3

Tab. 12.3: Channel properties (continuation)

Segment	LastSeg	NextSeg	Trib1	Trib2	Slope	Length	Width	Type
48	47	50	0	0	0.05612327	1123	5	3
49	0	50	0	0	0.052029	769	3	4
50	48	54	49	0	0.00964568	622	5	3
51	0	53	0	0	0.0614815	1448	4	4
52	0	53	0	0	0.07395225	622	2	4
53	51	54	52	0	0.05043808	1923	5	2
54	50	56	53	0	0.00374805	800	6	3
55	0	56	0	0	0.06585529	2065	5	4
56	54	57	55	0	0.01053023	1899	8	2
57	28	59	56	0	0.01368252	1023	20	1
58	0	59	0	0	0.06259932	2492	8	3
59	57	60	58	0	0.01265753	1817	20	1
60	59	64	0	0	0.00818023	1711	20	1
61	0	63	0	0	0.16490638	1940	5	5
62	0	63	0	0	0.19354314	1524	8	5
63	62	64	61	0	0.01349863	2074	5	4
64	60	83	63	0	0.00556382	4314	20	1
65	0	68	0	0	0.04428955	1806	6	4
66	0	68	0	0	0.03947967	1494	6	4
67	0	68	0	0	0.07386234	1354	5	4
68	67	70	66	65	0.0187226	267	5	3
69	0	70	0	0	0.05691073	1810	4	3
70	69	73	68	0	0.01142515	1926	6	2
71	0	72	0	0	0.02261107	2654	5	2
72	71	73	0	0	0.01784901	1849	7	1
73	70	77	72	0	0.00388653	1029	7	1
74	0	76	0	0	0.06785463	1179	6	4
75	0	76	0	0	0.05745784	1323	4	3
76	75	77	74	0	0.01127683	1596	8	1
77	73	78	76	0	0.00860413	1511	9	1
78	77	82	0	0	0.00183513	2180	10	1
79	0	81	0	0	0.06843585	1490	2	3
80	0	81	0	0	0.095023	1494	7	4
81	80	82	79	0	0.00518111	1351	10	2
82	81	83	78	0	0.00178484	560	15	1
83	64	88	82	0	0.00219467	456	20	1
84	0	86	0	0	0.12545896	3300	10	5
85	0	86	0	0	0.1462732	2906	8	5
86	85	88	84	0	0.00241965	2066	3	3
87	0	88	0	0	0.08219635	2677	10	3
88	83	90	86	87	0.00842181	1306	20	1
89	0	90	0	0	0.0144135	833	3	2
90	88	93	89	0	0.00561993	1779	18	1
91	0	92	0	0	0.08303557	2324	4	4
92	91	93	0	0	0.00536073	2985	9	1
93	90	107	92	0	0.01109496	631	16	1
94	0	97	0	0	0.05954919	2183	4	3

Tab. 12.3: Channel properties (continuation)

Segment	LastSeg	NextSeg	Trib1	Trib2	Slope	Length	Width	Type
95	0	97	0	0	0.01470313	272	1	4
96	0	97	0	0	0.06162542	941	3	4
97	94	100	95	96	0.02363102	635	4	3
98	0	100	0	0	0.05980817	1488	3	4
99	0	100	0	0	0.04508334	2662	4	4
100	97	104	98	99	0.00772697	1682	4	2
101	0	103	0	0	0.06060226	2360	3	3
102	0	103	0	0	0.05866722	2267	3	4
103	102	104	101	0	0.03360853	1190	5	3
104	100	106	103	0	0.0135307	1626	5	3
105	0	106	0	0	0.04324797	3746	2	3
106	104	107	105	0	0.00733293	1091	5	2
107	93	109	106	0	0.01351274	592	16	1
108	0	109	0	0	0.01250195	1680	5	2
109	107	110	108	0	0.01222484	1718	16	1
110	109	0	0	0	0.01534476	1564	20	1

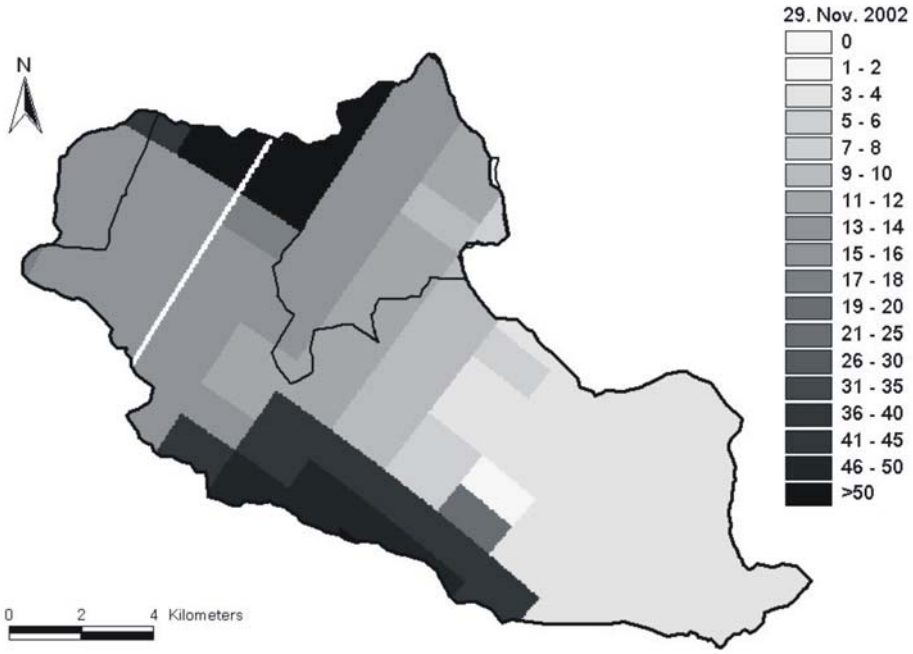

Figure 12.1: Daily rainfall in mm, Nov 29th 2002

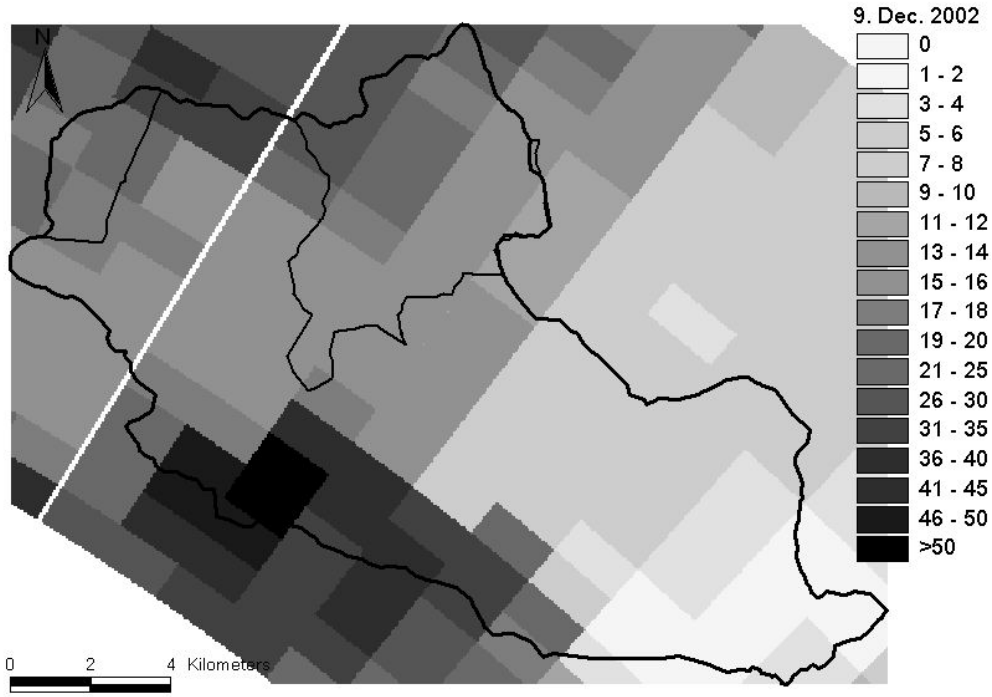

Figure 12.2: Daily rainfall in mm, Dec. 9th 2002

Figure 12.3: Daily rainfall in mm, Dec. 10th 2002

Figure 12.4: Daily rainfall in mm, Dec. 11th 2002

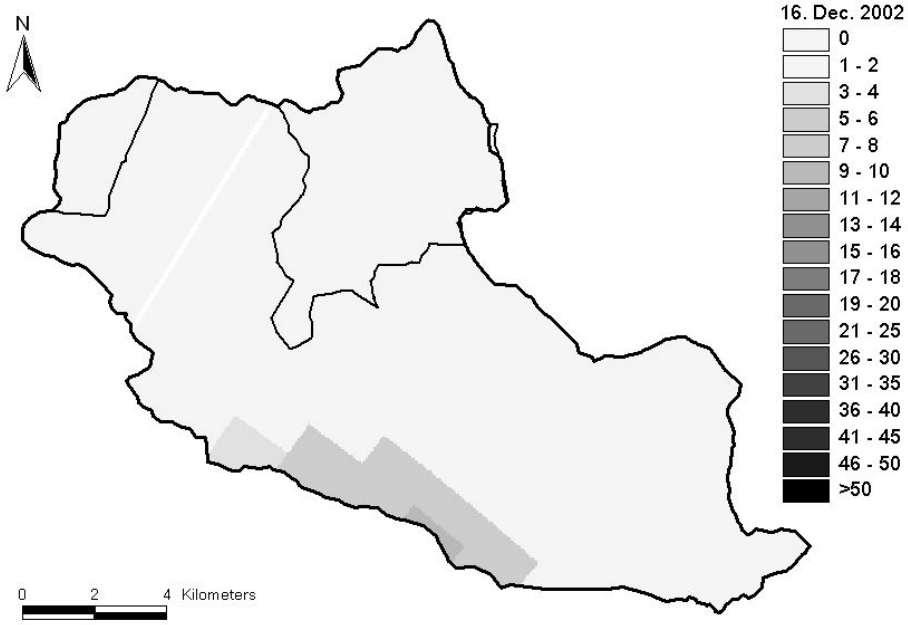

Figure 12.5: Daily rainfall in mm, Dec. 16th 2002

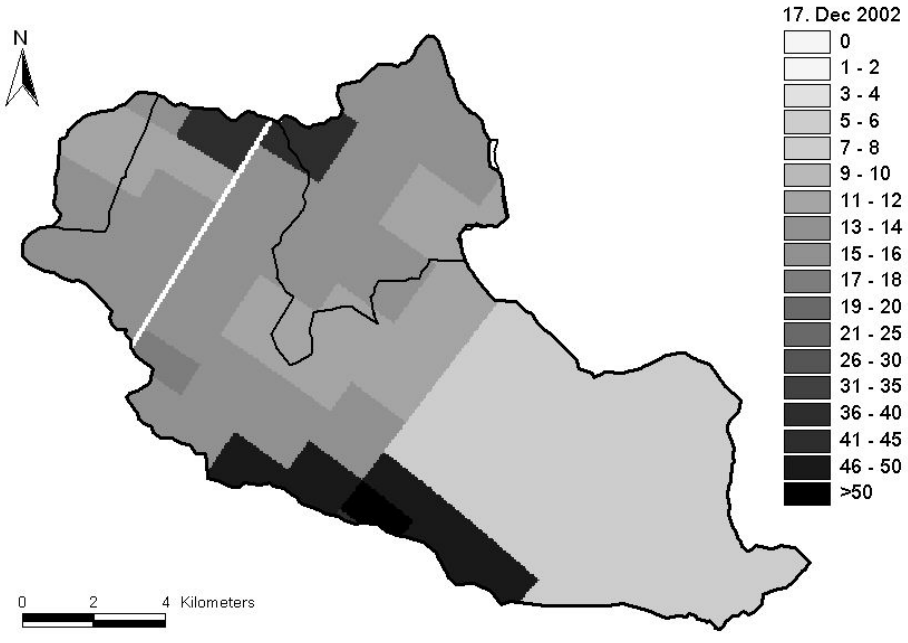

Figure 12.6: Daily rainfall in mm, Dec. 17th 2002

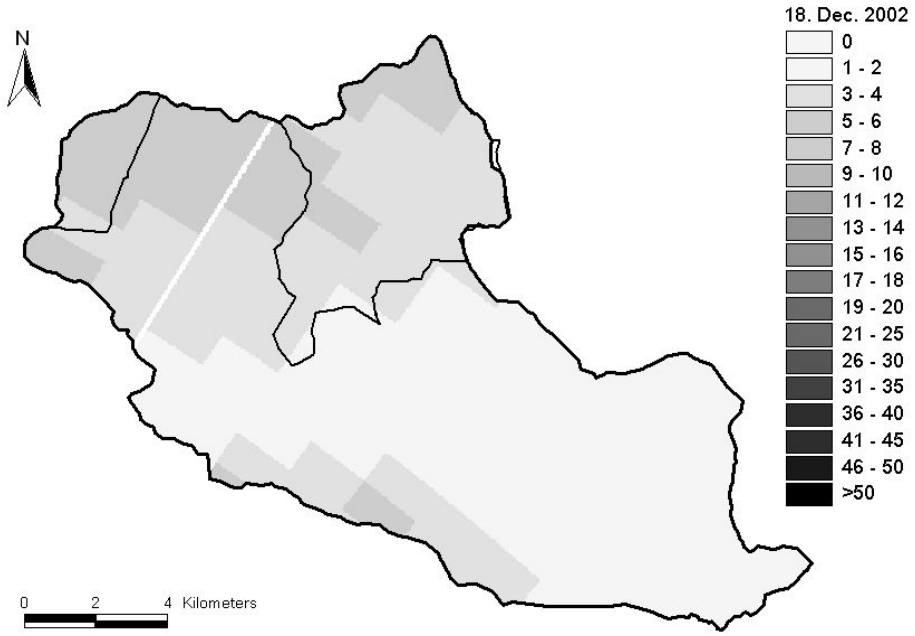

Figure 12.7: Daily rainfall in mm, Dec. 18th 2002

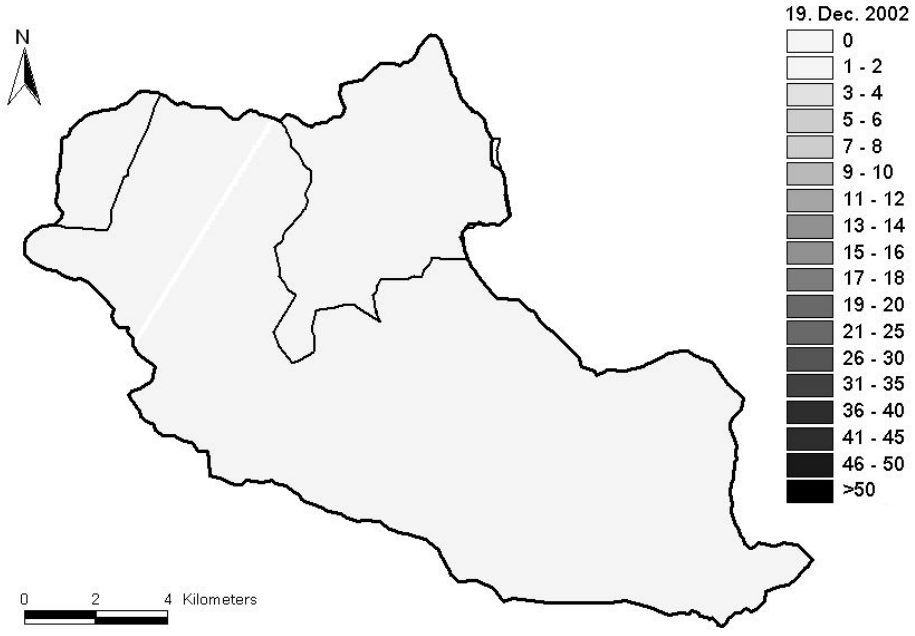

Figure 12.8: Daily rainfall in mm, Dec. 19th 2002

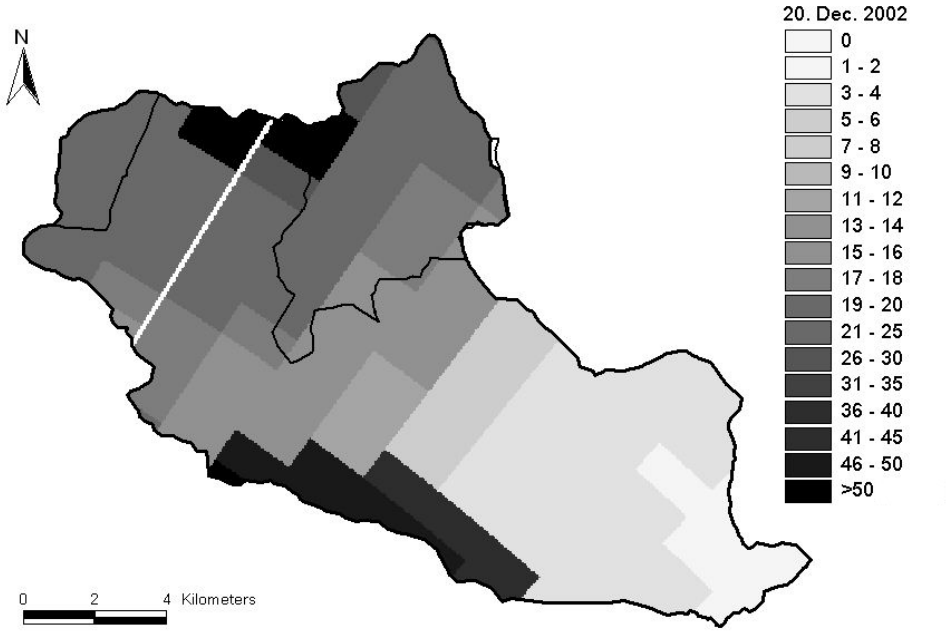

Figure 12.9: Daily rainfall in mm, Dec. 20th 2002

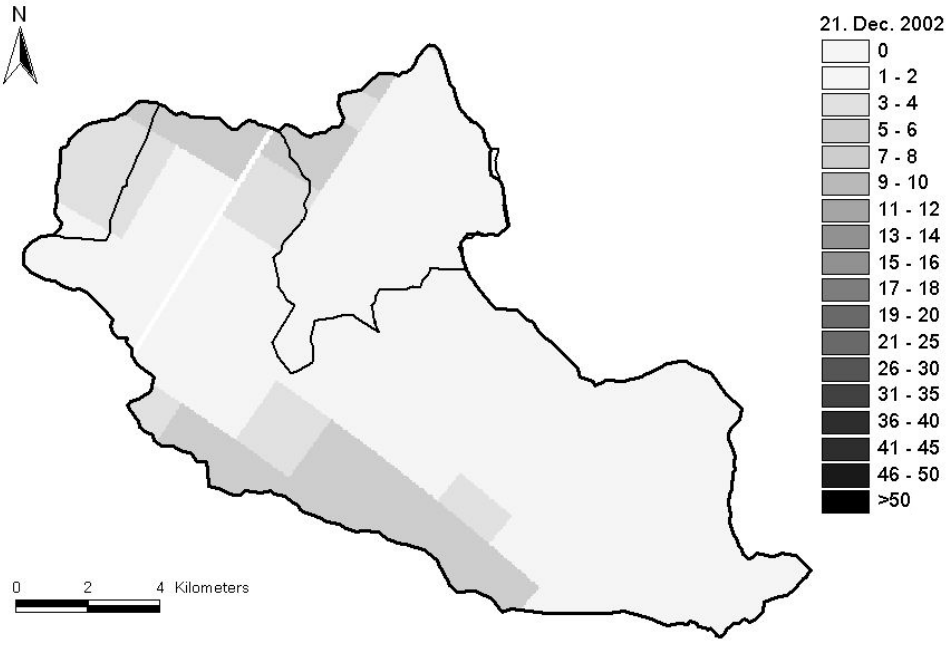

Figure 12.10: Daily rainfall in mm, Dec. 21st 2002

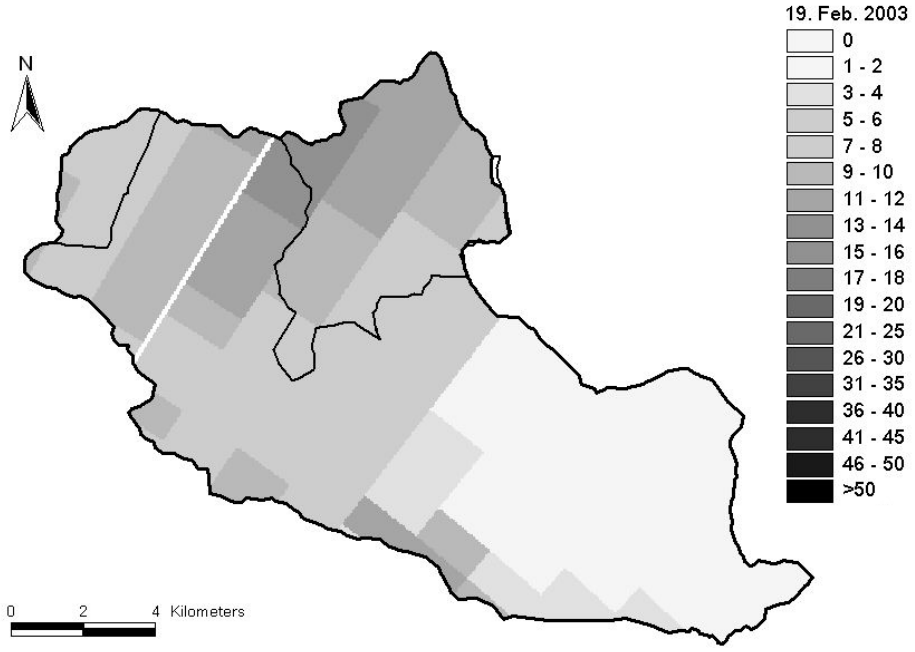

Figure 12.11: Daily rainfall in mm, Feb. 19th 2003

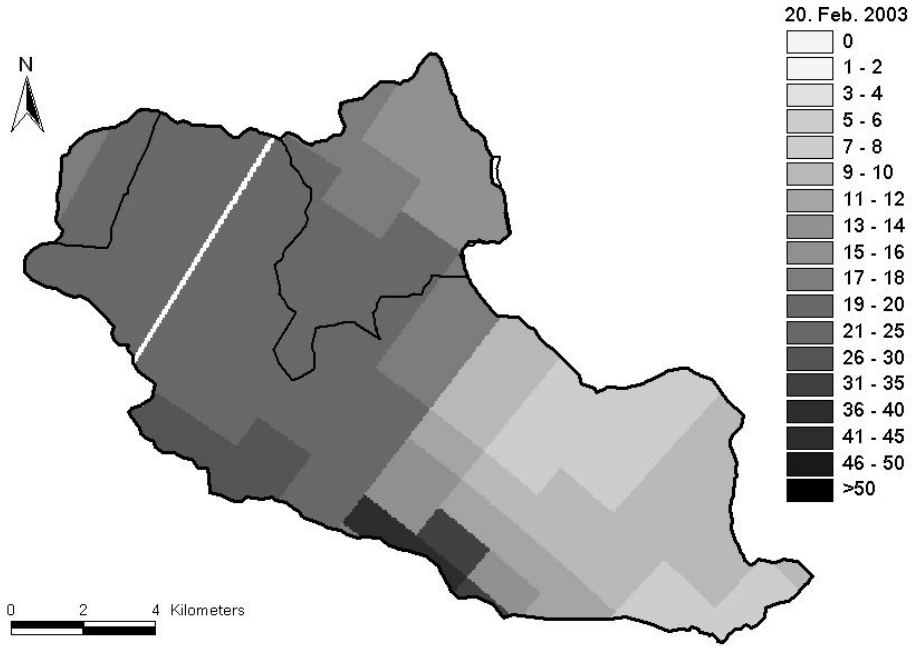

Figure 12.12: Daily rainfall in mm, Feb. 20th 2003

Figure 12.13: Daily rainfall in mm, Feb. 21st 2003

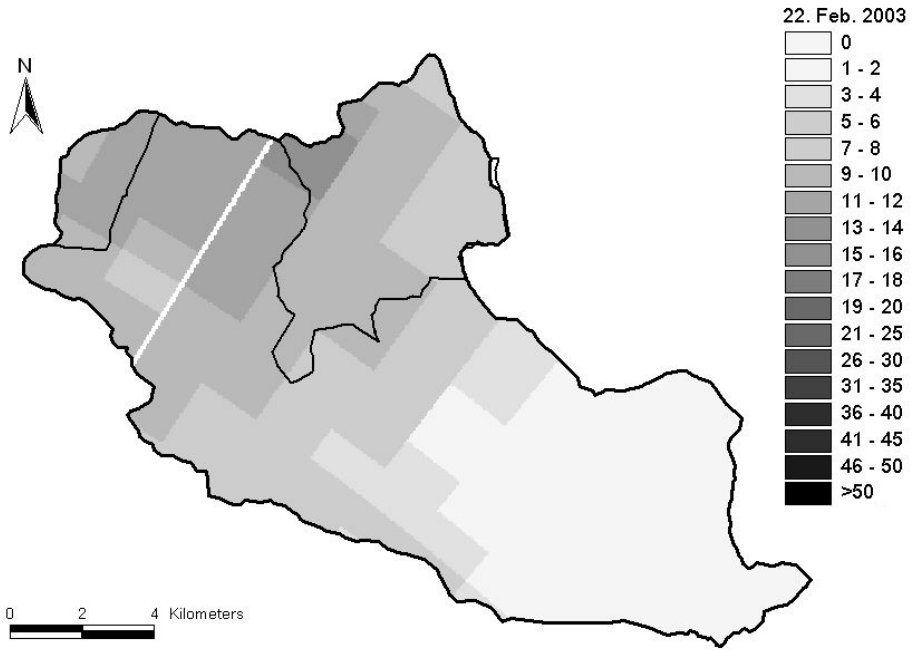

Figure 12.14: Daily rainfall in mm, Feb. 22nd 2003

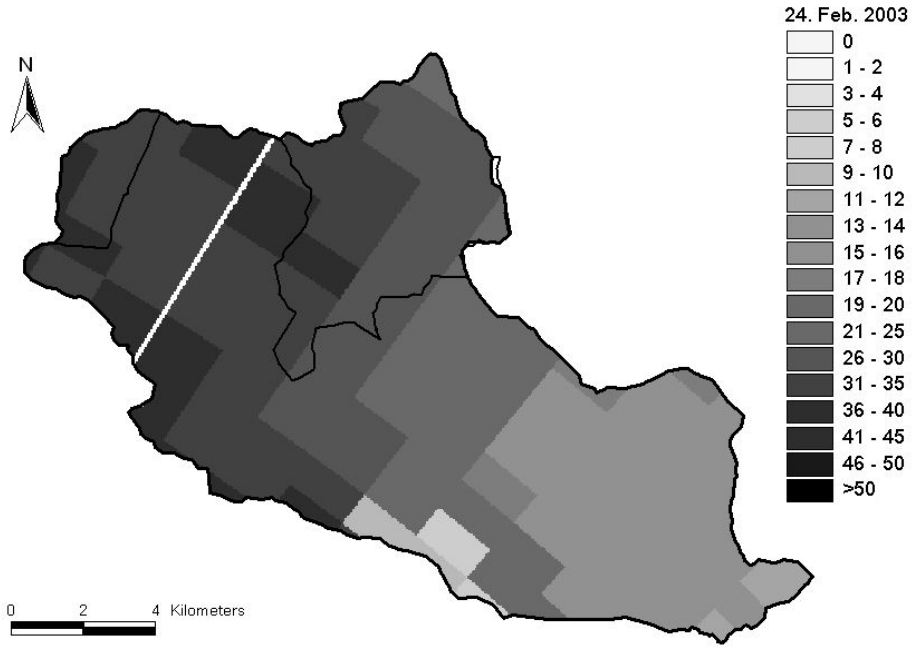

Figure 12.15: Daily rainfall in mm, Feb. 24th 2003

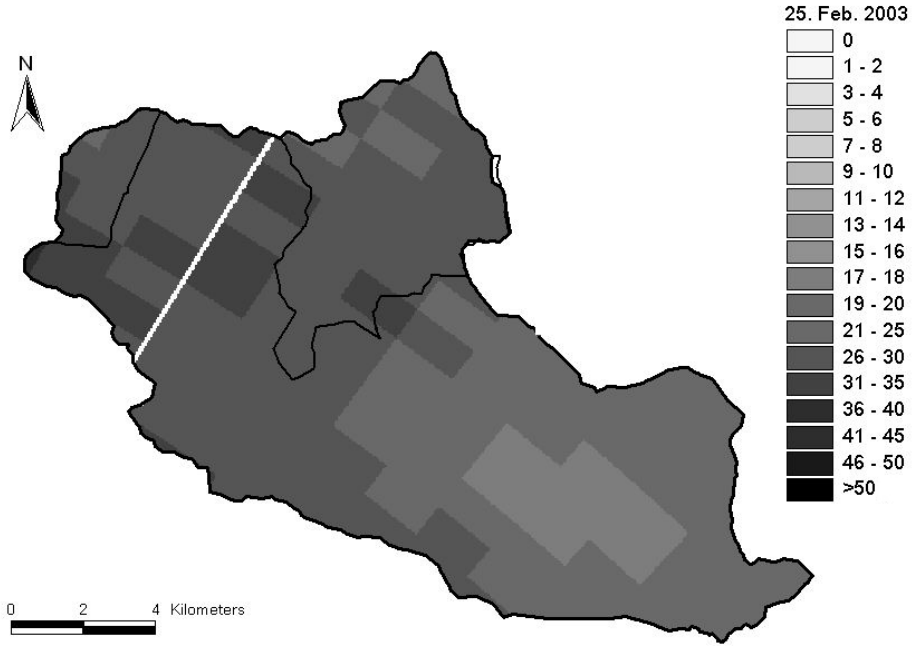

Figure 12.16: Daily rainfall in mm, Feb. 25th 2003

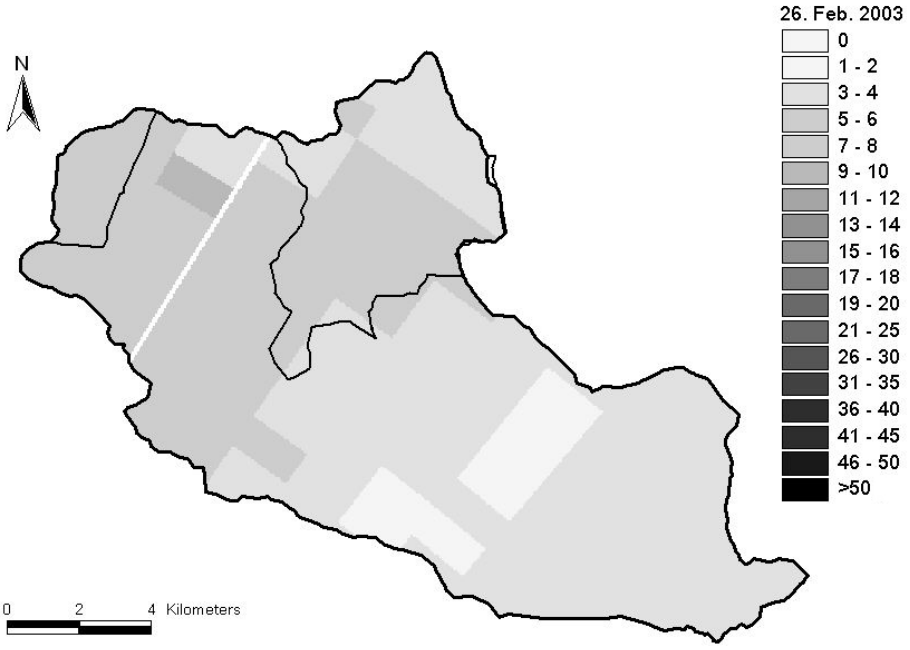

Figure 12.17: Daily rainfall in mm, Feb. 26th 2003

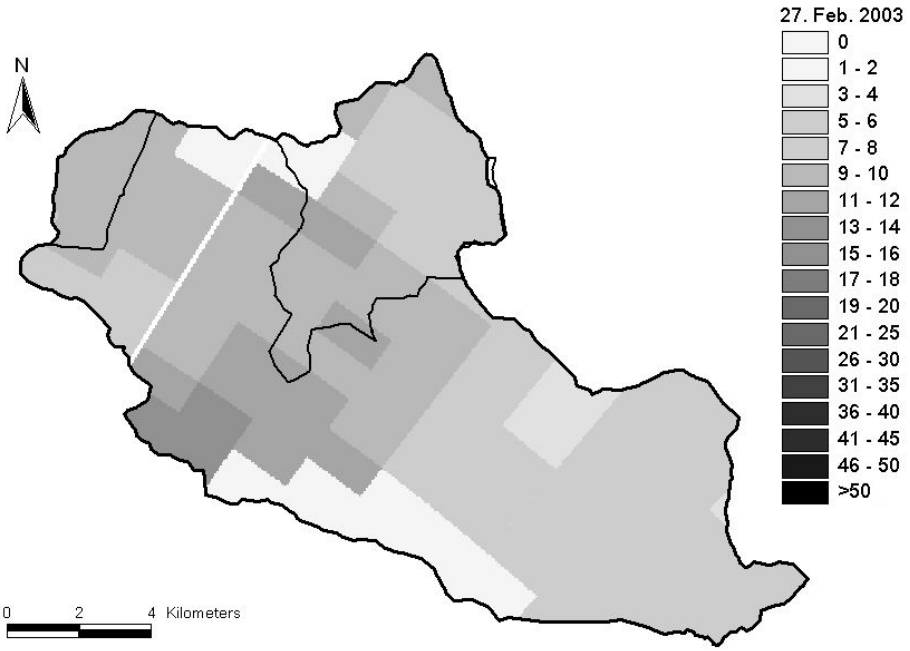

Figure 12.18: Daily rainfall in mm, Feb. 27th 2003

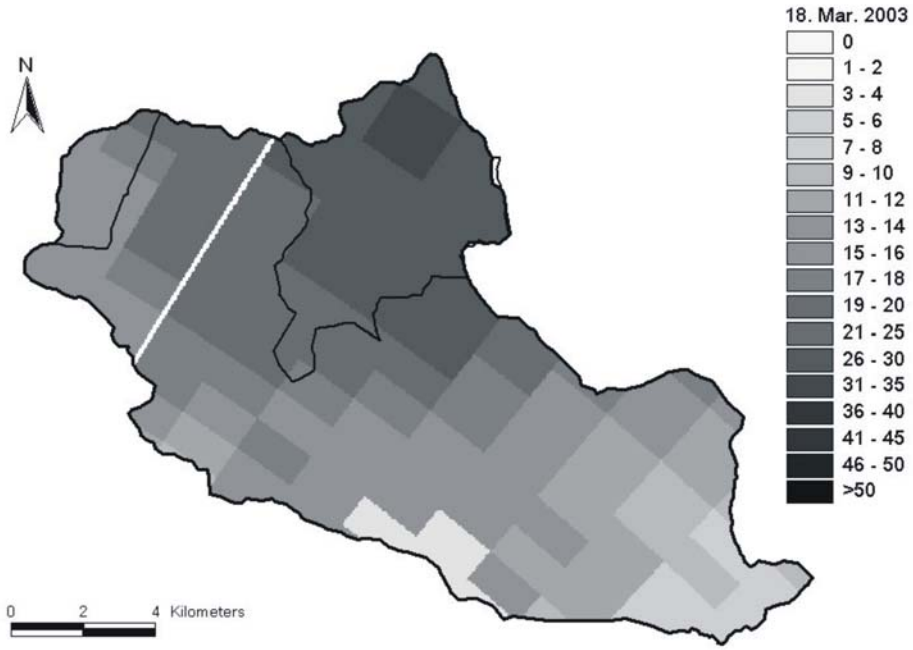

Figure 12.19: Daily rainfall in mm, Mar. 18th 2003

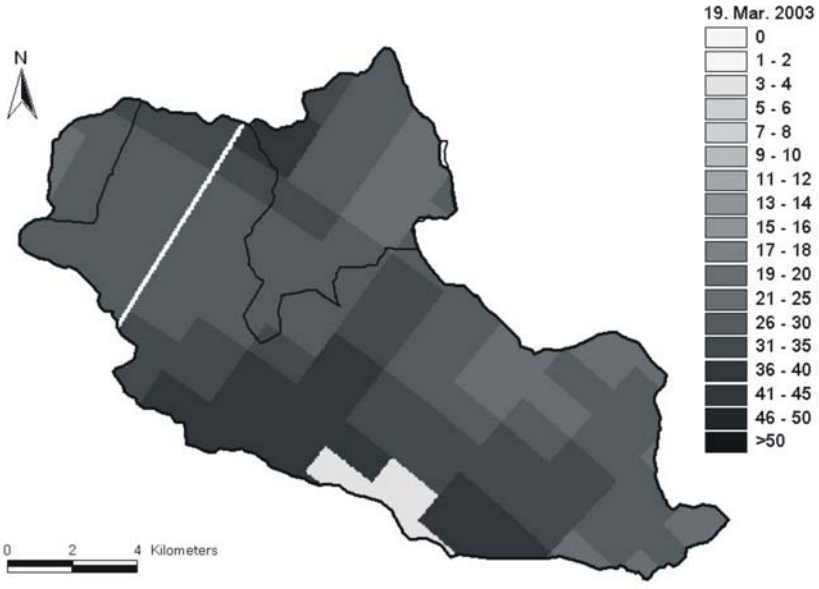

Figure 12.20: Daily rainfall in mm, Mar. 19th 2003

Figure 12.21: Daily rainfall in mm, Mar. 24th 2003

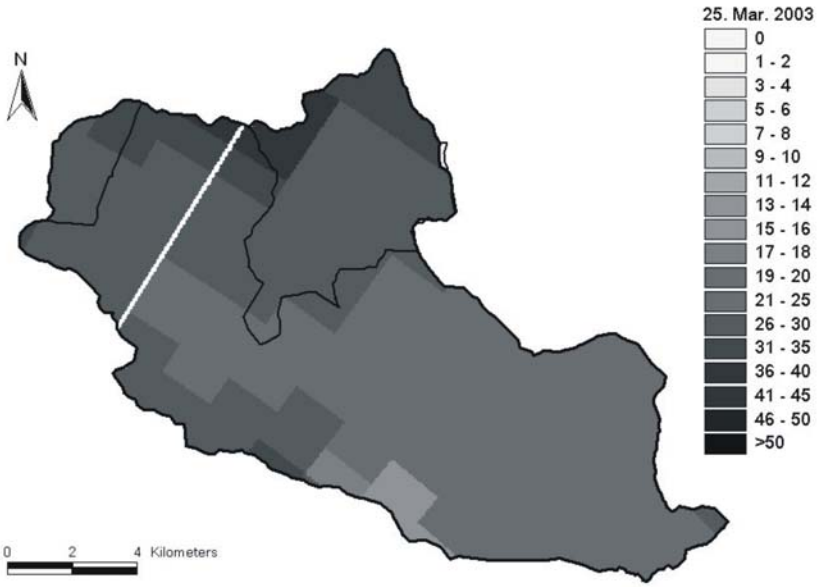

Figure 12.22: Daily rainfall in mm, Mar. 25th 2003

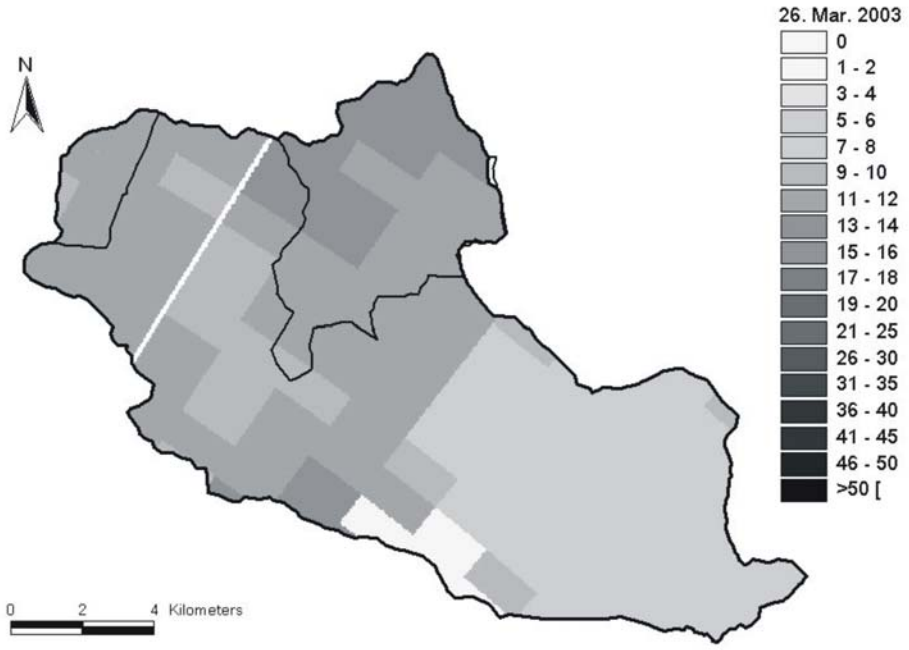

Figure 12.23: Daily rainfall in mm, Mar. 26th 2003

XIII. Ehrenwörtliche Erklärung

Hiermit erkläre ich, dass die Arbeit selbständig und nur unter der Verwendung der angegebenen Hilfsmittel angefertigt wurde.